HIRSZFELD INSTITUTE OF IMMUNOLOGY AND EXPERIMENTAL THERAPY
POLISH ACADEMY OF SCIENCES

DOCTORAL DISSERTATION

mgr Michał Olk

Synthesis and Cytotoxicity of $NaYF_4$ Nanoparticles Coated in a Layer of Porous Silica

Synteza i cytotoksyczność nanocząstek $NaYF_4$ pokrytych warstwą porowatej krzemionki

SUPERVISOR
prof. dr hab. Andrzej Gamian

AUXILIARY SUPERVISOR
dr Katarzyna Prorok

Department of Immunology of Infectious Diseases
Laboratory of Medical Microbiology

Wrocław, 2023

This thesis was financially supported by the National Science Centre Poland under Grant No. 2018/31/D/ST5/01328 at the Włodzimierz Trzebiatowski's Institute of Low Temperatures and Structure Research, Polish Academy of Sciences in Wrocław. Synthesis of nanoparticles, silica coating, and spectral as well as structural characterization was performed there. Cytotoxicity experiments were performed at the Hirszfeld Institute of Immunology and Experimental Therapy, Polish Academy of Sciences in Wrocław.

I would like to express my deepest gratitude and thanks to doctor Katarzyna Prorok from Włodzimierz Trzebiatowski's Institute of Low Temperatures and Structure Research, for her irreplaceable role in this dissertation by allowing me to work alongside her and study the subject of the upconversion process.

I am also grateful to professor Andrzej Gamian from Hirszfeld Institute of Immunology and Experimental Therapy for his supervision of the biological aspects of this work and the essential motivation for writing the dissertation.

Lastly, I would also like to mention Marzena Ciesielska for her precious words of advice.

TABLE OF CONTENTS

ABBREVIATIONS

@	*coated with*
APTES	*(3-aminopropyl) triethoxysilane*
ATP	*adenosine triphosphate*
BHMT	*bis (hexamethylene)triamine*
ChR2	*channelrhodopsin-2*
CD	*cyclodextrin*
DC	*dendritic cell*
DCM	*dichloromethane*
DMF	*dimethylformamide*
DOX	*doxorubicin*
$dSiO_2$	*dense silica*
EDC	*1-ethyl-3-(3-dimethylaminopropyl)carbodiimide*
FRET	*Förster resonance energy transfer*
ICG	*indocyanine green*
IR	*infrared*
LbL	*layer-by-layer assembly*
Ln / Ln^{3+}	*lanthanides*
$mSiO_2$	*mesoporous silica*
NHS	*N-hydroxysuccinimide*
NIR	*near-infrared*
PA	*polyacrolein*
PAA	*polyacrylic acid*
PDT	*photodynamic therapy*
PEG	*polyethylene glycol*
PEI	*polyethylenimine*
PI	*propidium iodide*
PMAO	*poly(maleic anhydride-alt-1-octadecene)*
PS	p*hosphatidylserine*
PVP	*polyvinylpyrrolidone*
QD	*quantum dot*
ROS	*reactive oxygen species*
TEOS	*tetraethyl orthosilicate*
UC	*upconversion*
UCL	*upconversion luminescence*
UCNP	*upconversion nanoparticle*
UV	*ultraviolet*
VIS	*visible*

STRESZCZENIE

Jakościowe i ilościowe metody takie jak mikroskopie czy spektroskopie, są jednymi z najbardziej popularnych technik wykorzystywanych we współczesnej biologii. W ostatnich latach nanocząstki konwertujące energię wzbudzenia w górę (ang. upconverting nanoparticles, UCNPs), domieszkowane jonami lantanowców, stały się przedmiotem intensywnych badań w ciągle rozwijającym się polu poszukiwań nowych i wydajnych metod obrazowania oraz detekcji struktur biologicznych.

Proces konwersji energii wzbudzenia w górę (ang. upconversion, UC) został odkryty już w latach 60-tych XX wieku, a w latach 2000-tych opracowano metody syntez chemicznych pierwszych domieszkowanych mikro- i nanocząstek opartych o matrycę $NaYF_4$, o wydajności kwantowej wyższej niż poprzednie materiały UC. Zjawisko UC polega na absorbcji dwóch lub więcej niskoenergetycznych fotonów, zazwyczaj z zakresu podczerwieni, i emisji fotonów o wyższej energii, zazwyczaj z zakresu widzialnego lub ultrafioletowego. Zjawisko to wykorzystuje przejścia elektronowe 4f-4f zachodzące w jonach lantanowców.

Dalsze wzmocnienie luminescencji nanocząstek UC można uzyskać poprzez zaprojektowanie tak zwanej aktywnej powłoki. Powłoka ta, poprzez konkretne jony lantanowców, jest zdolna do pochłonięcia dodatkowej energii fotonów i przekazania jej do rdzenia, w którym zachodzi zjawisko UC.

Nanocząstki $NaYF_4$ mają jednak istotną wadę w postaci niskiej wydajności kwantowej. Wzbudzenie w widmie IR wymaga intensywnego źródła tego światła. To generuje znaczną ilość ciepła w układzie, które jest szkodliwe dla struktur biologicznych. Problem ten próbuje się rozwiązać poprzez zastosowanie tak zwanych powierzchniowych anten uczulających. Antena pochłaniając promieniowanie IR, przekazuje energię bezpromieniście do jonów lantanowców w strukturze nanocząstki. Ta dodatkowa energia zwiększa intensywność zjawiska

UC. Cyjaninowe barwniki organiczne pochłaniające w widmie bliskiej podczerwieni (NIR) takie jak IR-806, lub kropki kwantowe są przykładami aktualnie badanych kandydatów do roli tychże anten.

Oferując właściwości takie jak możliwość wzbudzania w głębszych fragmentach tkanki, niższy szum tła i wyższą stabilność, nanocząstki $NaYF_4$ stały się przedmiotem badań nad nową grupą znaczników luminescencyjnych zdolnych do zastąpienia klasycznych znaczników takich jak związki organiczne czy białka fluorescencyjne.

Istnieją trzy główne metody syntezy nanocząstek $NaYF_4$. Metoda Ostwald-ripening, synteza hydrotermalna oraz najbardziej znana metoda dekompozycji termicznej - termolizy.

Metoda dekompozycji termicznej pozostawia na powierzchni nanokryształu ligandy kwasu oleinowego. Właściwości hydrofobowe nanocząstek $NaYF_4$ opłaszczonych tymi ligandami znacząco ograniczają zastosowanie biologiczne, z tego względu konieczne jest przeprowadzenie modyfikacji powierzchni nanokrystalitów, która pozwala uzyskać właściwości hydrofilowe. Te modyfikacje można przedstawić w następujących kategoriach: wymiana ligandów, przyciąganie ligandów, utlenianie ligandów, usuwanie ligandów, powlekanie powłoką polimerową, powlekanie metodą layer-by-layer, metoda oddziaływań host-guest oraz powlekanie nanocząstki warstwą powłoki krzemionkowej.

Nanocząstki ze zmodyfikowaną powierzchnią mogą być wykorzystywane w szerokiej gamie badań biologicznych, które można podzielić na kategorie takie jak: obrazowanie, detekcja związków i zjawisk, śledzenie dynamiki związków i procesów biologicznych, transport oraz dostarczanie leków lub innych cząsteczek chemicznych, terapia fotodynamiczna a także optogenetyka.

Podczas gdy wzbudzanie promieniowaniem z zakresu nadfioletowego i widzialnego ogranicza wysokie pochłanianie fotonów z tych zakresów, spektrum podczerwieni zapewnia kilka potencjalnie efektywnych tak zwanych okien optycznych w ramach których do około 90%

światła jest w stanie przeniknąć tkanki na głębokość 2 centymetrów i więcej. Perspektywa przenikania do tak głębokich warstw pozycjonuje wykorzystanie znaczników UC jako ważną alternatywę w obserwacji struktur wielokomórkowych, takich jak tkanki czy całe organizmy.

Cytotoksyczność i inne szkodliwe efekty uboczne nanocząstek $NaYF_4$ to pole debat i wielu prac badawczych. Obecnie ogranicza to ich zastosowanie. Prace w dziedzinie tych materiałów wskazują, że nanocząstki $NaYF_4$ ulegają rozpadowi w płynach ustrojowych uwalniając jony lantanowe i fluorkowe do otoczenia. Ze względu na swoją wielkość, nanocząstki typu core- i core@shell mogą bez problemów przenikać przez błonę komórkową bez udziału aktywnych mechanizmów endocytozy i akumulować się w cytoplazmie. Nanocząstki o większych rozmiarach, wynikających z potencjalnych modyfikacji powierzchniowych, są internalizowane na drodze endocytozy zależnej od kaweolin lub klatryn. Konieczność ścisłego przebadania tych nanocząstek wynika z faktu, że endocytoza zależna od kaweolin i klatryn jest ściśle powiązana z wieloma szlakami apoptotycznymi. Dodatkowym argumentem przemawiającym za koniecznością prowadzenia szeroko zakrojonych badań w tej kwestii są doniesienia wykazujące wysoki poziom akumulacji nanocząstek $NaYF_4$ w konkretnych narządach.

Podsumowując, materiały oparte o nanokryształy $NaYF_4$ wymagają w dalszym ciągu szeregu badań. Wymagają także pewnego stopnia indywidualnego podejścia dla różnych rodzajów materiałów różniących się między sobą składem chemicznym, rozmiarem nanocząstki, obecnością rożnych modyfikacji powierzchni, mogących przekładać się na diametralnie różną odpowiedź ze strony całego organizmu lub konkretnie układu odpornościowego.

W niniejszej rozprawie przedstawiono wyniki wstępnych badań nad zasadnością zastosowania nanocząstek core@shell typu β-$NaYF_4$: Er^{3+}, Yb^{3+} @ β-$NaYF_4$: Nd^{3+}, Yb^{3+}, o wielkości 55 nm i 96 nm, pokrytych warstwą porowatej krzemionki będącej platformą nośnikową dla potencjalnych środków terapeutycznych oraz wcześniej opisanych

wzmacniających luminescencję anten uczulających, takich jak barwnik IR-806 wykorzystany w przedstawianych tutaj badaniach.

Nanocząstki β-$NaYF_4$: 2% Er^{3+}, 20% Yb^{3+} @ β-$NaYF_4$: 30% Nd^{3+}, 20% Yb^{3+} o wielkości 28 nm, których syntezę przeprowadził zespół w Instytucie Niskich Temperatur i Badań Strukturalnych im. Włodzimierza Trzebiatowskiego PAN we Wrocławiu, zostały pokryte warstwą krzemionki poprzez zmodyfikowaną metodę Ströbera u podstaw której leży kondensacja krzemionki na drodze chemicznej degradacji prekursorowego związku TEOS w środowisku zasadowym.

Potencjalne właściwości ochronne powłoki krzemionkowej badano pod kątem trzech aspektów. Pierwszym był wpływ na ogólną stabilność chemiczną IR-806 w czasie. Porównano barwnik w roztworze i barwnik zaadsorbowany do krzemionki. W po dwóch tygodniach, 21% optycznie aktywnego IR-806 zostało w roztworze wodnym, podczas gdy 74% barwnika pozostało w krzemionce. Dodatkowe siedem miesięcy przechowywania w ciemni pokazuje, że 16% barwnika osadzonego na krzemionce było nadal aktywne, podczas gdy tylko około 1% pozostającego w formie roztworu. Analogiczne eksperymenty, badające degradację pod wpływem działania światła, przeprowadzono poprzez naświetlanie promieniami UV o długości 254 i 366 nm. Po 200 minutach naświetlania cała populacja cząsteczek IR-806 w wodzie uległa degradacji, podczas gdy około 27% molekuł barwnika pozostało niezdegradowane wewnątrz porowatej warstwy krzemionkowej. Ostatnim badanym aspektem degradacji była ocena skuteczności w zapobieganiu utleniania IR-806 przez nadtlenek wodoru jako przedstawiciela grupy reaktywnych form tlenu. Eksperymenty sugerują, że powłoka krzemionkowa nie chroni cząsteczek IR-806 przed działaniem H_2O_2, gdyż szybkość degradacji jest stosunkowo podobna pomiędzy barwnikiem zaadsorbowanym do krzemionki i barwnikiem w roztworze wodnym.
Do eksperymentów badających cytotoksyczność użyto komórek linii makrofagowo-podobnych THP-1, linii komórek nabłonkowo-podobnych MDA-MB-231 i nabłonkowo-podobnych

komórek linii A375 od pacjenta z przerzutowym czerniakiem. Zastosowano nanocząstki $NaYF_4$ pokryte krzemionką o różnej grubości jak też nanokryształy $NaYF_4$ z usuniętymi ligandami oleinowymi i bez otoczki krzemionkowej. W przypadku makrofagowej linii THP-1 mniejsze nanocząstki typu core zwiększały proliferację komórek. Wzrost proliferacji w przypadku nanocząstek typu core@shell także był obserwowany, nawet wyższy niż w przypadku NPs typu core. Dla nabłonkowo-podobnej linii MDA-MB-231 nie zaobserwowano właściwości stymulujących zarówno dla nanocząstek typu core, jak i core@shell. Stymulacja nanocząstkami $NaYF_4$ pokrytymi krzemionką pokazuje znaczną toksyczność tych nanocząstek. Żywotność hodowli THP-1 spadła do 16% grupy kontrolnej, natomiast przeżywalność linii MDA-MB-231 obniżyła się do 49%. Następnie, linie THP-1 i A375 zostały wybrane do eksperymentów mających na celu ocenić wpływ różnej wielkości powłoki krzemionkowej oraz potencjalną cytotoksyczność barwnika IR-806. W przypadku nanocząstek pokrytych krzemionką o średnicy 96 nm nie zaobserwowano istotnego efektu cytotoksycznego. Podobnie jak w przypadku wyników eksperymentów z liniami THP-1 i MDA-MB-231, nanocząstki pokryte krzemionką o średnicy 55 nm istotnie zmniejszały żywotność komórek, jednocześnie nie zaobserwowano żadnego dodatkowego efektu cytotoksycznego próbek nanocząstek z barwnikiem osadzonym w krzemionce. Barwnik IR-806 rozpuszczony w medium hodowlanym nie wpłynął na żywotność hodowli komórkowej. Analiza cytometryczna żywotności komórek pokrywa się z wynikami cytotoksyczności, jednocześnie wskazując na indukcję szlaków apoptozy w hodowlach komórkowych prowadzących do znacznej śmierci populacji komórek po upływnie 48 godzin od rozpoczęcia stymulacji.

Uzyskane wyniki, wraz z danymi literaturowymi, sugerują istnienie przedziału wielkości nanocząstek w zakresie którego są one wysoce cytotoksyczne dla linii komórkowych.

ABSTRACT

Qualitative (microscopy) or quantitative (spectroscopy) optical methods are one of the most prominent techniques in biology. In recent years rare-earth element doped upconversion nanoparticles have become a new subject of research in an ever-growing field seeking new and efficient methods of imaging and detection.

The upconversion process was discovered in the 1960s and by the 2000s, the first lanthanide-doped $NaYF_4$-based micro- and nanoparticles, with enhanced luminescent properties, were synthesized. These upconverting materials absorb two or more low-energy photons, typically from the infrared spectrum, and throughout 4f-4f transitions on the lanthanide ions they emit one higher energy photon, generally in the visible or ultraviolet spectrum.

Further enhancement of luminescence can be done by engineering an active shell capable of absorbing additional energy and transferring it into the active luminescent core.

Upconverting $NaYF_4$ nanoparticles suffer from a low quantum yield efficiency. Excitation at this spectrum generates considerable heat, which significantly rises the temperature of the system, to the point of being harmful to biological structures. This problem could be possibly mitigated by sensitizing antennas. An antenna would non-radiatively transfer the harvested energy to upconverting nanoparticle increasing the luminescence intensity. NIR-absorbing organic dyes (like IR-806) or quantum dots show promise as viable candidates for that role.

These lanthanide doped $NaYF_4$ nanoparticles have become a focus of study for new types of luminescent labels, which offer enhanced properties like excitation at deeper sections of the tissue, lower background noise, and higher photostability.

There are three main $NaYF_4$ upconversion nanoparticle synthesis approaches. These methods are the Ostwald-ripening method, hydrothermal synthesis, and the most prominent thermal decomposition, also known as thermolysis.

The thermal decomposition synthesis leaves oleic ligands on the surface of the nanocrystal which severely restricts biological applications. Hydrophilic properties can be gained by modifying the surface of the nanoparticle. These modifications can be presented in the following categories such as ligand exchange, ligand attraction, ligand oxidation, ligand removal, polymeric shell coating, Layer-by-layer assembly, Host-Guest self-assembly, and sialinization, which coats nanoparticles with a silica shell layer.

Surface-modified nanoparticles can be utilized in a broad gamut of biological research, which can be classified into categories like bioimaging, biosensing, tracking, drug and molecule delivery, photodynamic therapy, and optogenetics.

While UV and Vis excitations are restricted, the infrared spectrum provides few optical windows for efficient excitation within which around 50 to 90% of a signal can penetrate up to the depth of 2 centimetres or more for specific tissues. Deeper penetration into the layers of tissue could make utilization of upconverting labels as a valid strategy in observations of multi-cellular structures like tissues or whole organisms.

The uncertainty of cytotoxic and other potentially harmful side-effects of upconversion nanoparticles limits the use of lanthanide doped UCNPs. Reports show that bare $NaYF_4$ nanoparticles can degrade in bodily fluids. According to the current knowledge on the subject, due to the size, core- and core@shell-type nanoparticles can penetrate the cell membrane without the involvement of any active mechanisms of endocytosis. Nanoparticles of a more substantial size and with surface modifications are internalized by the cell through Caveolin- or Clathrin-mediated endocytosis. The necessity for thorough investigation stems from Clathrin- and Caveolin-mediated endocytosis being tightly related to the apoptotic pathways.

The argument for extensive research into the subject of cytotoxicity is additionally strengthened by *in vivo* studies suggesting high rates of accumulation in certain organs for specific kinds of $NaYF_4$ nanoparticles.

In conclusion, $NaYF_4$ upconverting materials require more investigation and some degree of an individual approach to thoroughly investigate their viability. The subject of composition, size, surface modification, and response from the cellular or immune systems necessitates this individualized approach for each kind of lanthanide-doped $NaYF_4$ upconversion nanoparticle.

This thesis presents the results of a preliminary investigation into the validity of the application of the 55 nm and 100 nm mesoporous silica-coated β-$NaYF_4$: Er^{3+}, Yb^{3+} @ β-$NaYF_4$: Nd^{3+}, Yb^{3+} nanoparticles as carriers of therapeutic agents and emission-enhancing organic molecules such as IR-806 used as an example of a carried molecule.

Synthesis of 28 nm β-$NaYF_4$: 2% Er^{3+}, 20% Yb^{3+} @ β-$NaYF_4$: 30% Nd^{3+}, 20% Yb^{3+} nanoparticles, was performed by a team in the Włodzimierz Trzebiatowski's Institute of Low Temperatures and Structure Research, Polish Academy of Sciences in Wrocław. These nanoparticles were used as a template for a synthesis of the silica shell *via* the modified Ströber method of silica condensation by the means of degradation of TEOS compound in a basic environment.

The protective properties of silica shells were studied in three different aspects. The impact of IR-806 on the overall chemical stability shows increased stability of the dye over two weeks from 21% for an aqueous solution to around 74% for silica-embedded IR-806. After seven months of storing this compound, it was shown that 16% of silica-embedded dye was still active while only around 1% remained in the soluble form. Analogous experiments concerned the study of light degradation by exposing to UV light of 254 and 366 nm. After 200 minutes of exposition, all water-dissolved molecules of IR-806 degraded while around 27% of the dye was left within the mesoporous silica shell. The last studied aspect of degradation was the effectiveness of preventing reactive oxygen species in the form of hydrogen peroxide from oxidizing molecules and rendering them spectrally inactive. Silica shell did not protect IR-806

molecules from the reach of H_2O2 and the rates of degradation are relatively similar between silica-embedded and aqueous dyes.

The macrophage-like THP-1, epithelial-like MDA-MB-231 cell line and epithelial-like A375 cell line from a patient with malignant melanoma were used for cytotoxic experiments with MTT assay and flow cytometry. Different silica-coated, as well as uncoated $NaYF_4$ nanoparticles, were used. For the macrophage-like THP-1 cell line, smaller core-type nanoparticles increased proliferation. The increase in proliferation of the core@shell-type UCNPs was even higher. For the epithelial-like MDA-MB-231 cell line, stimulatory properties for both core- and core@shell-type nanoparticles were not observed. Stimulation with silica-coated upconversion nanoparticles shows significant cell toxicity of these nanoparticles. The viability of the THP-1 cells decreased to 16%, while MDA-MB-231 dropped to 49%. THP-1 and A375 lines were selected for the experiments involving various sizes of silica shell and the potential cytotoxicity of IR-806 dye. Nanoparticles of the same composition, with two different sizes of silica shells, were chosen. For the thicker 96 nm silica-coated NPs, there was no major cytotoxic effect observed. Similarly, to the results of THP-1 and MDA-MB-231 experiments, the 55 nm silica-coated nanoparticles reduced the viability of the cells, but there was no additional cytotoxic effect from the silica-embedded dye. The media solution of the dye didn't impact the viability of the cell culture and any significant cytotoxicity of IR-806 was observed. Cytometric analysis of cell viability confirms MTT assay results and indicates induction of apoptotic processes in cells which leads to significant death of cells during 48 hours stimulation period.

These results combined with literature data, indicate existence of a spectrum range of diameter in which $NaYF_4$ nanoparticles are highly cytotoxic to the cells.

INTRODUCTION

Optical methods, qualitative (microscopy) or quantitative (spectroscopy), are the most prominent techniques available to researchers in the field of biology. In recent years rare earth element doped upconversion nanoparticles (UCNPs) have become a new tool for this ever-growing field which is constantly seeking new and efficient methods of study and observation.

The upconversion (UC) process was discovered in the 1960s and as a result of decades-long attempts to create an efficient platform to utilize the UC phenomenon. By the 2000s, the first lanthanide-doped $NaYF_4$-based micro- and nanoparticles were synthesized.

Exhibiting anti-Stokes characteristics, these upconverting materials absorb two or more low-energy photons, typically from the infrared spectrum, and throughout 4f-4f or 4f-5d transitions they emit one higher energy photon, generally in the visible or ultraviolet spectrum.

These UCNPs have become a focus of study for a new types of luminescent labels. Upconverting nanoparticle offers enhanced properties like excitation at deeper sections of the tissue, lower background noise, and higher photostability. Presently lanthanide-doped UCNPs are the subject of extensive biocompatibility studies by various surface modification strategies.

All these properties suggest that upconversion nanoparticles could provide a significant edge over traditional fluorescent markers like low molecular dyes, fluorescent proteins, or quantum dots.

■□□□ Upconversion Process and History of $NaYF_4$ Nanoparticles

While the upconversion (UC) process itself was known before, it was not until the mid-1960s that prof. Auzel suggested a potential mechanism of energy transfers within two lanthanide ions.[1,2] 40 years later, the first physical basics for energy transfer in upconversion were proposed. By the 2000s various models for multiple-photon upconversion were discussed.[3]

The upconversion process in lanthanide-doped crystals is achieved with an intertwined system of sensitizing and emitting ions in a rigid crystalline host lattice.[4] Sensitizer (e.g. Yb^{3+}, Nd^{3+}) ions absorb the photons of light in the near-infrared spectrum (e.g. 808 and 980 nm),[5] and in the excited state transfer the energy to the emitting ions. That harvested and transferred energy allows the emitter (e.g. Er^{3+}) ions to achieve an excited state higher than the usual state of excitation after the absorption of infrared photons.[6] Subsequently, emitter ions release higher-energy photons that correspond with the visible (VIS) or ultraviolet (UV) spectrum.

Anti-Stokes emission was introduced to the studies of colloidal solutions circa 2003 with the first phosphate-based lutetium ($LuPO_4$) and ytterbium ($YbPO_4$) nanosized crystals doped with different lanthanide ions, capable of emitting a broad spectrum (blue, green and red) of visible light after excitation with near infra-red wavelengths.[7]

Phosphate-matrix (PO_4^{3-}) was soon followed by sodium yttrium-fluoride ($NaYF_4$) lattices (Figure 1).[8] $NaYF_4$ provides much higher quantum efficiency of the upconversion process allowing more energy to be transferred between ions.[9] Among two of the crystal structures, cubic and hexagonal, the latter proved to have greater enhancement of energy transfer effect and thus higher emission intensity.[10]

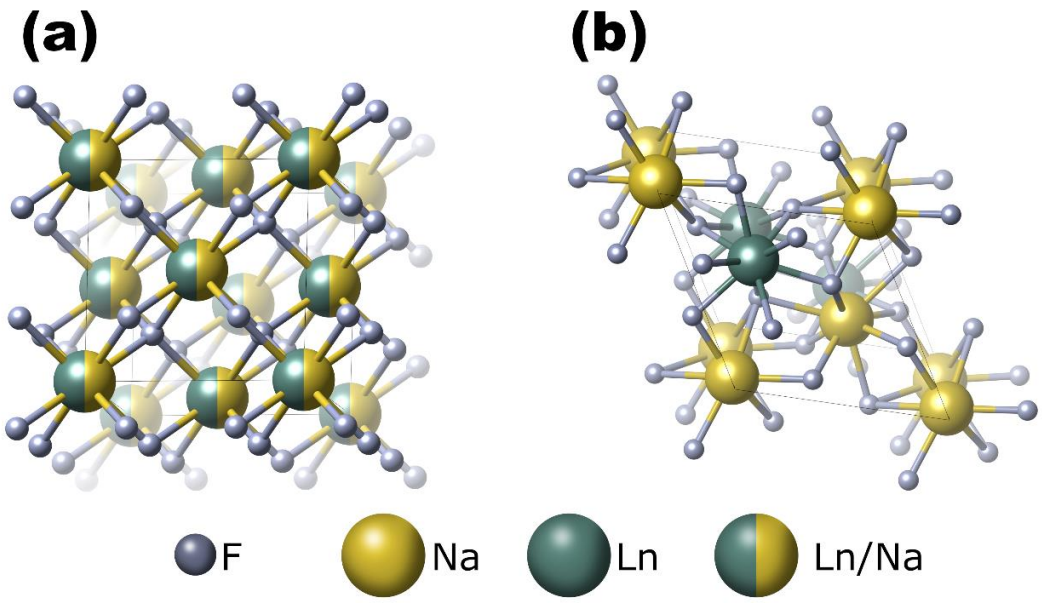

Figure 1. Two structures of $NaYF_4$ lattice | Depending on the type of synthesis, $NaYF_4$ crystal can be synthesized in a) cubic and b) hexagonal systems. Reprinted with permission of the author of the publication.[11]

The initial restriction of having to work only with dry powder of $NaYF_4$ nanoparticles was overcome in 2006 when Mai et al. and Boyer et al. published results of the first colloidal cubic and hexagonal $NaYF_4$ UCNPs obtained *via* the method of thermal decomposition. Suspension of nanoparticles capped with oleic acid ligands demonstrated high stability in non-polar organic solvents such as chloroform and hexane.[12,13]

In the early 2000s, alongside the first phosphate-matrix nanocrystals, the development of core/shell architecture started. It was a response to the high surface area in relationship to the size, which is a disadvantage for these nanomaterials. The nanoparticle typically will have multiple defects in the crystal structure on its surface. This limits energy transfers needed for efficient upconversion emission.[14] The core/shell architecture was designed to overcome that problem. Coating the luminescent core with an additional layer of material removes the negative effect on emission intensity.[15]

Core/shell design (figure 2) was adopted for the development of nanoparticles based on the $NaYF_4$ matrix. Some studies report that compared to the core-only structure, the UCNPs with

undoped with Ln^{3+} ions inert sodium yttrium-fluoride shell have shown a 30-fold increase of emission intensity.[16]

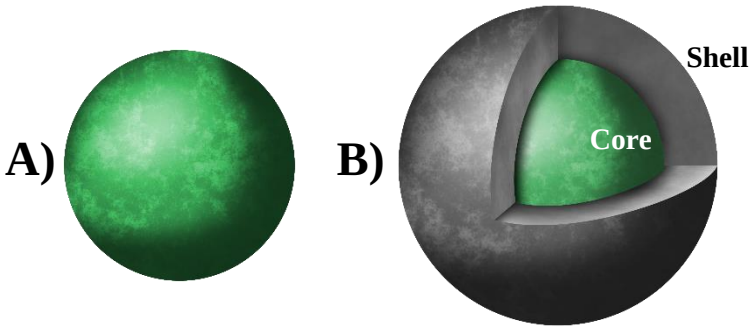

Figure 2. Architectures of $NaYF_4$ upconverting nanoparticles | Two architectures of $NaYF_4$ nanoparticles. A) Core-type nanoparticle with a single hexagonal lattice with all ions uniformly spread throughout. B) Core@shell-type of nanoparticle with two hexagonal lattices doped with different lanthanide ions.

Further enhancement of UCNPs capabilities can be accomplished through doping the shell layer with sensitizing lanthanide ions like Yb^{3+}, thus engineering an active shell capable of absorbing additional excitation energy and transferring it into the active core (figure 3). An active shell can further increase upconversion emission up to 10 times in comparison with an inert shell.[17] Additional strategies of doping various segments with different activating ions can be deployed for achieving spectral characteristics as well as strengthening emission intensity to a greater extent.[18]

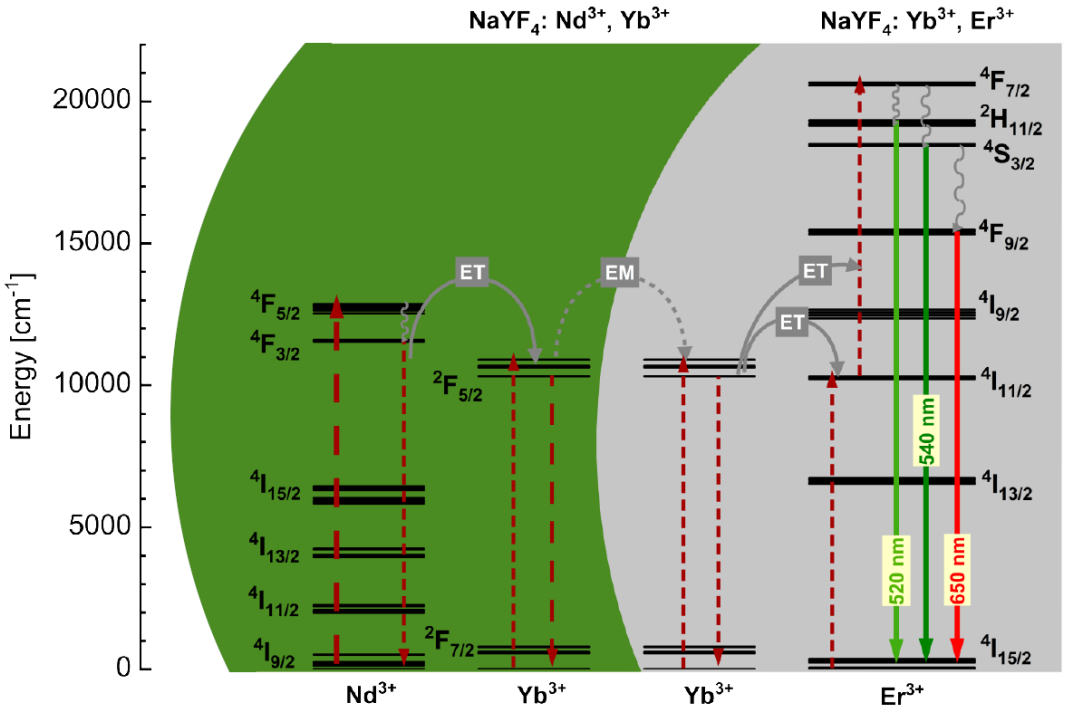

Figure 3. Energy transfer between the active shell and active core | Energy transfer between an active shell doped with neodymium and ytterbium ions and an active core doped with ytterbium and erbium ions. Nd^{3+} ions with a NIR absorption peak at 808 nm and Yb^{3+} ions at 980 nm, transfer the energy to the active core throughout Yb^{3+} ions to the erbium ions. Excitement of Er^{3+} ions causes emission at various wavelengths in the spectrum of visible light. Courtesy of dr Katarzyna Prorok.

■□□□ Surface Modification of $NaYF_4$ Nanoparticles

There are three main $NaYF_4$ upconversion nanoparticle synthesis approaches. These methods are the Ostwald-ripening method,[19] hydrothermal synthesis, [20] and the most prominent thermolysis (thermal decomposition).[9]

The thermal decomposition synthesis leaves oleic ligands on the surface of the nanocrystal.[21] While it provides excellent solubility in organic solvents,[22] it severely restricts biological applications. Hydrophilic properties can be gained by a range of surface modification strategies and there are different ways to classify these modifications.[4,23–25] These modifications can be

presented in the following categories: **I) Ligand exchange**, with replacing hydrophobic capping with other ligands (e.g. folic acid, dendrimers);[26,27] **II) Ligand attraction**, by utilizing ligand hydrophobic interaction with another amphiphilic molecule;[28] **III) Ligand oxidation**, throughout the chemical reaction and introducing chemically active moiety at the hydrophobic end of the ligand;[20] **IV) Ligand removal**, by stripping hydrophobic ligands from the surface of UCNPs;[29] **V) Polymeric shell coating**, with various polymers (e.g. PVP, PEG, glucose dehydrate);[30–34] **VI) Layer-by-layer assembly**, of introducing consecutive layers of oppositely charged molecules or particles;[35–37] **VII) Host-Guest self-assembly**, utilizing the spontaneous interactions between UCNPs ligands with a hydrophobic pocket of specific cyclic molecules;[38] **VIII) Sialinization**, which coats nanoparticles with a layer of silica shell;[39–42] and other modifications that are less commonly used in the study of UCNPs, like ZnO-antimicrobial coating of $NaYF_4$ that generates reactive oxygen species (ROS) against *Staphylococcus aureus* bacteria.[43]

Ligand Exchange | Replacing hydrophobic ligands (figure 4) can be employed for procuring water-soluble upconverting nanoparticles. Replacing the oleic-capping of $NaYF_4$ with a polyvinylpyrrolidone (PVP) layer can be accomplished in a DCM/DMF mixture.[44] Poly(amidoamine) (PAMAM) dendrimers are effective in displacing ligands on the $NaGdF_4$ nanocrystal surface.[45] $NaYF_4$ nanoparticle oleic-coating can be also replaced with (polyacrylic acid) PAA[46] which is also efficient in achieving the same result for $NaGdF_4$ nanocrystals.[47] Another polymer used for exchanging oleic ligands on $NaYF_4$ NPs is polyethylenimine (PEI).[48]

Replacing hydrophobic ligands can also be performed *via* the nitrosonium tetrafluoroborate ($NOBF_4$) method, with inserting intermediate BF_4^- ligands, which are

characterized by low binding affinity to the surface of nanoparticles thus allowing further replacement with other ligands.[49,50]

Another approach to ligand exchange uses solutions akin to ligand removal methods. It involves an intermediate step of removing the original ligand in an acidic environment, allowing the introduction of a new ligand to the surface.[29,51] These modifications provide enhanced colloidal stability in aqueous solutions for long-term storage.[52] Ligand exchange techniques can be used to introduce chemical compounds such as glycine, cysteine, citric acid, biotin, AMPA, APTES, DHCA, MAEP, AEP, PAA, PVP or PEI.[53,54]

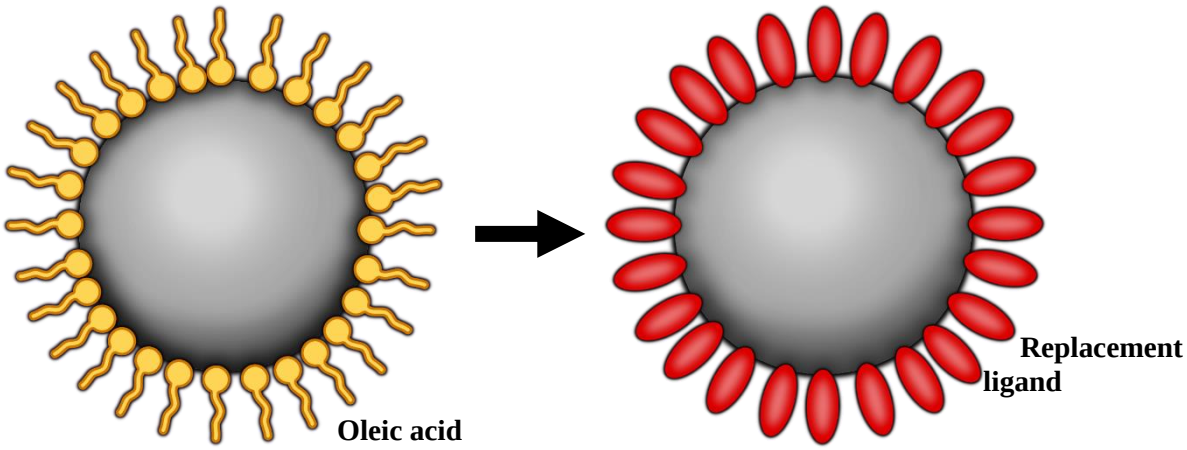

Figure 4. Ligand Exchange | Schematic representation of the process of replacing oleic acid ligands on the surface of $NaYF_4$ nanoparticle.

Ligand Attraction | Exposed to the outside environment, hydrophobic chains of oleic ligands, can be utilized for another modification strategy – ligand attraction (figure 5).[55] Nanoparticles capped with oleic ligands can be coated with another amphiphilic molecule to produce a bilayer on the surface of NPs. Through van der Waals forces, both layers of molecules interact with each other to generate stable and water-soluble structures. Ligand attraction can utilize oleic acid molecules, modified with PAA-PEG to provide higher hydrophilic properties than the carboxylic moiety of oleic acid.[56] Oleic-capped $NaYF_4$ nanocrystals can be coated with

Pluronic F127 amphiphile.[57] Another example of attraction is the use of poly(maleic anhydride-alt-1-octadecene) (PMAO) cross-linked with bis (hexamethylene)triamine (BHMT).[28] Yi et al. presented water-soluble nanoparticles synthesized by incubation of oleic-capped UCNPs with modified PAA.[58] The same type of UCNPs can also attract PEG-modified molecules.[55] Attracting phospholipids to oleic ligands are studied as a biocompatible mimicry of cell membrane[59] and other studies have shown an effective utilization of more than one type of phospholipid.[60]

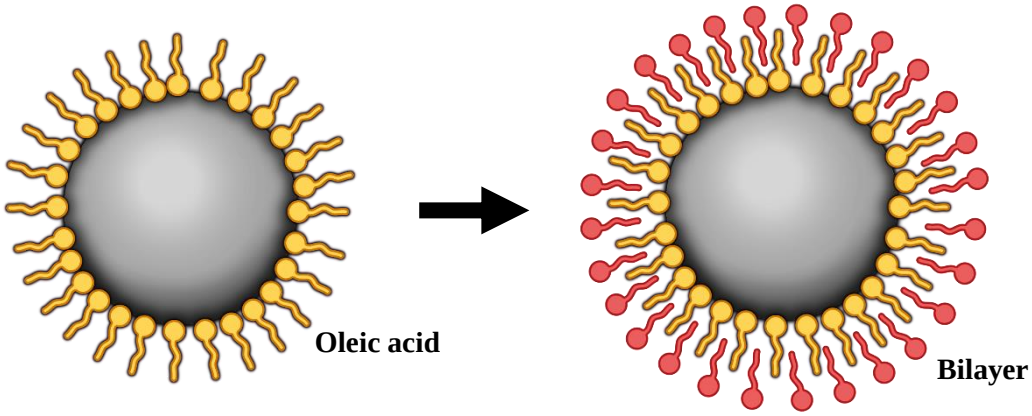

Figure 5. Ligand Attraction | Schematic representation of the process of attracting ligands capable of interacting with oleic acid ligands on the surface of $NaYF_4$ nanoparticle.

Ligand Oxidation | Oleic ligands on the surface of UCNPs can be targeted for chemical modification. Oxidation performed with a Lemieux-von Rudloff reagent generates carboxylic moieties at the end of a hydrophobic chain of the ligand (figure 6).[20] Ozone steaming, combined with acetic acid and H_2O_2 or CH_3SCH_3 can respectively introduce carboxyl -COOH and aldehyde -CHO groups to the chains of the ligand.[61] The double bond between two atoms of carbon in the middle of the ligand's hydrophobic chain can be a target of epoxidation reaction with 3-chloroperoxybenzoic acid as an oxidizer and further functionalized with various monomers such as polyethylene glycol monomethyl ether.[62]

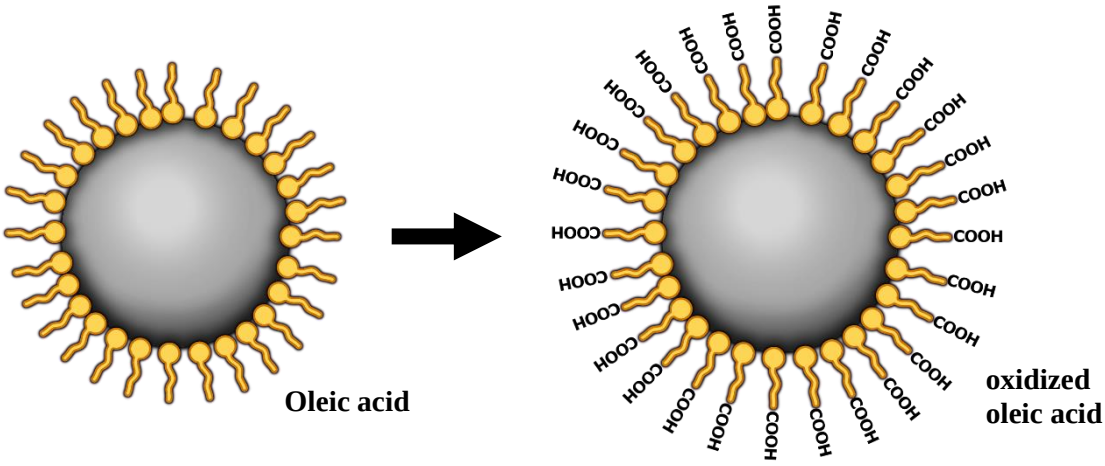

Figure 6. Ligand Oxidation | Schematic representation of the process of oxidation of oleic acid ligands on the surface of $NaYF_4$ nanoparticle.

Ligand removal | If required, ligands on the surface of the nanocrystal can be simply removed, leaving water suspensible $NaYF_4$ nanocrystal (figure 7). Ligand removal can be performed by mixing hydrophobic nanoparticles with a concentrated water solution of hydrochloric acid[51,63], formic acid[29], or $SOCl_2$/DMF mixture.[64] Although this method seems to be optimal since it is the most simple, the matter of instability of naked $NaYF_4$ nanoparticles in specific conditions limits the utilization of this method.[29]

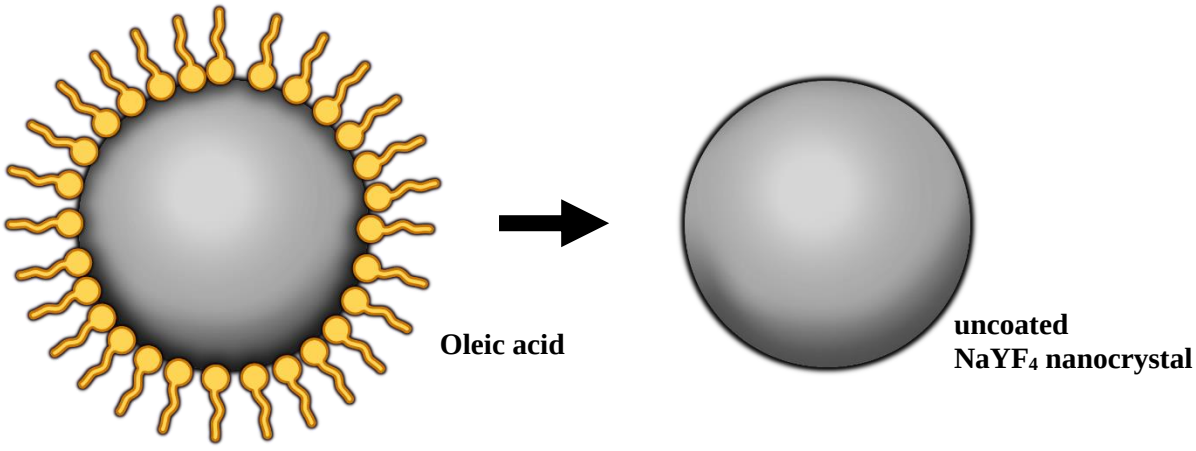

Figure 7. Ligand Removal | Schematic representation of the process of removing oleic acid ligands from the surface of $NaYF_4$ nanoparticle.

Polymeric shell coating | Coating nanoparticles with polymer materials is one of the most recurrent means of surface modification (figure 8).[65] UCNPs can be layered with a neutral l(e.g. polyvinylpyrrolidone, PVP), positive (e.g. polyethylenimine, PEI), or negative (e.g. polyacrylic acid, PAA) charged polymers that will impact its water solubility and biocompatibility.[66] Various polymers can be applied for this type of surface modification. These can be polyethylene glycol (PEG), PAA,[67] PEI,[66] PVP,[68] P(MEO$_2$MA-co-SEMA) copolymers,[69] Pluronic F127,[70] Polyacrolein (PA).[71]

For the PVP modification, the pyrrolidone groups of the polymer coordinate with Ln^{3+} ions on the surface of the nanoparticle, stabilizing the structure,[72] and for PAA-coated nanoparticles, the hydrophobic octyl and isopropyl groups of PAA interact with exposed oleic ligand chain achieving the same result.[58]

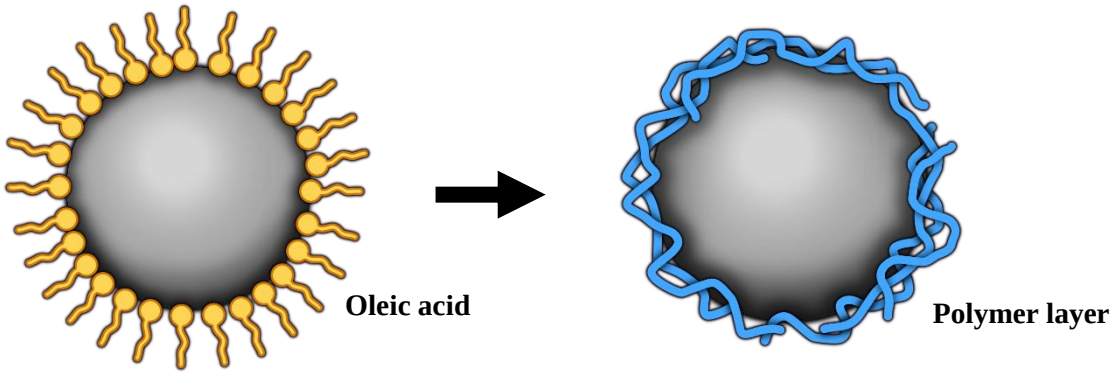

Figure 8. Polymeric shell coating | Schematic representation of the process of replacing oleic acid ligand on the surface of $NaYF_4$ nanoparticle with a layer of polymer.

Layer-by-Layer assembly | The layer-by-layer (Lbl) assembly method (figure 9) utilizes electrostatic interactions between polymer materials. This approach involves coating nanoparticles with consecutive layers of oppositely charged polymers. Lbl-coating can be

engineered from negatively charged polymers like PMAO, dextran sulphate sodium salt (DSS), poly(D,L-lactide) (PLa), poly(lactide-co-glycolide) (PLG), poly(sodium 4-styrenesulfonate) (PSS) or poly(acrylic acid) (PAA); and with positively charged layers of poly(ethyleneimine) (PEI) or poly(allylamine hydrochloride) (PAH) in between.[22,73]

Alternative approaches to Lbl assembly can utilize electrostatic adsorption properties of additional but smaller nanoparticles made from materials like colloidal gold. $NaYF_4$ nanoparticles coated in a silica layer can be further modified by adsorbing subsequent layers of small or big gold nanoparticles.[74]

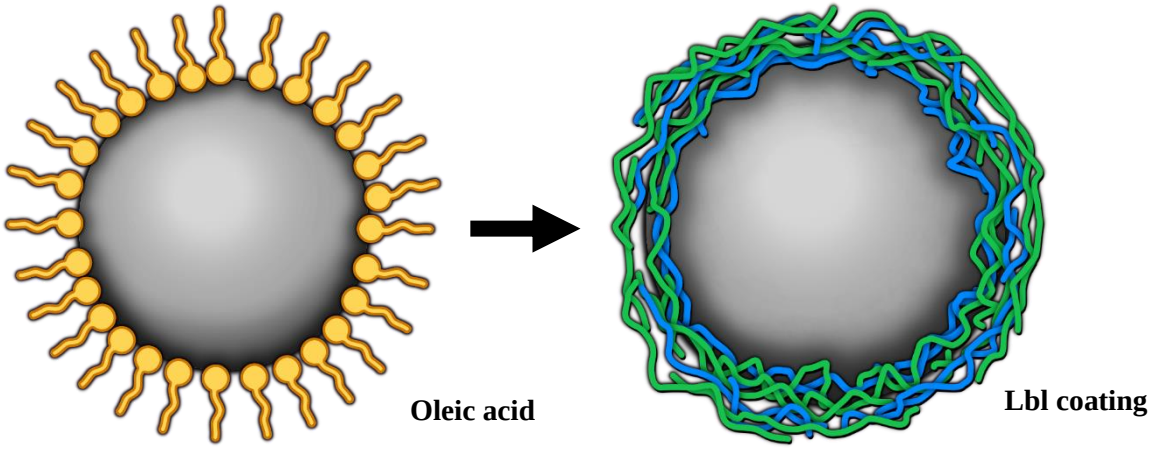

Figure 9. Layer-by-layer assembly | Schematic representation of the process of replacing oleic acid ligand on the surface of $NaYF_4$ nanoparticle with Lbl coating.

Host-Guest self-assembly | The method was derived from highly specific biological interactions occurring in nature.[75] Bound to the surface of the nanoparticle, molecules of the so-called "host" interact and tether the "guest" molecules without the need for any further chemical reactions (figure 10).[75,76]

Two macrocyclic types of molecules, cyclodextrins, and pillararenes are commonly used for host-guest systems. One side of the cyclic structure binds the surface oleic ligand and creates the host component, the host-coated UCNP. The other side of the host molecule binds

various guest elements.[77] Throughout its hydrophobic and lipophilic cavity, cyclodextrin (CD), binds various molecules with long hydrophobic chains or aromatic rings.[78] Pillar[5]arene modification is another form of host-guest system and functions on the same principle as cyclodextrins.[79,80]

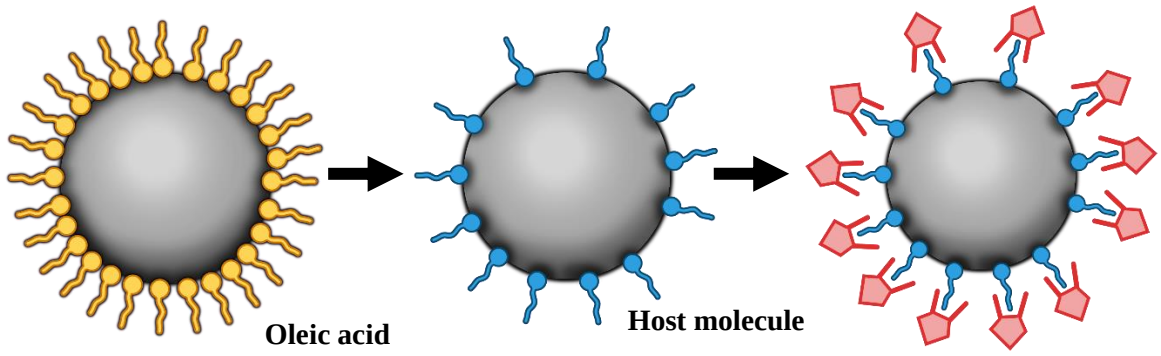

Figure 10. Host-Guest self-assembly | Schematic representation of the process of replacing oleic acid ligand on the surface of $NaYF_4$ nanoparticle with Host-Guest system.

Sialinization | Another surface modification involves the coating the nanoparticle in an layer of amorphous silica (figure 11). Originally designed as an efficient method for the synthesis of silica particles, from micro- to nanosize, the Ströber method[81] has become a starting point for coating nanoparticles in silica. In years following the development of the original methodology, further synthesis strategies like reverse microemulsion method[82] and synthesis on polymer beads[83] were developed.

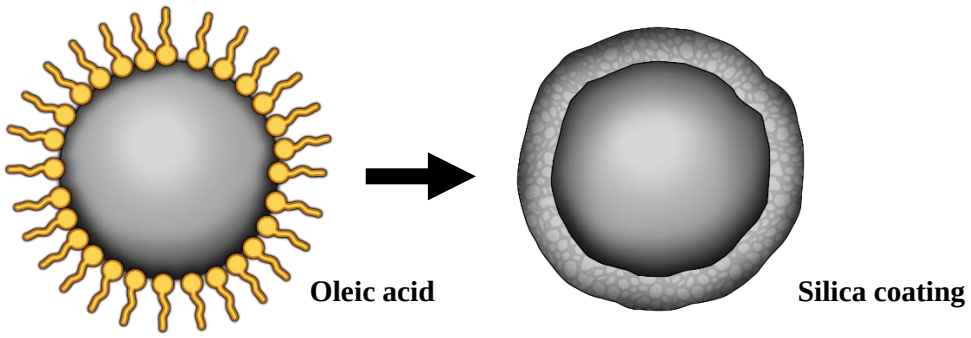

Figure 11. Silica coating | Schematic representation of the process of replacing oleic acid ligand on the surface of $NaYF_4$ nanoparticle with a layer of silica.

Depending on the synthesis approach, two forms of silica layer can be produced, dense ($dSiO_2$) and mesoporous silica ($mSiO_2$).[84] Dense silica provides a rigid protective coating for the nanoparticle, while mesoporous silica has the characteristic porous structure, which is capable of adsorbing various compounds for enhancing the luminescent properties of the nanoparticle or having potential applications such as drug carrier for photodynamic therapy.[85]

The mesoporous structure is obtained in the presence of a surfactant compound that generates a template for pores at the surface of the nanoparticle (figure 12).[86–88] Silica growth can be manipulated to obtain the desired thickness of the shell. Very thin 5 nm,[89] 10 nm,[90] 20 nm[91] layers can be manufactured. Different factors involved in synthesis (e.g. temperature, solvents, surfactants, catalysts) can control silica growth.[92] Pore volume can reach around 0.9 $cm^3 \times g^{-1}$ and surface area almost 1400 $m^2 \times g^{-1}$.[86]

Silica coating offers several beneficial qualities. It has high thermal stability of up to 750°C.[93] It offers good aqueous stability of colloidal silica.[94] It is transparent to light, which makes it a good candidate for coating luminescent materials.[95] There are caveats such as decreasing the quantum yield of luminescence due to strong absorption from functional groups like $-NH_2$[96] or increasing distance between the luminescent core and outside elements, which could decrease the efficiency of potential FRET-based solutions. Silica is regarded as a highly biocompatible material. Previous reports have cited silica being absent of any cytotoxic properties (e.g. in case of dissolution in physiological fluids, it produces nontoxic soluble silicic acid species)[97], however, additional research into the subject is required.

The coating surface can be designed with further modifications in mind. The standard precursor for the synthesis, tetraethyl orthosilicate (TEOS), can be replaced with a derivative. These derivatives introduce specific moieties at the surface and are subsequently targeted in further chemical modifications. (3-Aminopropyl) triethoxysilane (APTES) is a commonly used

reagent for the synthesis of silica shell with amino groups on the surface.[98] Use of carboxyethylsilanetriol (CTES) introduces carboxylic groups.[99] Another derivative, (3-glycidyloxypropyl)trimethoxysilane (GPTMS) generates the coating with epoxy groups.[100]

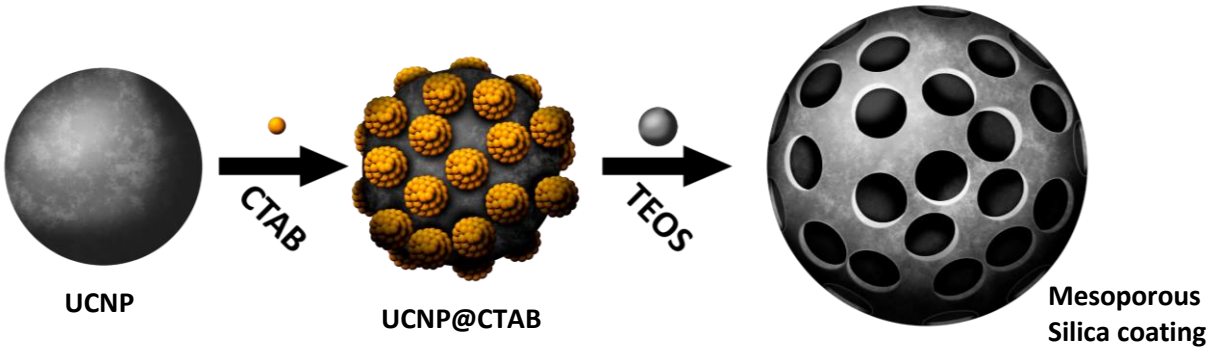

Fig 12. Illustration of coating the nanoparticle in mesoporous silica | A schematic representation of the process of coating the upconverting nanoparticle in a layer of porous silica. CTAB incubated with UCNPs forms a micelles on the surface of the nanocrystal which then prevents TEOS from forming silica layer in these spots, thus forming a porous structure of the shell.

■□□□ Application of Upconversion Nanoparticles

Surface-modified nanoparticles can be utilized in a broad gamut of biological research (figure 13), which can be classified into categories such as **I) Bioimaging** of cells and tissues,[30] small[101] or more complex[102] multicellular model organisms; **II) Biosensing** of biomolecules,[103] potentially harmful compounds,[104] metal ions,[105] or protein interactions;[106] **III) Tracking**, of molecule dynamics within cells or entire organism; **IV) Drug and molecule delivery**, that takes advantage of NIR radiation;[107,108] **V) Photodynamic therapy**, with cytotoxicity activated throughout energy transfer from UCNP into photolabile drug precursor or free radical and reactive oxygen species generating molecule;[109] and **VI) Optogenetics**, a newly emerging

technique of introducing light-induced genes to the control mechanism of studied biological processes.[110]

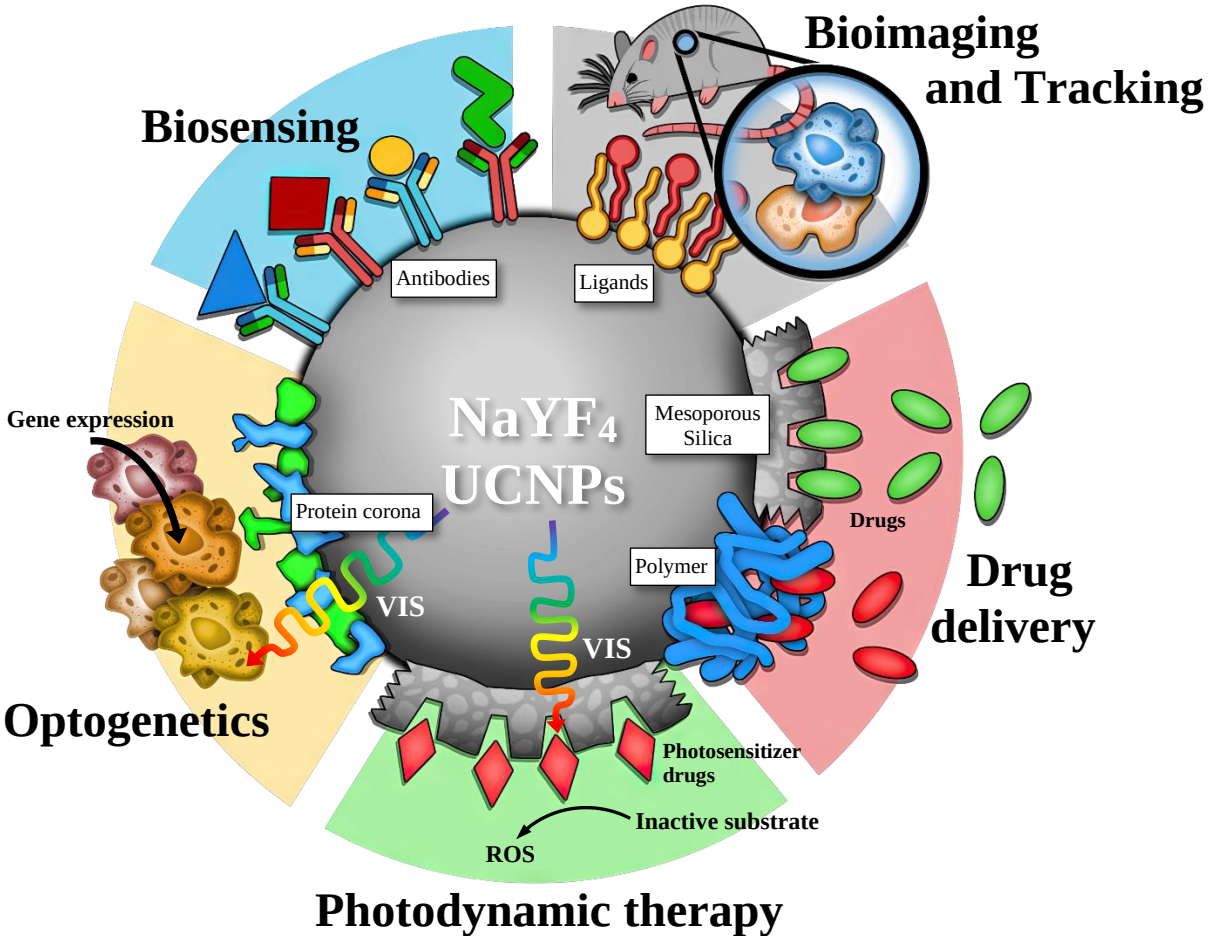

Figure 13. Various biological applications of $NaYF_4$ nanoparticles | A visual representation of the examples of lanthanide-doped upconversion nanoparticle biological application with different surface modifications.

Outside the field of biology, studies of the non-biological application of Ln-doped UCNPs involve anti-counterfeit safeguards[111], photovoltaic technologies[112], and engineering of optical fibres[113] or volumetric displays.[114]

Bioimaging | The evolutionary design of the human eye makes it an adequate tool for observation and analysis of the surrounding environment. It had paved the way for microscopy-based imaging to become one of the most popular analytical methods available in biology.

Bioimaging, with the use of the upconversion process, aims to replace the typical photolabile organic fluorophores with more stable dyes based on UC nanoparticles. Studies show potential application possibilities for almost all types of organisms, from single cell to multicellular organisms, as well as prokaryotic, eukaryotic, plant, or animal cells.

Single-cell imaging is one of the common utilization method for upconversion nanoparticles.[115–119] Staining eukaryotic cells is possible for various cancer lines like malenins,[120] hepatocellular carcinoma (HepG-2),[121] HeLa,[89] or human pancreatic cancer (Panc 1) cells,[102] among many others. Combined with high-resolution microscopy, bioimaging in mammalian cancer A549 cell lines allows tracking single upconversion nanoparticles.[122] Plant studies report successful intake of $NaYF_4$ nanoparticles into the root cells of *Arabidopsis thaliana*.[123]

Regarding single-cell imaging, prokaryotic cells can be labelled as well. Specific strains of *Escherichia coli* can be distinguished from other bacteria with the use of UCNPs.[124] Common food pathogens (e.g. *Staphylococcus aureus*, *Salmonella*, *Shigella fexneri*) could be detected to improve food safety.[125] Much smaller non-cellular infectious particles, like particular strains of avian influenza virus (AIV), can be detected *via* immunolabeling techniques of impure samples that renders commercial test less effective.[126]

Infrared radiation can penetrate deeper into tissue layers than what is possible for visible or ultraviolet light.[127] Therefore, moving the scope of imaging in the opposite direction is a valid strategy that sees the utilization of upconverting dyes in observations of multi-cellular

structures like tissues or whole organisms. Light scattering and absorption of living tissue, greatly decrease the penetration depth of most microscopic techniques based on UV and visible light imaging, even for advanced microscopic techniques such as multiphoton microscopy.[103,128–130] For example, a highly absorbing pigmentation of the skin generates a significant *in vivo* autofluorescence signal which decreases the signal-to-noise ratio and decreases the resolution of imaging.[131]

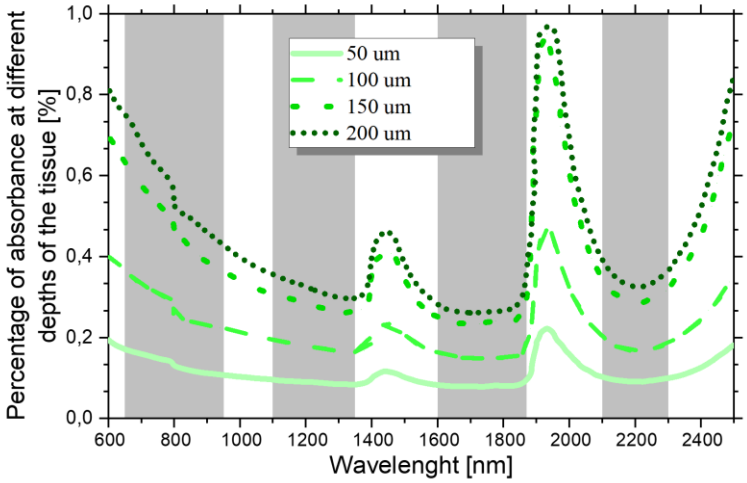

Figure 14. Optical windows in brain tissue of mouse and the absorbance at various penetration depths | Greyed-out areas are subsequent optical windows (650-950, 1100-1350, 1600-1870, and ~2200 nm). 50, 100, 150, and 200 µm represent the percentage of absorbance at respective depths of the mouse brain tissue. Based on Shi et al.[132]

While UV and Vis excitations are restricted, the infrared spectrum provides few optical windows for efficient excitation within which around 50 to 90% of a signal can penetrate up to 200 µm into the brain tissue (Fig 14).[132] Other studies report bioimaging to depths of 2 centimetres and more for other tissues.[133,134] At the moment, four optical windows for possible imaging are defined: the first window at around 650 – 950 nm, the second at 1100 – 1350 nm, the third at 1600 – 1870 nm, and the fourth centred around 2200 nm.[132,135] The first spectral

window between around 650 and 1000 nm is presently considered the most optimal for tissue penetration for luminescent materials available today.[136]

The application of UCNPs in tissue imaging was reported for biostructures such as human skin,[120] or mouse brain tissue cortical vasculature.[27] Highly absorbing blood tissue (hemolyzed blood) could use UCNPs to overcome that issue by providing an excitation signal from the outside of the blood absorption spectrum.[137] Pathologically changed tissues, such as tumors in mice can be observed with silica-coated UCNPs[138,139] and zwitterion-coated nanoparticles.[60]

Upconverting nanoparticles could also provide solutions for whole-organism imaging. It can be applied for relatively simple nematodes species of *Caenorhabditis elegans*[101] as well as imaging of more complicated organisms like mice.[102,140]

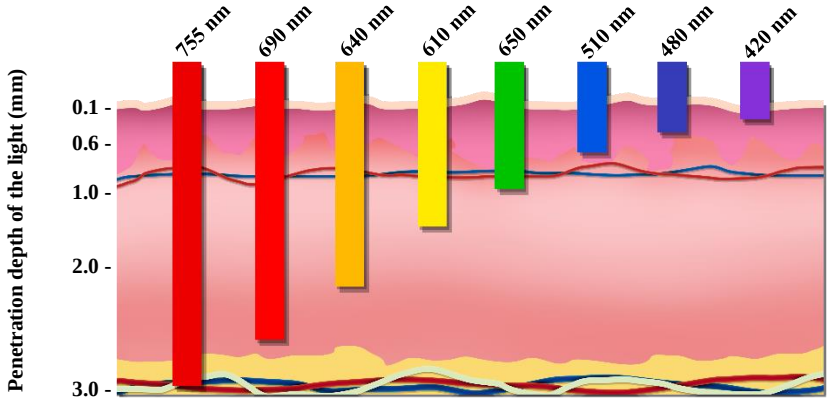

Figure 15. Penetration depth of the light | A visual illustration of the visible and near-infrared light penetration of the human skin tissue at different wavelengths. Figure based on Han et al.[127]

Another potential benefit of UCNPs-based labels is the characteristics of their spectra in comparison to other luminescent labels (figure 16). By doping the nanoparticles with different lanthanides, the spectra can be more easily distinguished. The overlap of peaks between different lanthanide ions is lesser than the spectral overlap between fluorescent proteins,

quantum dots or carbon dots. This could allow utilization of multi-UCNPs systems with different nanoparticles designed for a different role at the same site.[141]

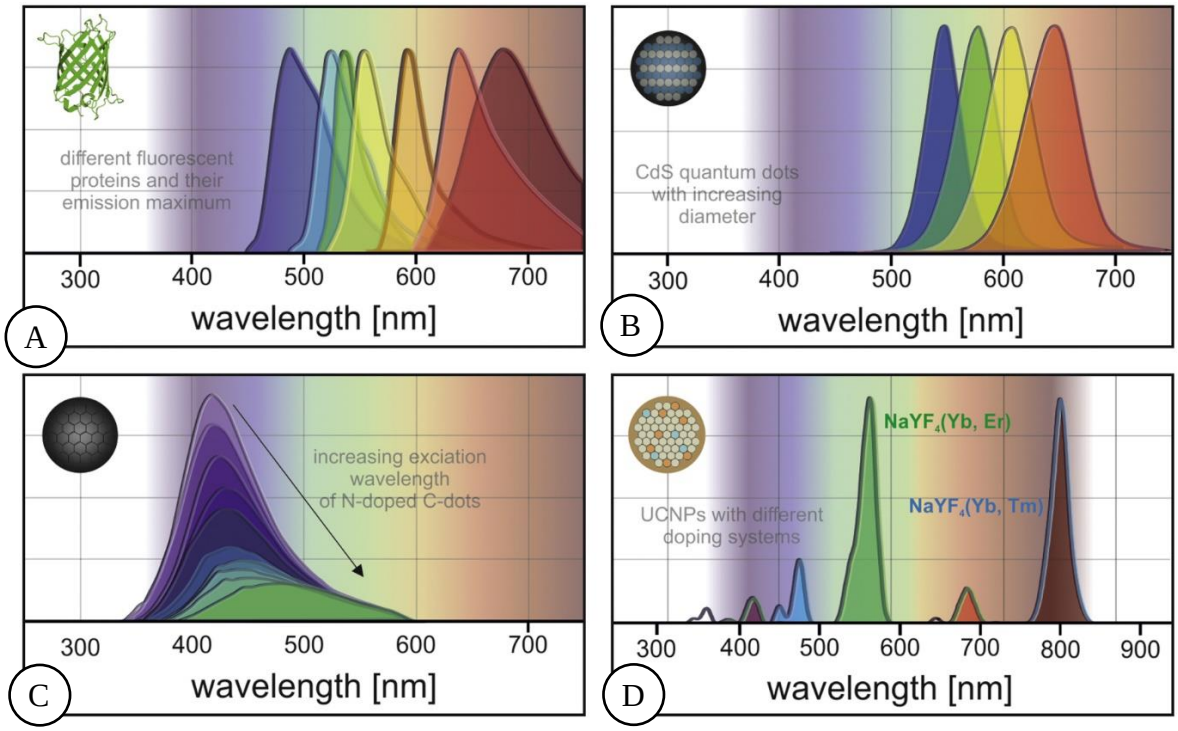

Figure 16. Overlap comparison between different luminescent materials. | A graphical comparison of the overlap of spectral peaks between different types of potential luminescent labels such as: A) fluorescent proteins, B) CdS quantum dots, C) Carbon dots and D) lanthanide-doped $NaYF_4$ nanoparticles. Reprinted with permission from Methods Appl. Fluoresc. 7 022002. Copyright© 2019 IOP Publishing Ltd.[141]

Optical imaging can be combined with other methods like x-ray radiography,[142] computed tomography,[143] magnetic resonance[144] or photoacoustic imaging.[145] This is the basic principle of a strategy called multimodal imaging.[146] Combining various methods allows for the study of more than one aspect by utilizing additional upconversion material.[147]

Biosensing | There are a number of studies investigating the use of tools based on lanthanide-doped upconverting nanoparticles for the detection of biomolecules, and observation of

biological processes. Among these are assessments of the changes in pH levels for which having a tight control is crucial for cell metabolism,[27] detecting of the activity of caspase-9 in studying the mechanisms of apoptosis process,[148] antibody that has been conjugated with Mn^{2+}- and Ln-doped UCNPs for sensing biomarkers of developing tumor,[149] dopamine neurotransmitter sensing during differentiation of stem cell into neurons,[103] sensing of miRNA which play a major role in the regulatory mechanism of the cell,[150] assessing protein conjugation *via* the method of EDC/NHS-chemistry[151] or real-time monitoring of changes in ATP.[152]

While being considerably bigger than some of the proteins,[153] the nanoparticles can be utilized to image biological processes by labelling these vital elements of the cell. Biolabeling of interactions of proteins can be marked by antibody-conjugated upconverting nanoparticles.[106] Targeting extracellular cell membrane proteins can also be used to study interactions between cells *via* important gap junction connections.[154]

The umbrella term of biosensing and detecting also encompasses the detection of harmful elements and potential pathogens in the environment outside the cell but is equally critical for its functioning. Detection of harmful elements with UCNPs is possible for lead[105] and copper ions.[155] Overuse of antibiotics in medicine, science, and industry generated problems of necessity (harmful side effects on animals) to monitor their concentration which is presently addressed by studies that report the use of upconverting nanoparticles in the detection of chloramphenicol.[104] The ever-growing consumption of food within the rising global population could benefit from various UNCPs-based approaches for monitoring food quality and safety by the means of screening for specific metabolites secreted by microorganisms.[156,157]

Tracking | The goal of tracking aims at mapping the dynamics of biological processes, and observation of potentially significant changes. Given enough intensity of luminescence, this can involve tracking single molecules within the cytoplasm.[122] Polymer (e.g. PMAO / PEG-DGE) coated UCNPs are reported to exhibit stability of up to one hour in the bloodstream before being removed from circulation.[30] UCNPs-stained transplanted stem cell movement can be monitored in live animals for assessing therapeutic properties for cryoinjured tissues[158] and potential candidates for other types of cell therapies.[159] Dendritic cells (DC) stimulated with antigen and labelled with upconverting nanoparticles are the subject of immunotherapy DC-based vaccine research in which nanoparticles are used to observe migration into the lymph nodes.[160] Upconversion luminescence of lanthanides shows potential in studying the degradation dynamic of hydrogels used in medicine for transplantation or drug delivery.[161]

Drug (biomolecule) delivery | The use of highly toxic agents in cancer therapies cause significant off-site damage to the organism,[116] hence it is most important to create a platform for very specific delivery and release of the aforementioned compounds. Drug delivery research for upconverting nanoparticles focuses primarily on two types of surface modifications, polymeric coating and sialinization. These provide a large surface area with a porous structure,[162] that serves as an adsorption site for cancer therapy drugs and other molecules.

Nanoparticles coated in a layer of mesoporous silica can host a number of different molecules such as antitumor drug doxorubicin (DOX), [163] curcumin,[164] or ibuprofen.[165] Silica-coated UCNPs, conjugated with antibodies, are shown to be efficient platforms for siRNA delivery.[166] Silica coating can be further modified by additional layers of polymers like PEG

and used to deliver DOX.[167] Mesoporous SiO_2 layer modified with pH-sensitive PAA polymer is an example of delivering doxorubicin to specific sites with acidic environment.[168]

Another type of sialinization strategy that can be used for delivery is the synthesis of yolk-structured silica/PEG coating that carries molecules located in the space between the synthesized layer and the luminescent core.[42]

Nanoparticles coated with different polymers are investigated as intensively as silica-coated counterparts.[65] Nanoparticles coated with polyethylene glycol and C18PMH copolymer are studied for the delivery of DOX whose specificity is facilitated by folic acid conjugation.[169] Lanthanide-doped nanocrystals can be coated with a pH-sensitive layer (e.g. PAA-coat) and carry anti-tumour drugs which will be released upon a change of the pH.[170] Compared to typically smaller drugs, much bigger molecules of siRNA can be incorporated into the structure of PAA@PEI polymer coating and delivered to the target site.[171] Light-sensitive polymer of PEO-b-PBNMA is reported as a carrier for Nile Red dye.[172] Jayakumar et al. presented $NaYF_4$ nanoparticles carrying photocaged DNA plasmids on the mesoporous silica. Then, treated with these nanoparticles, B16-F0 melanoma cancer cells were transplanted into the skin tissue of Balb/C mice. Upon exposure to NIR radiation, blue light generated by the upconversion process uncaged the plasmid from the porous surface of UCNPs, and expression of green fluorescent protein (GFP) encoded on it was observed.[173]

Outside polymer or silica coating strategies, different methods of delivering drugs involve oxidation of surface hydrophobic ligands and introducing -COOH moiety at its hydrophobic chain, which later serves as a site for highly specific DOX conjugation reaction.[174]

stimuli	polymers	UCNPs	excitation (nm)/ intensity (mW cm^{-2})	emissions (nm)	payload
thermosensitive polymers	PEO-*b*-P(NIPAM-*co*-NBA)	$NaYF_4$:Tm^{3+},Yb^{3+}	980/8000	365	Nile Red
	P(NIPAm-*co*-AAm) hydrogel	$NaYF_4$:Yb^{3+}/Er^{3+}	980/1200	525, 543	lysozyme
	poly(AZO-*co*-OEGMA)	$NaYF_4$:Gd/Yb/Tm	980/3000	350, 440	DOX
pH-sensitive polymers	PAA	$NaYF_4$:Yb^{3+}/Er^{3+}	980/N.A.	550, 650	DOX
	poly(HEMA-*co*-AMPS)	$NaYF_4$:Yb^{3+}/Er^{3+}	980/N.A.	550, 650	methylene blue
	PEI	$NaYF_4$:Yb^{3+}/Er^{3+}	980/N.A.	530, 650	siRNA
light-sensitive polymers	PEO-*b*-PBNMA	$NaYF_4$:Tm^{3+},Yb^{3+}	980/5000	350, 450	Nile Red
	PNB-*b*-POEG	NaYF4:Yb/Tm@NaYF4	980/1	350, 450	DOX
	PNBMA-*b*-PEG	NaYF4:Yb/Tm/Er	980/500	540, 650	hydrophobic AB3
	AZO-PDPAn-PEG_{45}@cyclodextrins (*β*-CD)	$NaYF_4$:Yb^{3+},Tm^{3+}	980/1300	365, 470	DOX
	AZO-PEG	$NaYF_4$:Tm,Yb@ $NaYF_4$:Er,Yb	980/1300	365, 470, 550	DOX
	PIPAM-*co*-SPMAA	$NaYF_4$:Tm^{3+},Yb^{3+}	980/4300	365, 470	Coumarin 102
nonfunctional hydrogel	4-arm-PEG-NH_2	$NaYF_4$:Tm^{3+},Yb^{3+}	808, 980/5310, 2830	350, 450	DOX/lysozyme
hydrophobic polymers	PLGA	YF_4:Yb,Er@$NaGdF_4$	980	520–540, 654	DOX
pH-degradable polymer	PEG-PAH-DMMA	$NaYF_4$:Yb,Tm	980	289, 361	Pt(IV)-prodrug
ROS-responsive polymers	sialic acid-PEG-thioketal-PLGA	*β*-$NaYF_4$:Yb,Er	980	540	DOX

Table 1. Examples of drug delivery systems | Table with examples of drug delivery systems, the types of $NaYF_4$ nanoparticles, their various coating, excitation and emission peaks, and the kind of molecules carried by them. Reprinted with permission from Biomacromolecules 2021, 22, 8, 3168–3201. Copyright© 2021 American Chemical Society.[65]

Photodynamic therapy | Photodynamic therapy (PDT) is a relatively new strategy in modern medicine, which aims to replace standard and destructive chemotherapy.[175] PDT utilizes photosensitive and photolabile compounds called photosensitizers (PS). Stimulated by light, these compounds generate toxic agents such as reactive oxygen species (ROS)[176] and other free radicals.[109] In other cases, the compounds undergo chemical rearrangement from non-cytotoxic into cytotoxic molecules.[177] PDTs are intensively investigated for cancer studies and therapies[178] as a safer replacement for the highly toxic drugs used for chemotherapy

treatments.[179] These therapies typically use visible light, sometimes UV light,[180] for activation of a therapeutic agent. Both UV and Vis photons have limited penetration depth, which could be enhanced by the use of an upconversion process that moves excitation into the infrared spectrum. Nanoparticle-based platform can be used as a means of delivering and a mean of activating the PDT agent.

Silica-coated upconverting $NaYF_4$ nanoparticles loaded with Merocyanine 540 (MC540) and Zinc phthalocyanine (ZnPC) photosensitizers can be used to generate singlet $^1O_2$ oxygen out of triplet $^3O_2$.[181] Other similar types of $NaYF_4$@$mSiO_2$ system with 2 nm pores, show potential in bladder cancer therapies.[88] Thin layers of mesoporous silica on $NaYF_4$ nanocrystals can be modified with APTES, subsequently providing -NH_2 moieties for EDC/NHS chemistry and conjugating Chlorin e6 (Ce6) photosensitizer.[180] Vitamin B_{12} is studied as a less toxic alternative to typical PS compounds for ROS generation against human breast cancer MDA-MB-231 cells.[182] Mesoporous silica-coated UCNPs loaded with MC540 photosensitizer and conjugated with ovalbumin shows low cytotoxicity against fibroblast L929 cell line and strong cytotoxicity against colon cancer CT29 cells while irradiated under 980 nm.[179] Rose Bengal-loaded nanoparticles coated with silica/PEG shell are reported as an effective PDT solution for inhibiting the growth of highly resistant cancerous cells of HeLa line.[183] Photodynamic therapy can be deployed in the fight against cancerous immune cells with mesoporous silica-coated UCNP carrying chlorin e6 photosensitizer which shows a capacity to selectively kill macrophage-like THP-1 cell lines upon laser excitation.[184] Mixed $NaYF_4$@$NaGdF_4$@$mSiO_2$ carrier shows efficacy against the HeLa cell line by utilization of hypocrellin A photosensitizer and folic acid as a ligand that facilitates crossing the cell lipid membrane.[185]

The multimodal approach briefly discussed at the end of the Bioimaging subsection, finds some application in PDTs as well. Combined chemo-, radio- and photodynamic therapy

of another $NaYF_4$@$NaGdF_4$ nanoparticles coated in a mixed shell of dense and mesoporous silica with incorporated docetaxel (Dtxl) and hematoporphyrin (HP) photosensitizers inhibits cancer growth after injection into T_1 tumour-bearing mice.[186]

A less conventional approach to photodynamic therapy is antimicrobial treatment. Strains of *Staphylococcus aureus* and *Escherichia coli* bacteria are reported to be susceptible to singlet oxygen generated by silicon 2,9,16,23-tetra-tert-butyl-29H,31H-phthalocyanine dihydroxide (SiPc) photosensitizer adsorbed into a mesoporous shell of cubic $NaYF_4$ nanoparticles. [187] Another unconventional angle is shown by reports suggesting photodynamic therapy as a potentially viable option for treating Alzheimer's disease. Rattle-like upconversion nanoparticles, with mesoporous silica shell and loose core, are shown to disrupt amyloid beta aggregation into amyloid plaques by producing $^1O_2$ *via* rose bengal dye.[188]

Optogenetics | As mentioned in the brief introduction at the beginning of the Application Section, optogenetics is a newly emerging field that combines the physicochemical engineering of nanoparticles with genetic engineering. Genetic engineering provides a gene with a light-sensitive protein product, while chemical engineering provides upconverting nanoparticles playing the role of inducers.

Channelrhodopsin-2 (ChR2) is a photosensitive element used in optogenetics.[110] The protein is a light-gated ion channel, which modulation by UCNPs doped with different Ln^{3+} ions, allows wavelength-specific control of the channel.[189] Optogenetic control through ChR2 protein involves flow of H^+, Na^+, K^+, and Ca^{2+} ions through the cell membrane which subsequently modulate other Ca^{2+}, Na^+ and K^+-specific ion channels, crucial for homeostasis of the cell.[190]

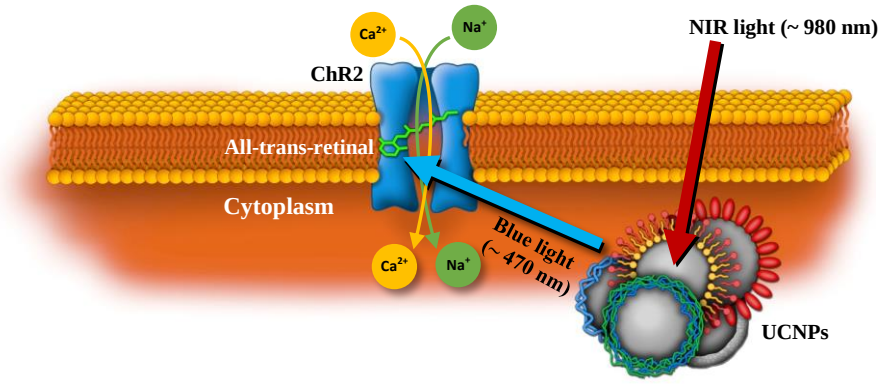

Figure 17. The principle of optogenetic method based on Channelrhodopsin-2 | Optogenetic method that utilize genetically modified cells transfected with ChR2 gene is based on induction on ions transport *via* membrane protein of ChR2. The change of ion concentration induces further signalling pathways within the cell. Based on Pliss et al.[191]

Optogenetics is shown to be capable of manipulating the neurons which were genetically modified with adeno-associated virus (AAV) vector carrying channelrhodopsins ChR2 and *C1V1* genes. These transduced neurons of adult rats showed a response to NIR radiation converted by $NaYF_4$ nanoparticles into green light.[192] Efficiency of such a system can be further enhanced by introducing IR-806 sensitizer dye that increases luminescent properties of $NaYF_4$ nanocrystals used to modulate the activity of neurons transduced with red activable channelrhodopsin (ReaChR) gene.[115]

$NaYF_4$ upconverting nanoparticles are reported to efficiently modulate the influx of Ca^{2+} ions and thus manipulate other ion channels of cervical cancer HeLa cells, genetically modified with blue-sensitive ChR2 protein.[191]

The movement patterns of the transgenic strains of small nematode species of *C. elegans* can be impacted by exposition to NIR radiation. Channelrhodopsin proteins introduced and

expressed in mechanosensory neurons of these strains of *C. elegans* can be stimulated by silica-coated $NaYF_4$ UCNPs converting 980 nm NIR into 450 nm light.[193]

■□□□ Enhancing Luminescent Properties with Sensitizing Dye

The wide variety of possible applications for nanoparticles, given all the benefits of infra-red upconversion and a variety of modifications to the $NaYF_4$ nanocrystals, is diminished by the low quantum yield efficiency of the UCNPs.[194] Registering the UCL signal requires strong near-infrared excitation radiation in the first optical window. This is further complicated by overlapping the water absorption bands with the 808 and 960 nm peaks of UCNP excitation.[4] Excitation at this spectrum generates considerable heat, which significantly rises the temperature of the system, to the point of being harmful to biological structures.[195]

This problem could be possibly mitigated by sensitizing antennas on the surface of nanoparticles (figure 18).[196] This method of enhancement is based on the Förster energy resonance transfer effect. Excited with NIR radiation, the antenna should non-radiatively transfer the harvested energy to upconverting particle increasing the luminescence intensity (figure 19).[197] Dye emission must overlap with the absorption spectrum of sensitizing lanthanide ions.[198]

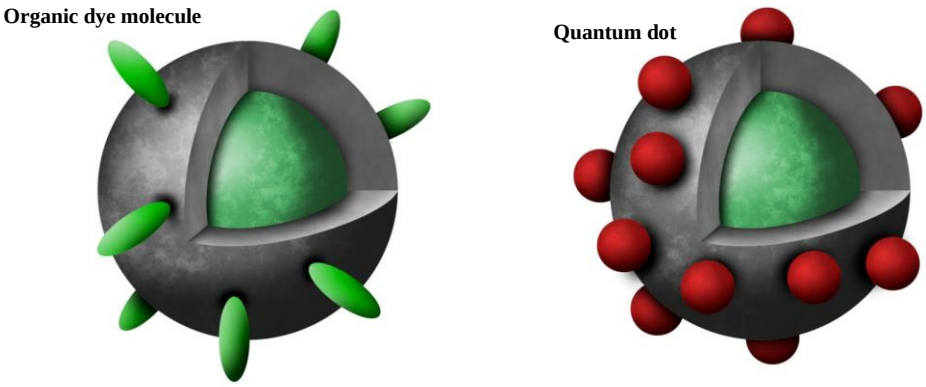

Fig 18. Potential strategies of enhancing luminescence with sensitizing antennas | Visual illustration of dye-sensitized and quantum dot-sensitized core@shell-type $NaYF_4$ upconverting nanoparticles.

NIR-absorbing organic dyes (like IR-806)[199,200] or quantum dots[201] show promise as viable candidates for that role. The same dye-sensitized design is the subject of non-biological research into topics like solar cell technologies.[194,202]

Infrared dyes | The idea to use organic infrared dye as a sensitizing agent was proposed by Zhang et al. in 2007. The group reported that tropolonate ligands can increase the luminescence lifetimes of $NaYF_4$ nanoparticles.[203] Following that work, in an early study on organic dye sensitization Zou et al. used a type of $NaYF_4$: Yb^{3+}, Er^{3+} nanoparticles sensitized with IR-806 to observe upconversion luminescence (UCL) increase of ~3,300 times.[204]

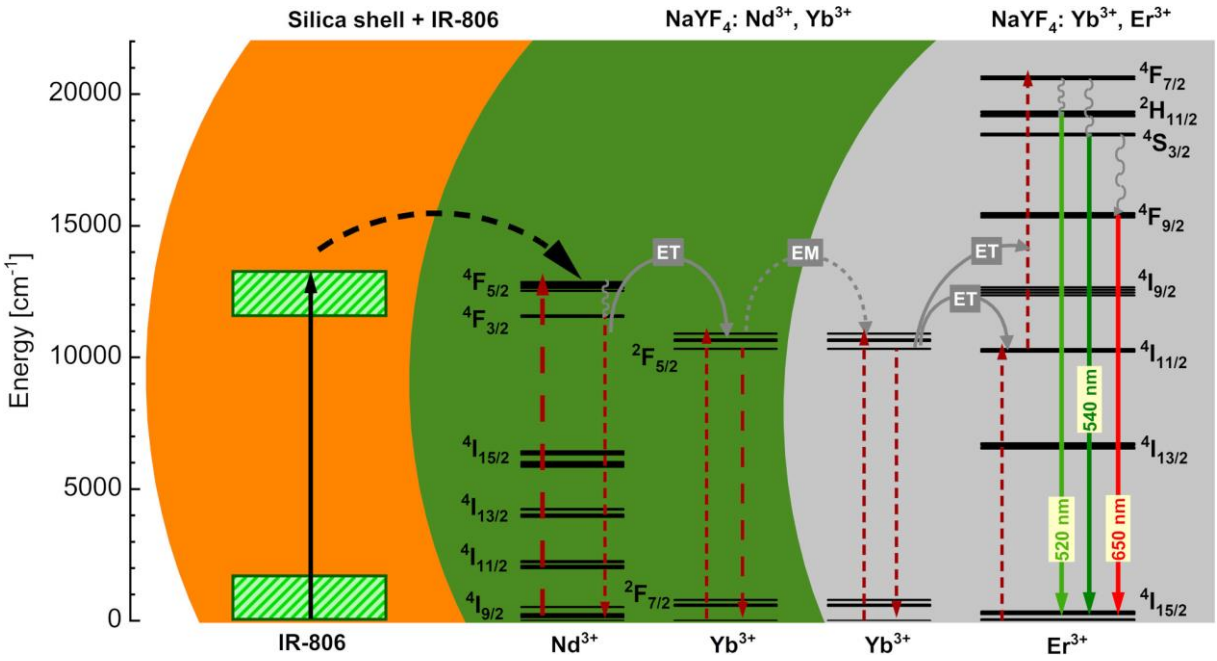

Figure 19. Energy transfer from sensitizing antenna | Energy transfer path between IR-806 sensitizing antenna, active $NaYF_4$: Nd^{3+}, Yb^{3+} shell, and luminescent $NaYF_4$: Yb^{3+}, Er^{3+} core. As previously described in figure 3, energy transfer between an active shell (green) doped with neodymium and ytterbium ions and an active core (grey) doped with ytterbium and erbium ions. Nd^{3+} ions with a NIR absorption peak at 808 nm and Yb^{3+} ions at 980 nm, transfer the energy to the active core throughout Yb^{3+} ions to the erbium ions. Excitement of Er^{3+} ions causes emission at various wavelengths in the spectrum of visible light. Layer of sensitizing antenna (orange) harvest additional portion of NIR light and transfer the energy to the neodymium ions in an active shell. Courtesy of dr Katarzyna Prorok.

Studies have shown that a dye-sensitizing strategy can yield in intensities enhancement of emission up to 10-20 times for infrared organic dye like IR-806[205] and IR-808[206] or around 17 times enhancement of luminescence for Cy7 dye.[207]

Core-type Nd^{3+}-doped $NaYF_4$ nanoparticles suspended in DMF solution of indocyanine green (ICG), shows 6- to a 37-fold enhancement of UC luminescence.[208] ICG-sensitized $NaYF_4$ nanoparticles with a 32x increase in UCL can be used in photoacoustic bioimaging.[209] Size of the nanoparticle impacts the efficiency of sensitization. Upconversion enhancement with ICG dye is shown to be the most efficient for $NaYF_4$ nanocrystals with a diameter of 19 nm.[210]

Core/shell-type $NaYF_4$:Yb^{3+}, Er^{3+}@$NaYF_4$:Nd^{3+} nanoparticles with surface-conjugated IR-806 dye demonstrate a 44-fold increase of upconversion luminescence in $CHCl_3$ solvent.[211] Similar $NaYbF_4$@$NaYF_4$ nanoparticles sensitized with IR-808 dye achieve UCL intensity increase of 33x and more when UCNP is co-sensitized with both IR-808 and IR-820 dyes.[199] Saleh et al. showed water-soluble micelle-like $NaYF_4$: Yb^{3+}, Er^{3+} platform sensitized with 1859 SL infrared dye that enhances UCL 21-fold.[212]

High rates of photobleaching limit the application of the infrared dye when combined with lanthanide-doped UCNPs, which are not photolabile.[213] Investigation focusing on embedding the dye in surface-modified UCNPs has shown to mitigate this problem to some extent. For example, a mesoporous shell of silica on the $NaYF_4$ nanocrystals can protect the ICG dye from photobleaching.[214]

Quantum dots | Although the interactions between lanthanide-doped upconverting nanoparticles and quantum dots are investigated primarily by focusing on the transfer of energy from cubic[5] or hexagonal[215–217] $NaYF_4$ nanoparticles to the quantum dot, the NIR-emitting Ag_2Se QDs[218] could be considered another class of sensitizers for upconverting nanoparticles. Initial reports by Song et al. show an 18-fold increase of UCL for small 18 nm $NaYF_4$ nanoparticles coated with 3-7 nm of size Ag_2Se quantum dots. [201]

■□□□ Cytotoxicity and Biocompatibility of $NaYF_4$ Nanoparticles

Cytotoxicity and other potentially harmful side-effects of upconversion nanoparticles are still an ongoing debate. This uncertainty limits the wide-scale deployment of lanthanide-doped UCNPs for any medical procedures that could benefit from their unique luminescent properties.

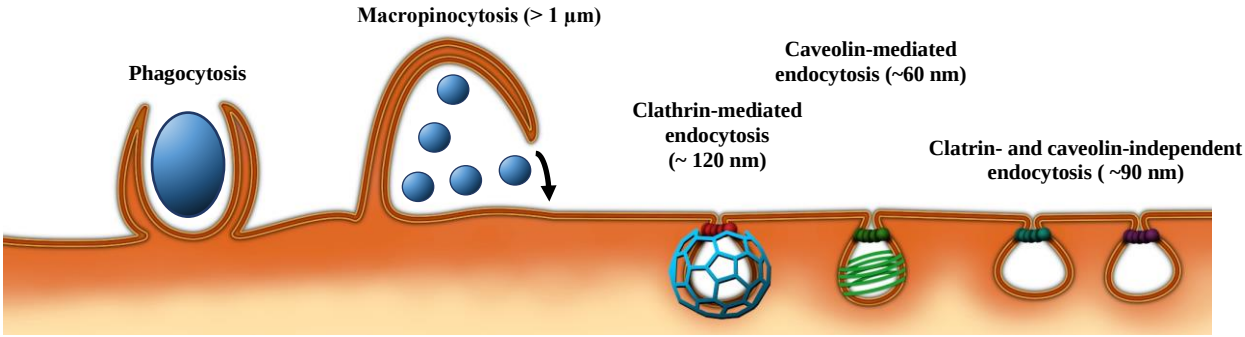

Figure 20. Endocytic pathways for micro- and nanoparticles | Examples of cellular mechanism of absorbing particles depending on the size of such particle. Based on Schmid et al.[219]

Reports have shown that ligand-stripped $NaYF_4$ nanoparticles can degrade in bodily fluids and biological buffers like phosphate-buffered saline (PBS).[220] Introduction of an isolating barrier, in the form of one of the modifications described in the "*Surface Modification of $NaYF_4$ Nanoparticles*" section is necessary to protect the stability of UCNPs. It also prevents nanocrystals from dissolving and leaking potentially harmful ions into organisms or the environment.[221–223]

Due to the size, typical core- or core@shell-type nanoparticles are small enough to penetrate the cell membrane without the involvement of any mechanism akin to Caveolin- or Clathrin-mediated endocytosis (figure 20).[219]

$NaYF_4$ nanoparticles of approximately 10 nm are internalized without requiring any surface modifications and are reported to be relatively low cytotoxic by reducing cell viability to around 80% after 20 hours of stimulation.[224] Investigation of doxorubicin-conjugated $NaYF_4$:Yb^{3+}/Tm^{3+} nanoparticles has shown that these 25 nm UCNPs do not induce death of L929 fibroblast cells.[174] *In vitro* cytotoxicity of $NaYF_4$:Tm^{3+}/Yb^{3+}/Gd^{3+} silica-coated 34 nm UCNPs in the MCF-7 breast cancer cell line are described as non-apoptotic-inducing as well, leading to the death of around 20% of the cell after 24-hour stimulation.[91]

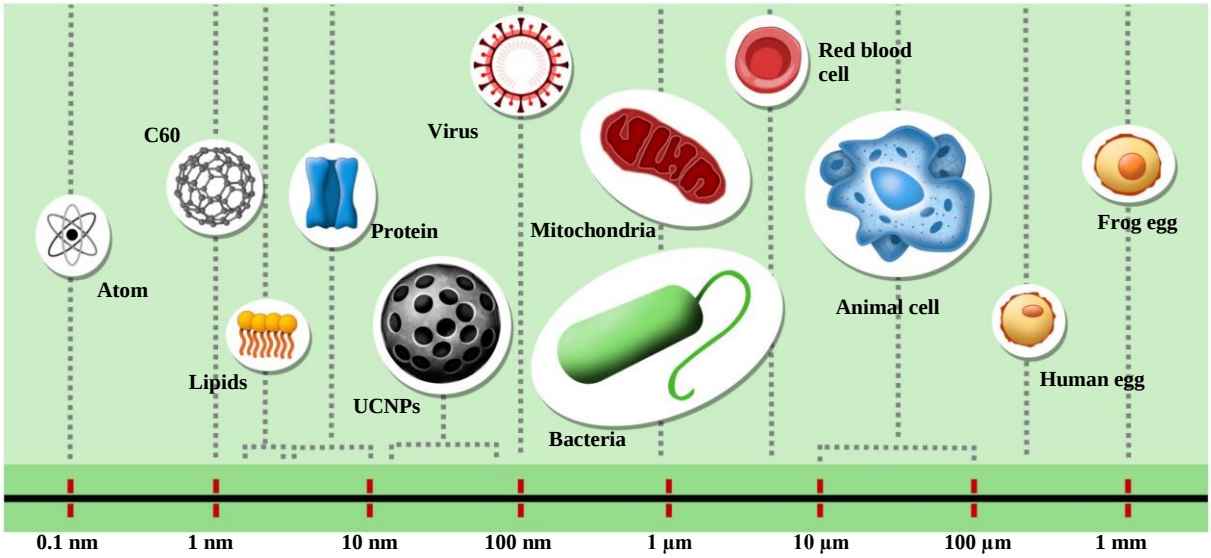

Figure 21. Comparison of sizes between UCNPs and other structures | Size comparison of $NaYF_4$ upconverting nanoparticles and other physical (e.g. atom, molecules) and biological (e.g. proteins, organelles, cells) structures. Relative sizes on a logarithmic scale.

Nanoparticles of a more substantial size and with surface modifications, like polymer- or silica-coated Ln-doped UCNP are internalized by the cell through Caveolin-mediated endocytosis (CME).[162,219] Studies show that bone marrow stromal and rat skeletal myoblast cells survive incubation with silica-coated core-type $NaYF_4$ 50 nm nanocrystals for 24 hours with cell viability of around 90%.[225]

Clathrin-mediated endocytosis occurs when the size of UCNPs exceeds 100 nm, and it is reported that PEG- and PAA-coated $NaYF_4$ nanoparticles utilize this internalization pathway without inducing apoptosis.[66]

The necessity for a thorough investigation of all the different lanthanide-doped $NaYF_4$ nanoparticles and their variation with multiple surface-modifications stems from Clathrin- and Caveolin-mediated endocytosis being tightly related to the apoptotic pathways.[226,227]

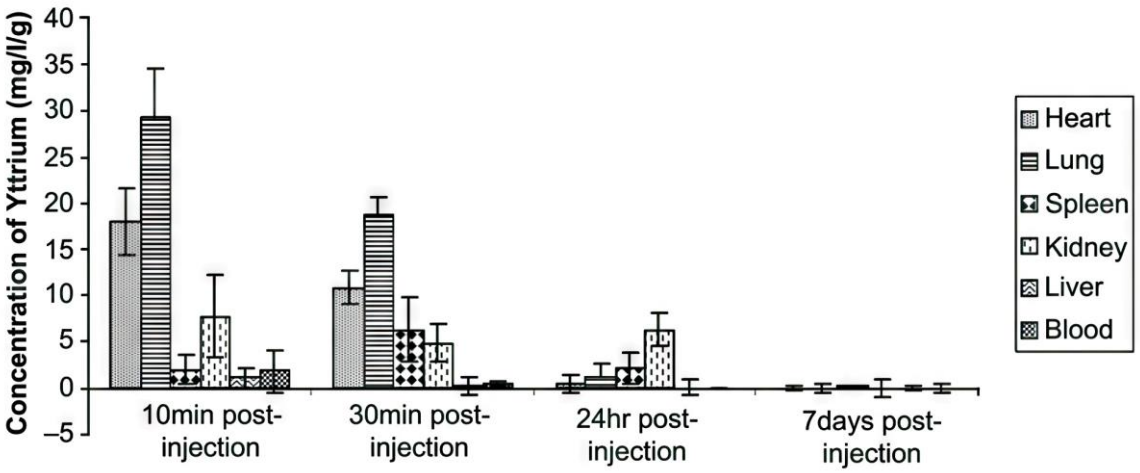

Figure 22. Accumulation of Y^{3+} ions | Dynamic of accumulation of yttrium ions in rat organism after injection of 50 nm silica-coated core-type $NaYF_4$ upconverting nanoparticles. Reprinted with permission from Biomaterials 2008, 29, 30. Copyright © 2008 Elsevier Ltd.[225]

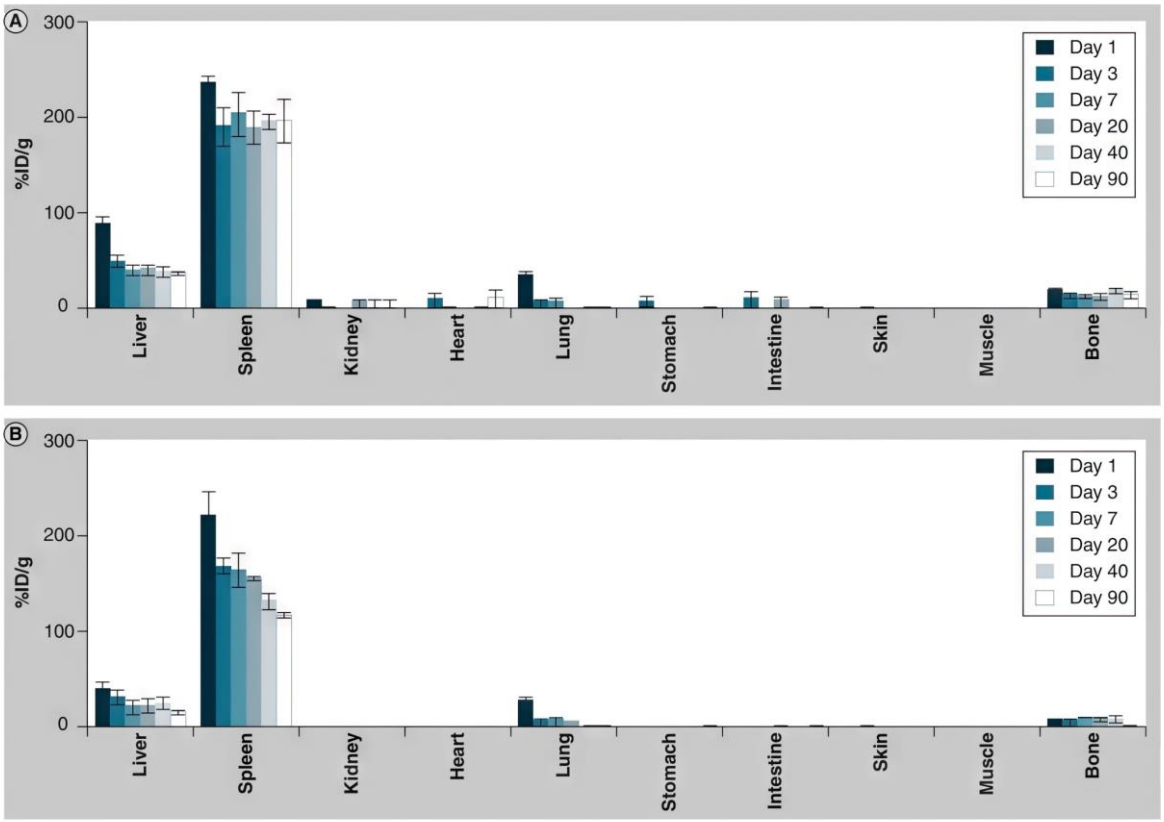

Figure 23 Organ distribution of polymer-coated $NaYF_4$ nanoparticles | An example of accumulation of ~30 nm A) polyethylene glycol-coated and B) polyacrylic acid-coated $NaYF_4$ nanoparticles in various organs of a mice. %ID/g stands for percentage of dose per gram of mouse tissue. Reprinted with permission from Nanomedicine vol. 6 no. 8. Copyright © 2011 Future Medicine Ltd[67]

The argument for extensive research into the subject of cytotoxicity is additionally strengthened by *in vivo* studies suggesting high rates of nanoparticle accumulation in certain organs like the liver or spleen.[228,229] Smaller 30 nm polymer-coated $NaYF_4$ upconversion nanoparticles are reported to be non-toxic for a mice organism but have a prolonged blood circulation time, and up to 3 months long retention in the spleen (figure 22).[67]

Substantially bigger 50 nm silica-coated core-type $NaYF_4$ nanocrystals are shown to be efficiently removed for rat organism within a period of 7 days after injection (figure 23).[225]

□□□ Apoptosis and Necrosis

In the context of $NaYF_4$ upconverting nanoparticles, among many types of cell death,[230] apoptosis and necrosis are the two that must be taken under the consideration while studying the subject of the application of UCNPs.

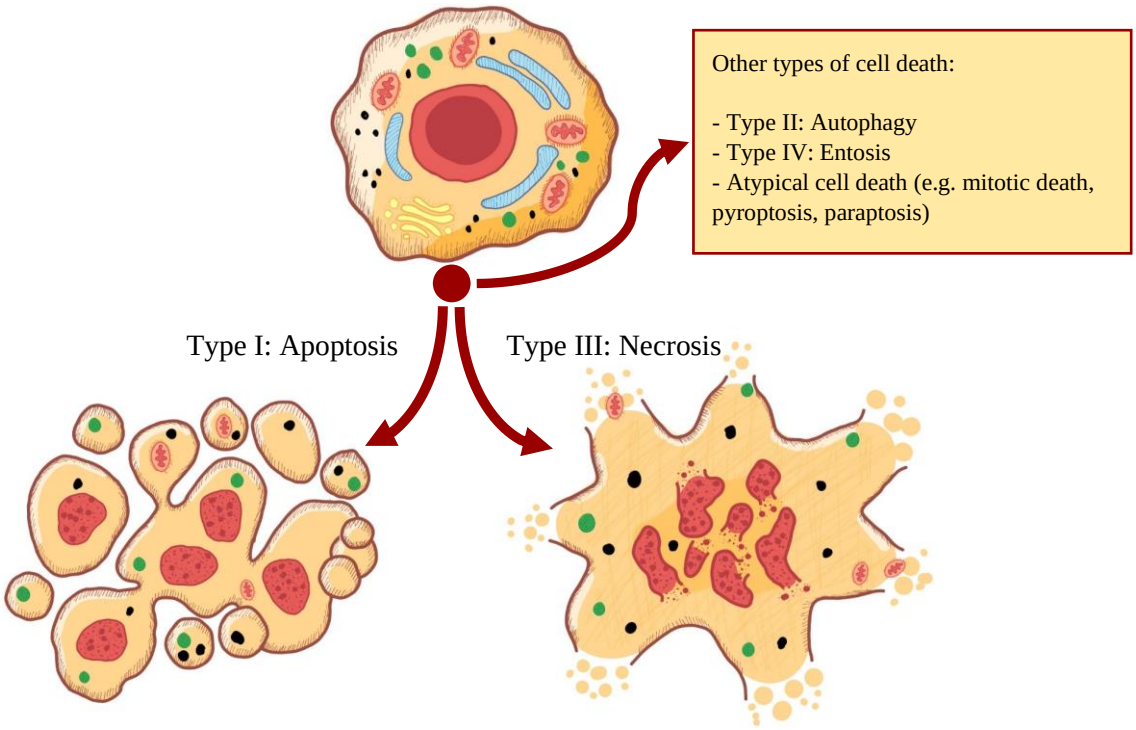

Figure 24. Types of cell deaths | Five types of cell deaths with a focus on the two discussed on the subject of toxicity of UCNPs. These are: apoptosis – the programmed cell death leading to the fragmentation of the cell, and necrosis – cell death leading to the disintegration of the cellular membrane and the release of the cell content into the environment. Other types of cell deaths are autophagy, entosis and various atypical processes. Based on Krüger et al.[230]

Apoptosis is a programmed cell death. Apoptotic cell undergoes many steps that includes chromatin condensation at the early stages of the process with further fragmentation of entire cell into smaller vesicles called apoptotic bodies (figure 24).[231,232] The process is crucial for the organization and survival of multicellular organisms.[233] Apoptosis is tightly controlled process that involves cross-communication between cells of multicellular organism as well as a number of intracellular signalling pathways involving complex protein interactions including ubiquitination, proteolysis or protein phosphorylation within a single cell (figure 25).[232,234] Dysregulation of apoptosis is involved in the pathogenesis of many cases of cancer but also in diseases related to neurological or cardiovascular diseases or autoimmune disorders.[235]

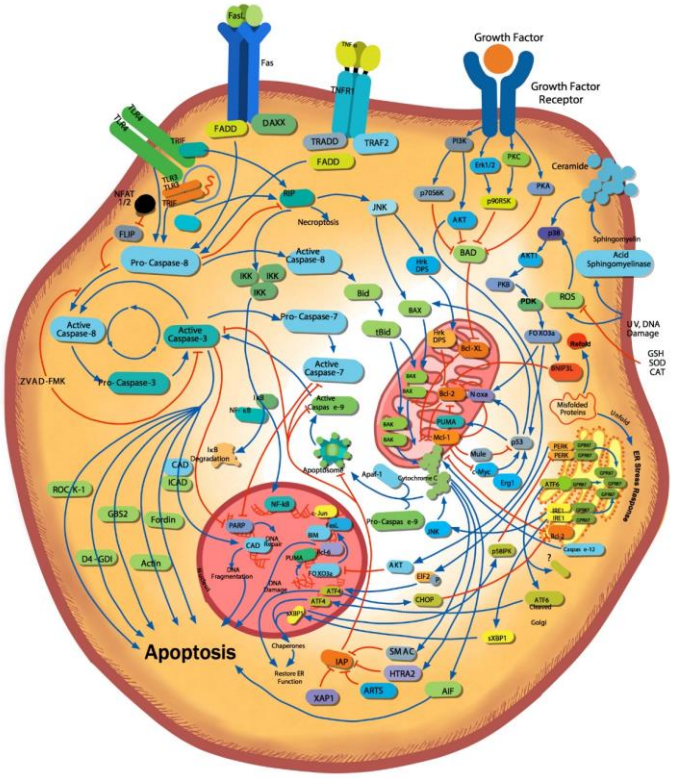

Figure 25. Regulatory mechanism of apoptosis | The complexity of regulatory mechanisms of apoptotic processes which makes it a challenging subject on research. Based on Novis Biologicals promotional materials.[236]

Another type of cell death is necrosis. Typically the necrosis is an uncontrolled process involving the lose of the integrity of the cell, occurring due in the presence of a chemically toxic or physically destructive factor, but there are types of necrosis controlled by specific signalling pathways.[237] In comparison to apoptosis, it is a far more impactful process for the overall condition of the organism as the loss of the integrity of cellular membrane leads to uncontrolled release of various dangerous intracellular components such as inflammation-promoting agents.[238] Necrosis generates a severe inflammatory state.[239] Additionally, necrosis can promote microenvironment changes that promote growth of tumour.[240] Necrosis can also occur as a side effect of apoptotic bodies not being properly disposed by the phagocytic cells which can lead to secondary necrosis.[241]

Because of the severe implications of both apoptotic and necrotic processes, the $NaYF_4$ nanoparticles and surface modified (e.g. with silica coating) UCNPs need to be thoroughly studied in the context of inducing these types of cell death. Particularly, the subject of chemical toxicity leading to necrosis must be assessed before adopting UCNPs as a new generation of highly stable luminescent labelling agents.

In summary, upconversion nanoparticle-based materials for medicine require more investigation and individual approaches to investigate their viability as contrasting agents, therapeutic carriers, diagnostic labels, etc. The subject of the nanoparticle's composition, size, surface modification, and thus response from the cellular or immune systems necessitates an individual approach for each kind of lanthanide-doped $NaYF_4$ upconversion nanoparticle.

This thesis presents the results of a preliminary investigation into the application of the validity of mesoporous silica-coated β-$NaYF_4$: Er^{3+}, Yb^{3+} @ β-$NaYF_4$: Nd^{3+}, Yb^{3+} nanoparticles as carriers of therapeutic agents or emission-enhancing organic molecules.

THE AIM OF THE STUDY

There are three main objectives of the study. First goal was to obtain a stable platform composed of $NaYF_4$ upconversion nanoparticles coated in porous silica shell of various properties such as different diameter of the pores and thickness of the silica. This platform will be studied in a second objective as a potential system of delivering target molecules by assessing efficiency with which silica can protect a volatile compound in form of cyanine IR-806 dye from chemical and photophysical degradation. Final goal will try to determine the validity of *in vivo* use of silica-coated $NaYF_4$ nanoparticles by performing cytotoxicity tests on selected cell cultures.

It will be done in following steps:

1. Synthesis of various silica coatings on $NaYF_4$ nanoparticles;

2. Assessments of silica shell protective properties with IR-806 embedded in porous structure;

3. Study of cytotoxicity of silica-coated $NaYF_4$ nanoparticle on cell cultures.

MATERIALS AND METHODS

■□□□ Chemicals and Cells

Ytterbium oxide (99.99%), erbium oxide (99.99%), neodymium oxide (99.99%), acetic acid (99%), pure oleic acid, 1- octadecene (90%), hexadecyltrimethylammonium bromide (CTAB, ≥98%), L-arginine (reagent grade, ≥98%), sodium hydroxide, IR-806 dye (90%), tetraethyl orthosilicate (TEOS, ≥99.0%), fetal bovine serum (FBS), L-glutamine, antibiotic antimycotic solution (Merck), thiazolyl blue tetrazolium bromide (MTT), and glucose were purchased from Sigma-Aldrich. Phorbol-12-myristate-13-acetate (PMA) was purchased form Pol-Aura, Poland. BD Pharmingen™ FITC Annexin V, Annexin V binding buffer, and BD Pharmingen™ Propidium Iodide Staining Solution were purchased from BD Biosciences Poland. Ethanol (96% pure p.a.), n-hexane (95%), acetone (pure p.a.), pyridine (pure p.a.), ammonia (30% pure p.a.), and chloroform were purchased from POCH S.A. (Poland). Phosphate-buffered saline, RPMI-1460 and Dulbecco's Modified Eagle media were obtained from the Laboratory of General Chemistry in the Institute of Immunology and Experimental Therapy. All of the chemical reagents were used as received, without further purification. THP-1, MDA-MB-231, A375, and SKOV cell lines, equivalent to American Type Culture Collection (ATCC) cell lines, were obtained from Polish Collection of Microorganisms (PCM) in the Institute of Immunology and Experimental Therapy.

■□□□ Synthesis of Upconversion Nanoparticles and Structural Characterization

β-$NaYF_4$: 2% Er^{3+}, 20% Yb^{3+} nanoparticles were obtained through a thermal decomposition reaction[6] and were used as a luminescent core template for further synthesis. The core NPs were covered with a layer of β-$NaYF_4$: 30% Nd^{3+}, 20% Yb^{3+} shell *via* a modified version of a thermal

decomposition reaction. Uniform size and shape were confirmed with the use of a transmission electron microscope.

Preparation of Lanthanide Acetate | Stoichiometric amounts of Tb_2O_3, Yb_2O_3, and Nd_2O_3 lanthanide oxides were mixed with 50% aqueous acetic acid. The mixture was stirred and heated to obtain a clear and transparent solution. The final precursor was obtained by evaporation of solvents and further drying at 130 °C for 24 h.

Synthesis of Core Nanoparticles | Lanthanide acetate, $(CH_3COO)_3Yb$ and $(CH_3COO)_3Tb$, 2.5 mmol, was added to the flask with 15 mL of oleic acid and 38 mL of octadecene. The solution was stirred and heated to 140 °C under vacuum for 30 min to form an $Ln(oleate)_3$ complex and to remove total oxygen and remaining water. Next, the temperature was lowered to 50 °C, and 10 mmol ammonium fluoride (NH_4F) and 6.25 mmol sodium hydroxide (NaOH) dissolved in 20 mL of methanol were added to the reaction flask. The resulting cloudy mixture which was stirred for 30 min at 70 °C. Next, the reaction temperature was increased, and the methanol was evaporated. After removing methanol, the solution was heated up to 300 °C under a nitrogen atmosphere and kept in such conditions for 1 h. Next, the nanoparticles were precipitated using acetone and n-hexane, centrifuged at 10.000 rpm for 10 min, and washed with ethanol. Finally, the prepared core NPs were dispersed in chloroform.

Synthesis of Core/Shell Nanoparticles | Lanthanide acetate, $(CH_3COO)_3Yb$ and $(CH_3COO)_3Nd$, 2.5 mmol, was added to the flask with 15 mL of oleic acid and 38 mL of octadecene. The solution was stirred and heated to 140 °C under vacuum for 30 min to form the Ln(oleate)3 complex and to remove the total oxygen and remaining water. The temperature was lowered to 60 °C, and the reaction flask was placed under a flow of nitrogen. A solution of

core nanoparticles in $CHCl_3$ was added to the solution. The solution was maintained at 80 °C until all the chloroform was removed. Next, the temperature was lowered to 50 °C, and 10 mmol ammonium fluoride (NH_4F) and 6.25 mmol sodium hydroxide (NaOH) dissolved in 20 mL of methanol were added to the reaction flask. The resulting cloudy mixture was stirred for 30 min at 70 °C. Next, the reaction temperature was increased, and the methanol was evaporated. After removing methanol, the solution was heated to 300 °C under a nitrogen atmosphere and kept in such conditions for 1 h. Next, the nanoparticles were precipitated using acetone and n-hexane, centrifuged at 10000 rpm for 10 min, and washed with ethanol.

Synthesis of β-$NaYF_4$:Er^{3+},Yb^{3+}@β-$NaYF_4$:Nd^{3+},Yb^{3+} nanoparticles presented in figure 23 was performed by dr Katarzyna Prorok in the Włodzimierz Trzebiatowski's Institute of Low Temperatures and Structure Research, Polish Academy of Sciences in Wrocław.

Structural characterization with the electron microscope was performed by dr Oleksii Bezkrovnyi in the Włodzimierz Trzebiatowski's Institute of Low Temperatures and Structure Research, Polish Academy of Sciences in Wrocław.

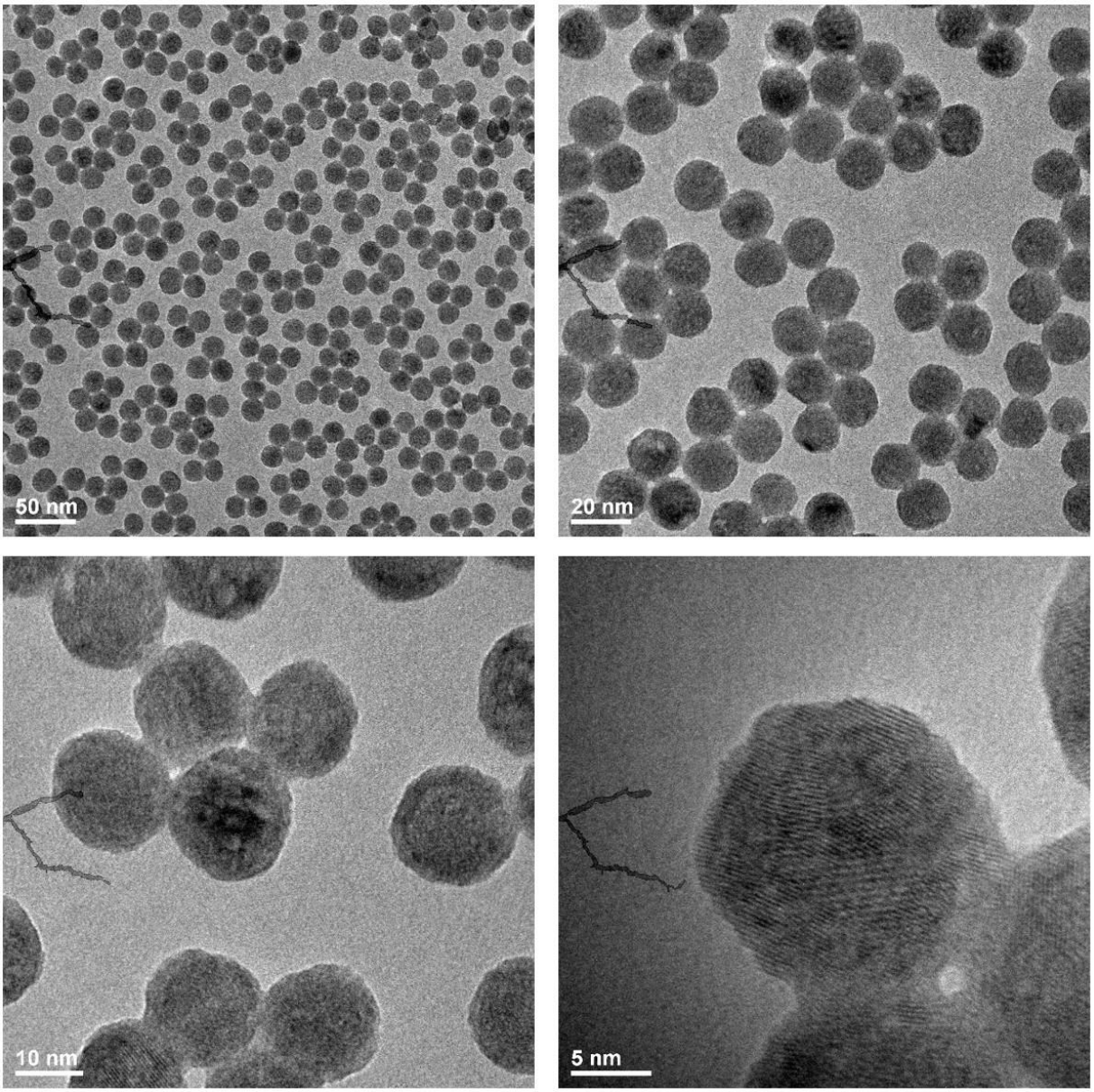

Figure 26. Morphology of upconversion nanoparticles | Transmission electron microscopic images of core@shell-type β-$NaYF_4$: 2% Er^{3+}, 20% Yb^{3+} @ β-$NaYF_4$: 30% Nd^{3+}, 20% Yb^{3+} nanoparticles under different magnification. Scale bar in the left bottom of images.

■□□□ Synthesis of Silica Coating

Core/shell nanoparticles with silica shell (UCNPs@$mSiO_2$) were synthesized with a modified TEOS hydrolysis method in a surfactant solution.[152] 20 mg of hydrophobic UCNPs, suspended in chloroform, were mixed with an aqueous CTAB solution with a concentration of 36 g/l. The mixture was stirred vigorously at 55°C until the solution became transparent. By a series of centrifugations, CTAB-coated UCNPs were washed with water from the excess CTAB. After the last washing, the pellet was resuspended in another CTAB solution, with a concentration of 8.2 g/l. The standard catalyst used for a reaction was 50 μL of 0.1 M NaOH. The solution was stirred for 30 min at 55°C. Various volumes of TEOS solution were added, depending on the size of the silica. Synthesis of the layer was performed for 4 h at 55°C. UCNPs@$mSiO_2$ were collected by centrifugation and suspended in water.

■□□□ Encapsulation of Inorganic Infrared Dye

The aqueous suspension of UCNPs@$mSiO_2$ and IR-806 dye solution were mixed and stirred for an hour at room temperature. Samples were centrifuged for 10 minutes at 15 000 RPM. A pellet with nanoparticles and supernatant with an excess of infrared dye was collected for further experiments.

■□□□ Characterization of Nanoparticles

Absorption measurements | Spectra were obtained with a Cary Varian 5E UV–VIS–NIR spectrophotometer.

Infrared spectra | The UV-VIS-NIR spectra were collected using the a Cary 5000 UV–VIS–NIR spectrophotometer from Agilent Technology (Santa Clara, CA, USA). Raman spectra in the 500–4000 cm^{-1} range were measured using the InVia Raman spectrometer from Renishaw (Gloucestershire, United Kingdom) equipped with the confocal DM 2500 Leica optical microscope (Wetzlar, Germany), a thermoelectrically cooled CCD as a detector, and an AR^{+} laser operating at 488 nm.

Electron Microscopy | The morphology of the samples was determined by transmission electron microscopy (TEM), using the Philips CM-20 Super-Twin instrument operating at 160 kV and the FEI Tecnai Spirit G2 instrument at an acceleration voltage of 120.0 kV, respectively.

■□□□ Cell Cultures, Cell viability Assays for Assessing Cytotoxicity and Flow Cytometry

Cell Cultures | The cells were cultured in RPMI-1640 or DMEM medium, according to ATCC protocols. Media were supplemented with 10% fetal bovine serum (FBS), L-glutamine, antibiotic antimycotic solution, and glucose. Cultures were carried out at 37 °C in a humidified incubator under an atmosphere of 5% CO_2. The medium was refreshed every 2-3 days.

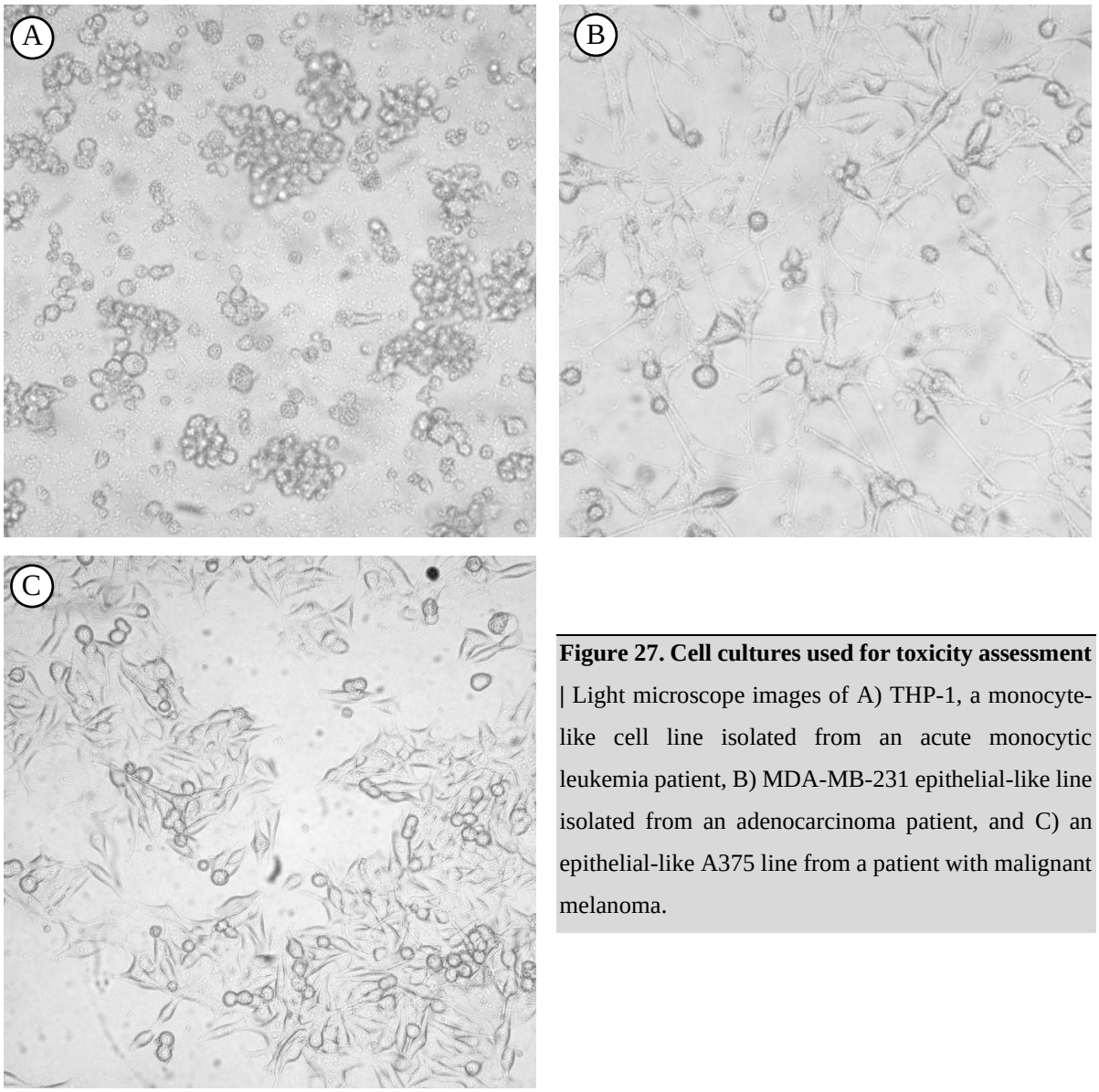

Figure 27. Cell cultures used for toxicity assessment | Light microscope images of A) THP-1, a monocyte-like cell line isolated from an acute monocytic leukemia patient, B) MDA-MB-231 epithelial-like line isolated from an adenocarcinoma patient, and C) an epithelial-like A375 line from a patient with malignant melanoma.

Cytotoxicity assessment | Cell viability was assessed with modified MTT assay protocol.[242] with further modifications. Cells were seeded at a density of 1.0 or 4.0 × 10^5 cells per well in a volume of 100 or 400 µl. 24- and 96-welled plates (NeoLab Bionovo, Poland) were used. The THP-1 line was differentiated into a macrophage line by 72 hours of stimulation with phorbol-12-myristate-13-acetate at a concentration of 200 ng/mL. Trypsinized MDA-MB-231 and SKOV cells were left for 72 hours to let the cells attach to the bottom of the well. Consequently, 400 µl of fresh media containing different concentrations of upconversion nanoparticles were

added. Four types of UCNPs were used: core-type β-$NaYF_4$: 2% Er^{3+}, 20% Yb^{3+} nanoparticles, core@shell-type β-$NaYF_4$: 2% Er^{3+}, 20% Yb^{3+} @ β-$NaYF_4$: 30% Nd^{3+}, 20% Yb^{3+}, silica-coated β-NaYF4: 2% Er^{3+}, 20% Yb^{3+} @ β-$NaYF_4$: 30% Nd^{3+}, 20% Yb3+ nanoparticles, and silica-coated β-NaYF4: 2% Er^{3+}, 20% Yb^{3+} @ β-$NaYF_4$: 30% Nd^{3+}, 20% Yb^{3+} nanoparticles with embedded IR-806 infrared dye. Concentrations of all nanoparticles ranged from 20 to 200 μg/ml. Cells were stimulated for 24 hours and then 10 or 40 μl of 0.5 mg/ml thiazolyl blue tetrazolium bromide (MTT) was added to each well. Plates were incubated for 4 hours at standard culture conditions. 100 or 400 μl of solubilization solution (10% SDS 0.01 M HCl) was added and plates were left overnight. Absorption at 570 nm was measured on a plate reader (BioTek, United States). The data in the *Results* represent an average of three or four wells for each treatment.

Cytotoxicity assessment *via* the MTT method is based on metabolic conversion of yellow dye thiazolyl blue tetrazolium bromide into the purple-coloured formazan derivative form of the chemical (figure 28). It is a reduction reaction performed by mitochondrial enzymes of living cells in the cell culture.[243]

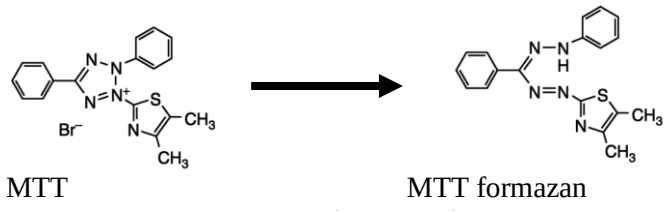

MTT MTT formazan

Figure 28. MTT conversion | The process of the chemical reduction and conversion of MTT into MTT formazan derivative compound by living cells in the cell culture. [242]

Flow Cytometry | Flow cytometry measurements were performed based on a modified protocol from Cold Spring Harbour Protocols.[244] THP-1 cells at the density of 2×10^5 per 500 µL were stimulated with 55 and 96 nm silica-coated nanoparticles of two sizes at a concentration of 90 µg/mL. Stimulation was carried out over a period of 24 and 48 hours. Cells were harvested into FACS tubes and centrifuged at a speed of 1500 RPM for 5 minutes. The pellet was suspended in 2 mL of Annexin V binding buffer. Cells were centrifuged at a speed of 1500 RPM for 5 minutes. The pellet was suspended in 100 µL of Annexin V binding buffer. Then, 0,3 µL of Annexin V-FITC (FITC) and 0,5 µL of Propidium iodide (PI) was added to each sample. After 1 minute and 30 seconds of incubation in the dark at room temperature, the samples were read using the Fortessa flow cytometer. The cells untreated with silica-coated UCNPs were used as the control group. The untreated cells as well as the UCNPs-treated cells stained with FITC and PI, both separately, were used for adjusting PMT voltage and ADP gains. Flow cytometry analyses were performed using a FACSFortessa with FACSDiva software (BD Biosciences, San Jose, CA, USA) and were presented as dot plots (figure 29) in the section Flow Cytometry (page 78).

Flow Cytometry is a technique used for the rapid analysis of cells. Cytometry can be used to assess the size of the cells, sort the cells into specific groups or analyse the presence of specific biomarkers in the cell population.[245] Historically, cytometry started as an analytical method of assessing one parameter – the size of the cell, but presently modern cytometer devices can analyse up to 20 different parameters.[246,247] Flow cytometer performs visible light scattering and fluorescent measurements on each cell that is moving through the system in an accelerated flow of one cell after another.[248] There are multiple types of flow cytometer devices and some are combined with different analytical methods such as mass spectrometry.[247]

Phosphatidylserine (PS) is a membrane lipid that asymmetrically occurs in the internal layer of aforementioned cell plasma membrane. During the process of apoptosis this asymmetry

is disturbed. Phosphatidylserine molecules migrate into external membrane layer. The Annexin V is a protein that binds to the PS lipid. Its fluorescent dye-conjugated derivative (Annexin V-FITC) can be used to observe apoptosis by detecting the presence of PS. Annexin V-FITC can also detect necrotic cells as the cell membrane disruption also occurs during this process, hence why the co-staining with propidium iodide (PI) that binds to nucleic acids is performed. Molecules of PI cannot permeate throughout the cell membrane so the dye does not stain genetic material of apoptotic cell which, although fragmented, sustains the membrane integrity.[244]

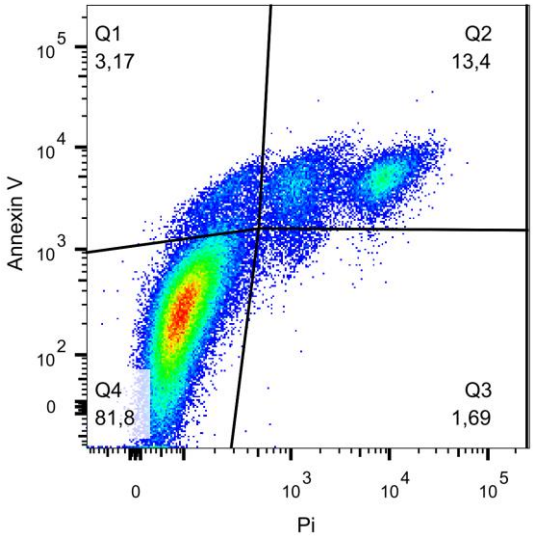

Figure 29. Flow cytometric dot plot example | An example of dot plot graph obtained with flow cytometry technique. During the data analysis the dot plot is divided into four section representing Q4 – live cells (A^-/PI^-), Q1 – cells in early apoptotic state(A^+/PI^-), Q2 – cells in a late apoptotic state(A^+/PI^+) and Q3 – necrotic and dead cells(A^-/PI^+).

($A^{+/-}$ / PI $^{+/-}$) means positive or negative signals from staining with Annexin V (A) and propidium iodide (PI).

RESULTS

■□□□ Synthesis of Silica Shell

β-$NaYF_4$: 2% Er^{3+}, 20% Yb^{3+} @ β-$NaYF_4$: 30% Nd^{3+}, 20% Yb^{3+} nanoparticles, with an average diameter of 28 nm, were used for the synthesis of the silica shell. A modified Ströber method of silica condensation by degradation of TEOS in a basic environment was chosen as a simple and widely applied method for coating various materials in a layer of mesoporous SiO_2.

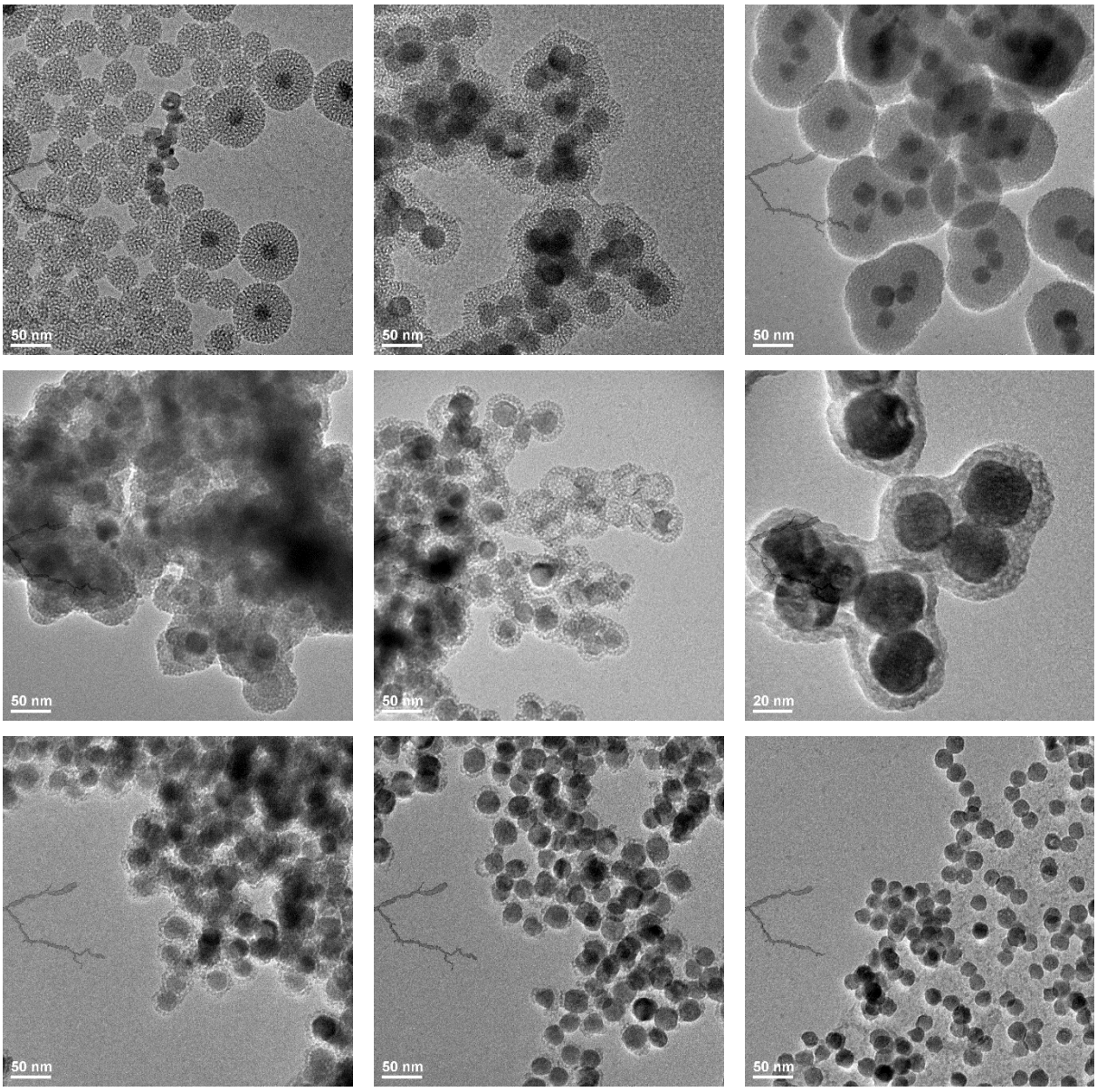

Figure 30. TEM images of unsuccessful synthesis attempts | Images of examples of unsuccessful attempts of synthesis of silica coating obtained via transmission electron microscope.

In total around 194 synthesis attempts were carried out. Only about 21 attempts were successful, accounting for around 10% of all experiments. Examples of TEM images of unsuccessful synthesis attempts are shown on figure 30. Different catalysts were tried. Ammonia, NaOH, L-arginine, and pyridine. According to the reports, different catalyst can impact the diameter of the pores.[92] As there was no observed synthesis efficiency increase for any specific catalyst, sodium hydroxide was chosen as the standard catalyst for most synthesis later during the production of silica-coated nanoparticles. This resulted in mentioned above 21 successful syntheses in form of particles with distinct parameters allowing for further study.

Different thicknesses of silica were obtained by changing the volume of added TEOS. Using 25 µl of TEOS yielded in silica shell of around 20 nm, and thicker shells of around 27-30 nm were obtained with 50 µl of TEOS (figure 31).

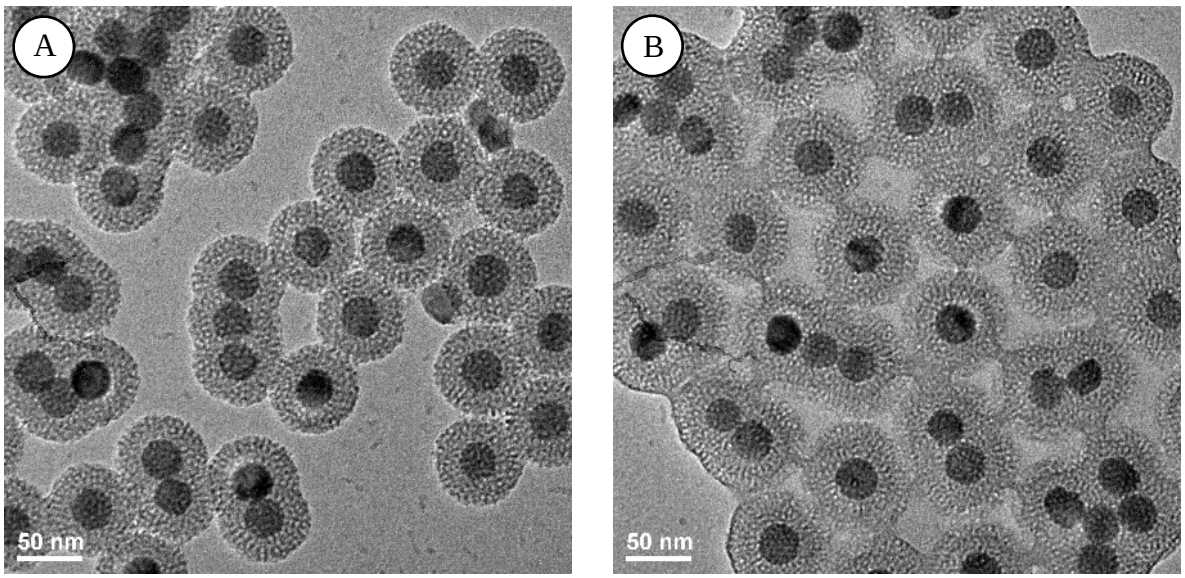

Figure 31. Morphology of silica shell | TEM images of mesoporous silica-coated nanoparticles synthesized under different volumes of TEOS. A) image of 20 nm thick silica obtained with 25 µl TEOS. B) image of around 27 nm thick silica shell obtained with 50 µl TEOS.

Out of the 20 mg of β-$NaYF_4$: 2% Er^{3+}, 20% Yb^{3+} @ β-$NaYF_4$: 30% Nd^{3+}, 20% Yb^{3+} nanoparticles, around 54 mg of 20 nm silica-coated UCNPs were obtained. For the thicker 27-30 nm shell, around 33mg of the sample was collected for further experiments.

■□□□ Protective Properties of Silica Coating

Silica coating on β-$NaYF_4$: 2% Er^{3+}, 20% Yb^{3+} @ β-$NaYF_4$: 30% Nd^{3+}, 20% Yb^{3+} nanoparticles were studied as a potential carrier for small organic molecules and as a protective layer limiting the exposure of these molecules to potentially destructive environmental factors. Due to undergoing parallel experiments at the Institute of Low Temperatures and Structural Research, with cyanine IR-806 dye as a sensitizing antenna enhancing luminescent properties of these $NaYF_4$ nanoparticles, the IR-806 was chosen as the carried molecule (figure 32). Spontaneous degradation over time, exposition to the physical factor of ultraviolet light, and effects of chemical oxidation with reactive oxygen species were studied in the following experiments.

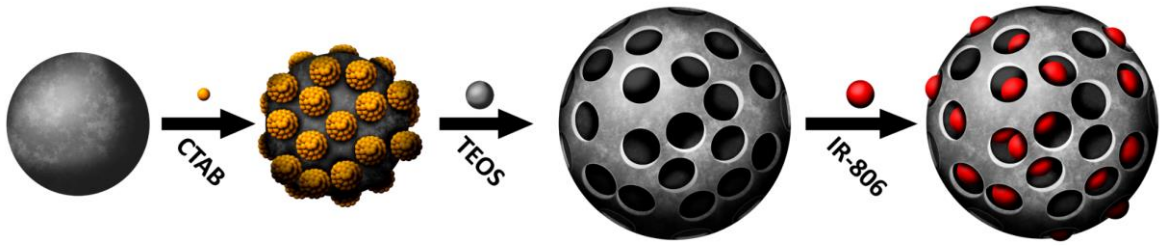

Fig 32. Silica-coating synthesis process and embedding IR-806 dye | Schematic illustration of the synthesis of mesoporous silica *via* the CTAB method and the embedding process of cyanine IR-806 dye used throughout this work.

□□□ Degradation over time

Two series of samples, an aqueous solution and silica-embedded dye with an equivalent amount of IR-806, were studied concurrently with each other to limit any random factors and variations while preparing these samples. Measurements were carried out over time, starting with freshly prepared samples. Spectral properties were then investigated after 48 hours, 6 days, and 13 days (figure 33). Between the experiments, the samples were stored at 4ºC and kept away from light.

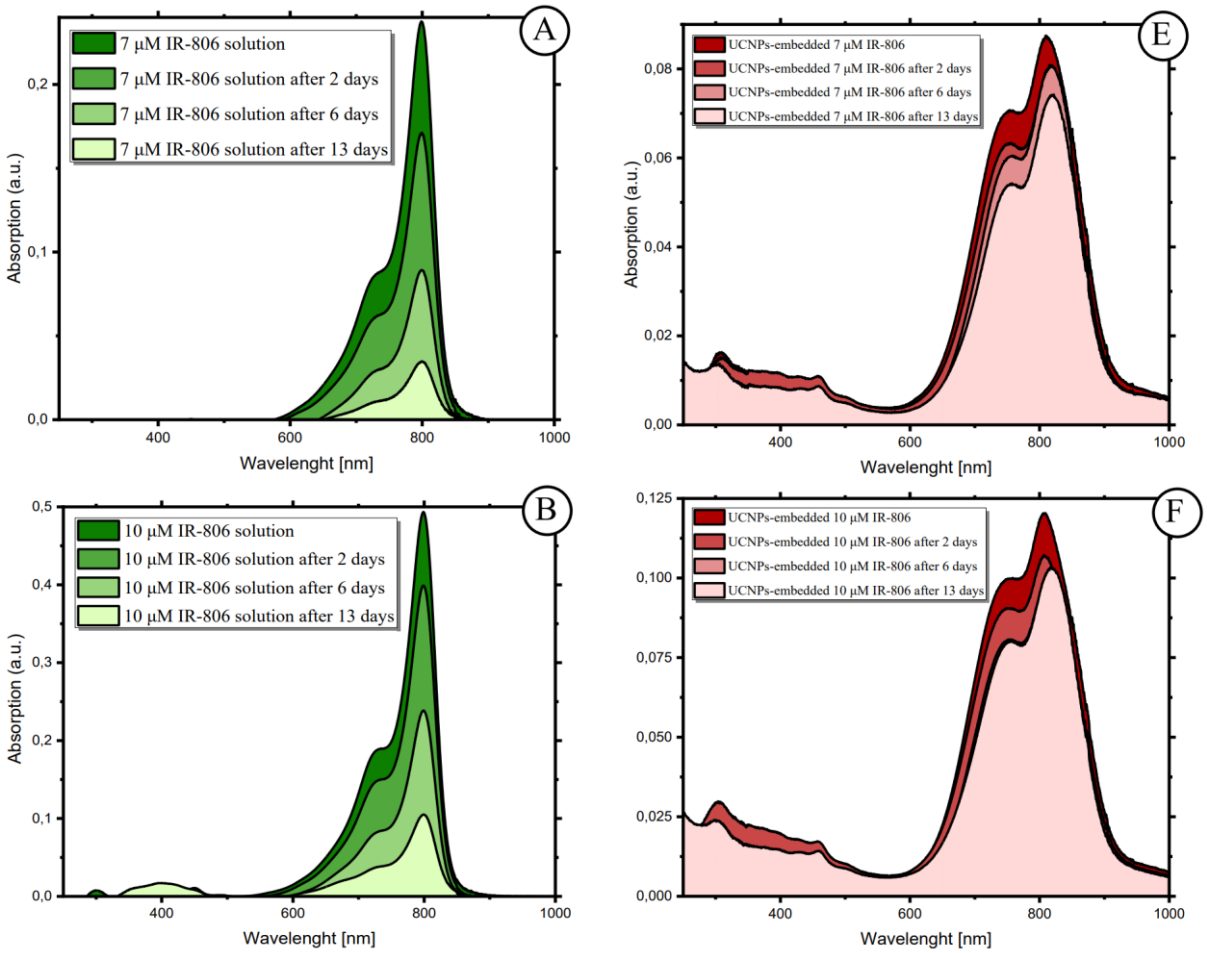

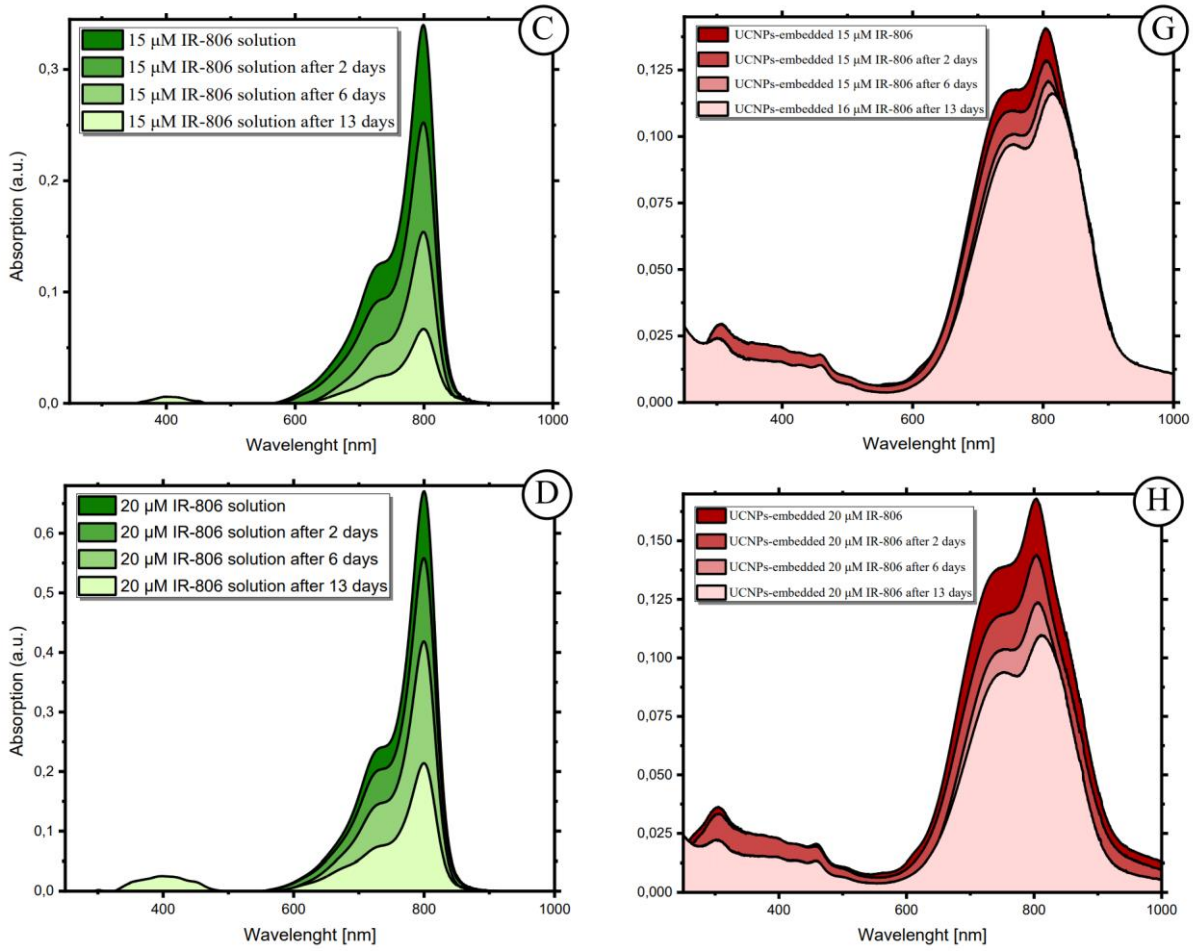

Figure 33. Stability of UCNPs@mSiO$_2$ loaded with various amounts of IR-806 dye | Assessment of IR-806 dye degradation in A-D) water solution and E-H) embedded in a silica shell. Aqueous solutions of standards: 7 nmol, 10 nmol, 15 nmol, and 20 nmol were used as a comparison with silica-embedded counterparts.

An aqueous solution of 7 nmol, 10 nmol, 15 nmol, and 20 nmol of IR-806 dye in 1 mL of water was chosen for the measurements. As well as an equal amounts of IR-806 dye embedded in 675 µg of UCNPs coated in a 20 nm silica shell. After 13 days, on average, about 21% of the photoactive dye remained in the solution (figure 34). The values vary between 33% to 10,6% from the highest and lowest concentration of samples (figure 33). In comparison, the IR-806 embedded in a silica shell showed higher stability, with on average 74% of photoactive dye remaining in a sample after the same amount of time (figure 34). In the case of embedded

dye, the values vary between 77,1% to 64,1% from the highest and lowest concentration of samples (figure 33).

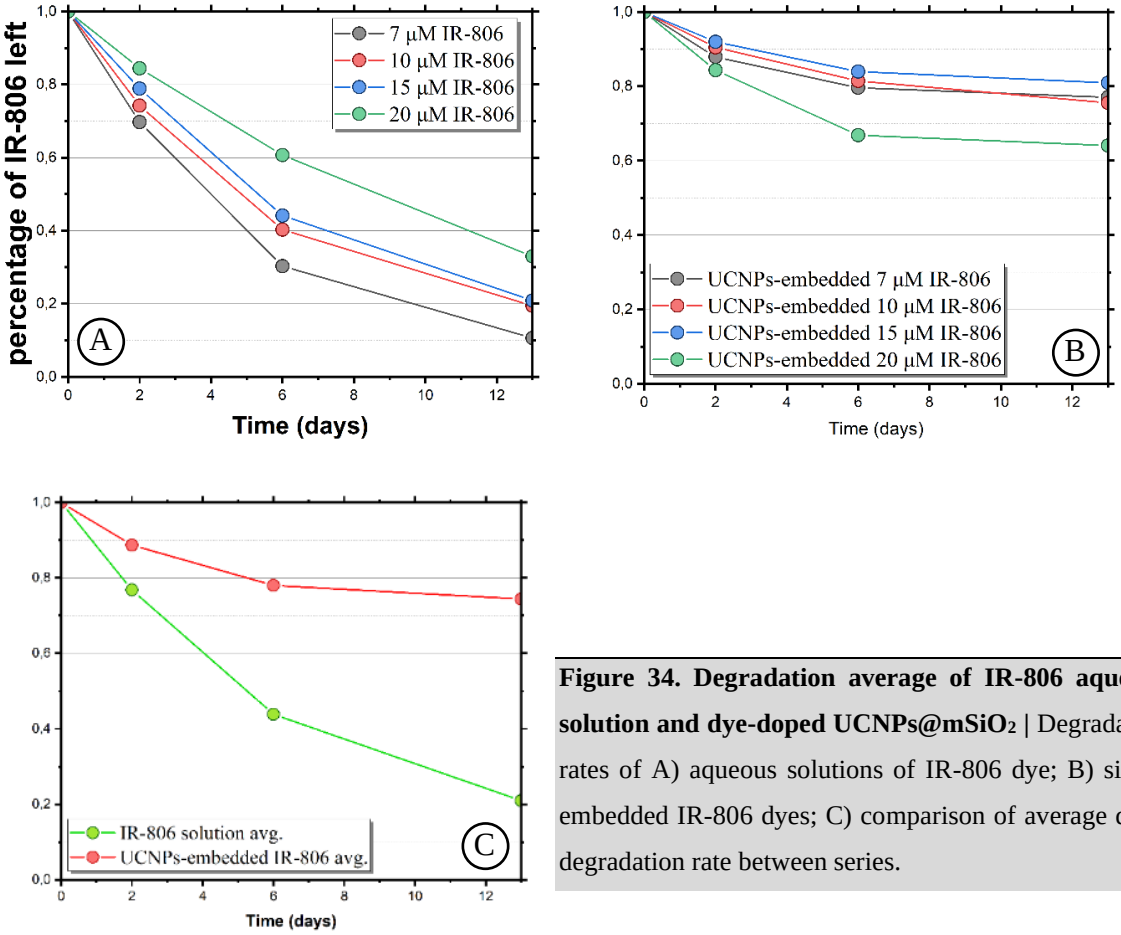

Figure 34. Degradation average of IR-806 aqueous solution and dye-doped UCNPs@mSiO$_2$ | Degradation rates of A) aqueous solutions of IR-806 dye; B) silica-embedded IR-806 dyes; C) comparison of average daily degradation rate between series.

Additional long-term studies of the degradation of dye solution and silica-embedded dye were carried out on separate samples. IR-806 was stored for up to 7 months. After this time, the IR-806 solution was almost completely degraded, leaving around 1% of absorbing dye in comparison to the absorbance of the freshly prepared sample. Analogically, on average, approximately 16% of a silica-embedded dye showed the capacity to absorb near-infrared light (figure 35).

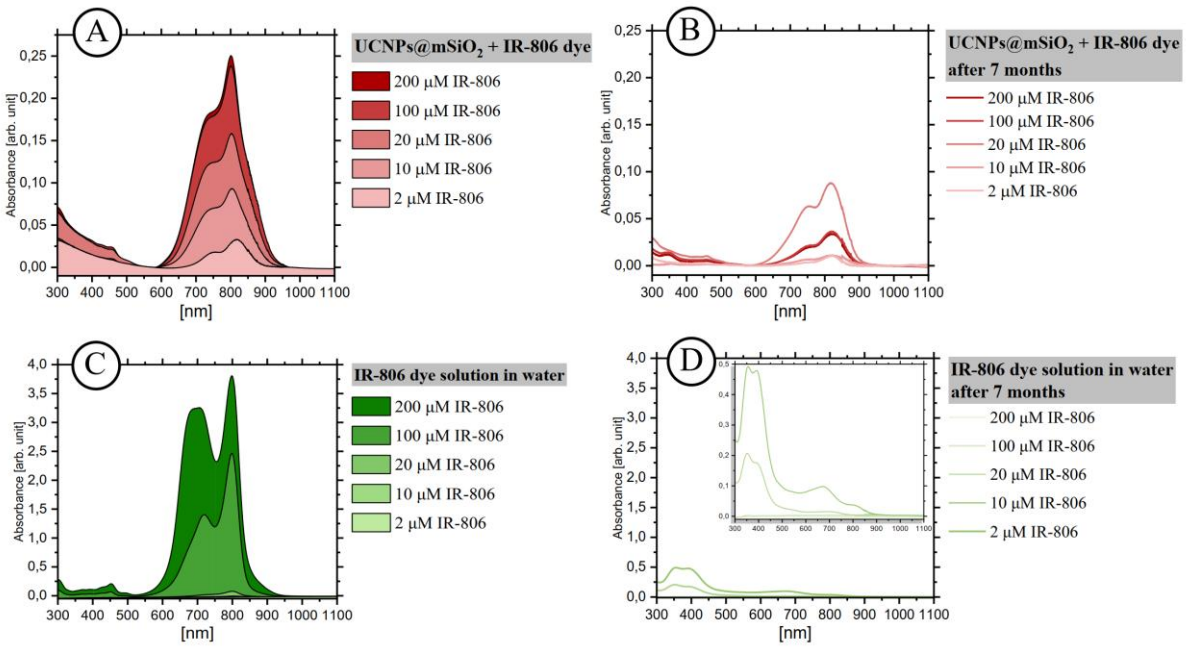

Figure 35. The long-term impact of time on the IR-806 solution and silica-embedded dye | Absorption spectra of A) silica-adsorbed IR-806 dye, B) the same sample of silica-embedded IR-806 dye after 7 months, C) IR-806 dye solution and D) the same sample of IR-806 dye solution after 7 months. For silica-absorbed dye, the values mean initial concentration of IR-806 used for incubation with upconverting nanoparticles.

□□□ Ultraviolet light-induced degradation

Light could be a major limiting factor for many photolabile organic compounds that could be utilized as therapeutic or diagnostic agents. The impact of silica shell on the photostability was studied by exposing samples of aqueous solution and silica-embedded IR-806 dye to ultraviolet radiation. Additionally, the high rates of photodegradation of organic dyes[249] can be a major obstacle to adopting IR dyes as stable sensitizing antennas.

Samples were prepared and stored as in over-time degradation studies described in the previous section. UV lamp with two emissions, 254 and 366 nm, was used as the source of ultraviolet light. Samples were irradiated consecutively for 20, 60, and 120 minutes. In total, samples were exposed for 200 minutes (figure 36).

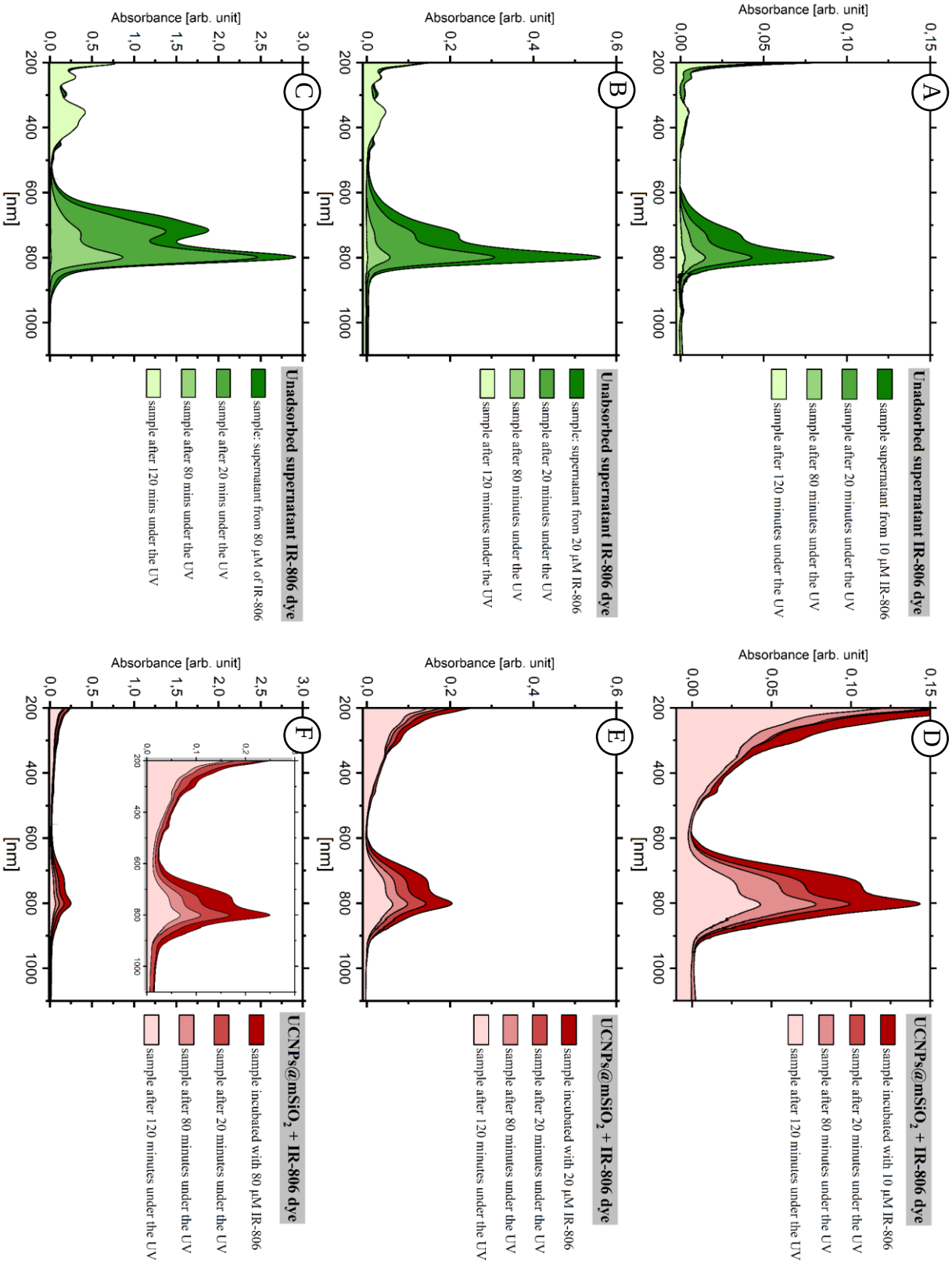

Figure 36. Dynamic of IR-806 degradation under UV light | Absorption spectra for A) 10 μM, B) 20 μM, C) 80 μM solutions of IR-806 dye and UCNPs incubated with D) 10 μM, E) 20 μM, F) 80 μM solutions of IR-806 dye. Samples were exposed to the 254 and 366 nm UV light for 20, 80, and in total 200 minutes.

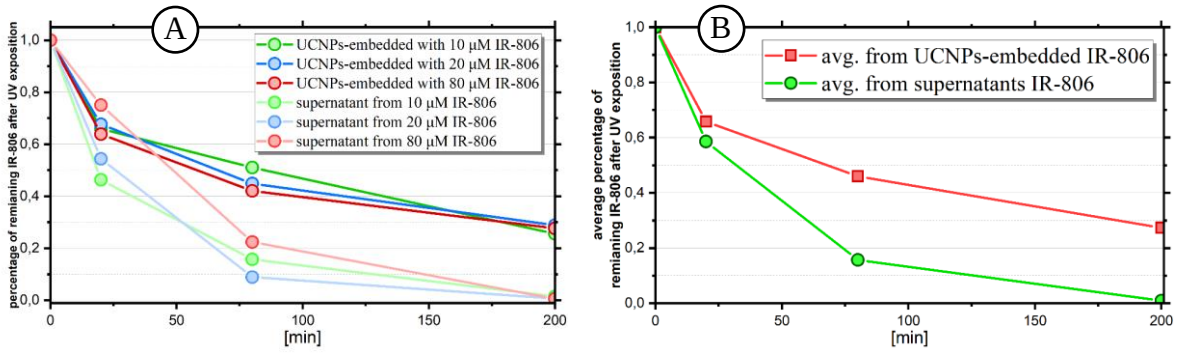

Figure 37. Percentage degradation rates of IR-806 exposed to UV light | Chart presents the dynamic of degradation of dye under UV light for selected samples. A) degradation of 10 µM (green lines), 20 µM (blue lines), and 80 µM (red lines) aqueous solutions of IR-806 dye. Dark lines represent silica-embedded dye. Bright lines represent separated supernatant with a solution of the dye. B) Combined average dynamic of degradation under UV. Green line represents silica-adsorbed dye samples, red line represents an average of supernatant solutions.

After the total exposition time, approximately 1% of photoactive IR-806 was left in all samples of water-dissolved IR-806 dye. Comparatively, after 200 mins of ultraviolet irradiation in the same conditions, around 27% of photoactive IR-806 remained embedded in the silica shell of upconversion nanoparticles (figure 37).

□□□ Chemical degradation

Reactive oxygen species (ROS) are destructive factors of biological structures and are generated by the metabolism of the cell itself, they are very abundant in extra- or intracellular environments.[250] ROS are destructive towards organic dyes, reacting with structural elements involved in the absorption and emission of the given molecule.[251]

Silica coating was studied for its potential anti-oxidative properties. A series of samples of silica-embedded dye and a solution of dye were incubated with H_2O_2 as an example of reactive oxygen species present in the extracellular matrix and cytoplasm of the cell.[252] Series of silica-embedded dye and the aqueous solution of the IR-806 were studied by incubation in the presence of hydrogen peroxide.

After 60 minutes of incubation at a higher concentration of 440 mM H_2O_2, around 33% of aqueous dye and 28% of silica-adsorbed dye remained spectrally active. Both solution and silica-embedded dye degraded at similar rates (figure 38), which suggests that silica does not protect against ROS, and subsequently other reactive chemical compounds.

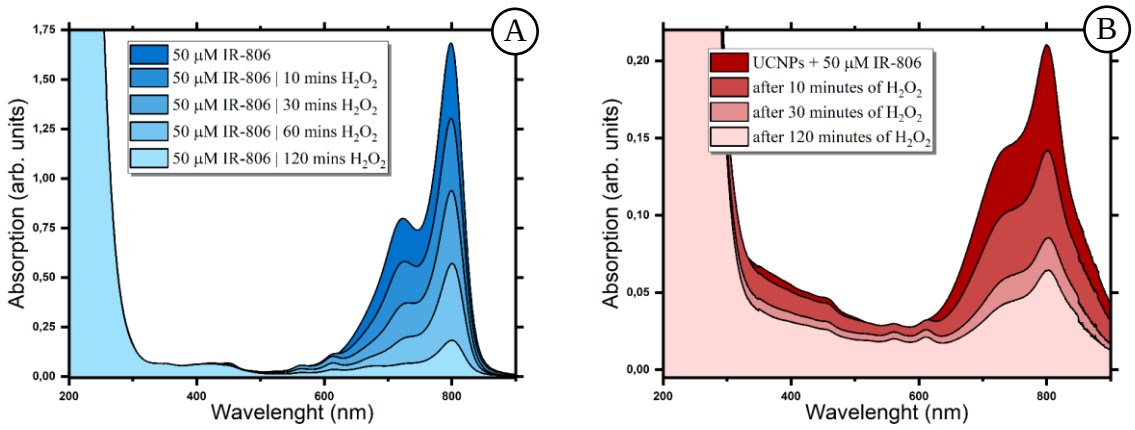

Figure 38. Chemical degradation of IR-806 exposed to high concentration of H_2O_2 | Absorption spectra of A) 50 µM dye solution and B) UCNPs@$mSiO_2$ silica-embedded dye incubated with 50 µM of dye solution. Experiments performed with 50 µl of highly concentrated 30% (440 mM) H_2O_2 solution. Experiments carried for two hours.

Complementary studies with a physiological concentration of 1 mM to mimic upper limits in an extracellular matrix[252] of concentration of hydrogen peroxide, were carried out (figure 39). As with high H_2O_2 concentration samples, degradation rates remained at a similar

level. Silica-embedded dye absorption decreased to 65,82% for the silica-embedded IR-806, and free dye solution decreased to 66,17% of the initial intensity of absorption.

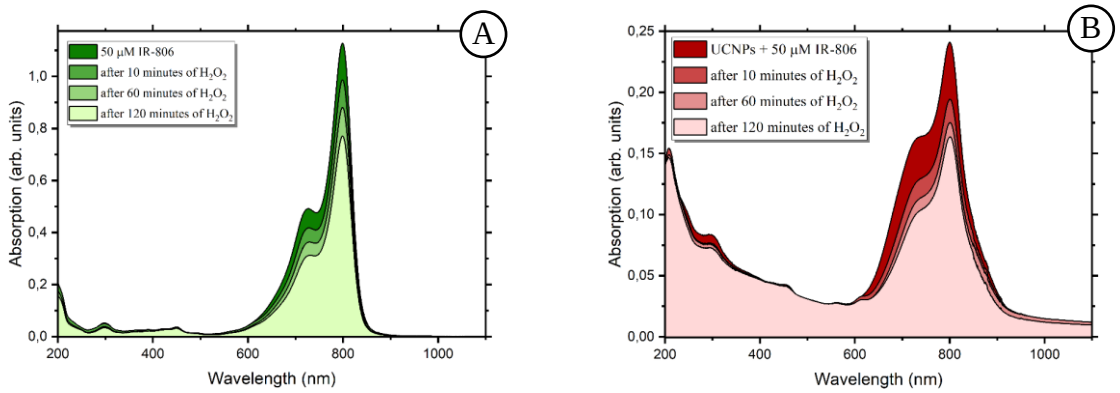

Figure 39. Chemical degradation of IR-806 exposed to extracellular levels of H_2O_2 | Absorption spectra of A) 50 µM dye solution and B) UCNPs@$mSiO_2$ silica-embedded dye incubated with 50 µM of dye solution. Experiments performed in 1 mM of H_2O_2 akin to the threshold of extracellular concentration of hydrogen peroxide for induction of apoptosis. Experiments carried for two hours.

Samples of incubation with 1 mM H_2O_2 were then kept for the next 12 days at 4ºC, and in the dark, to investigate any potential long-term impact of reactive oxygen species on the payload embedded in pores of silica layer (figure 40).

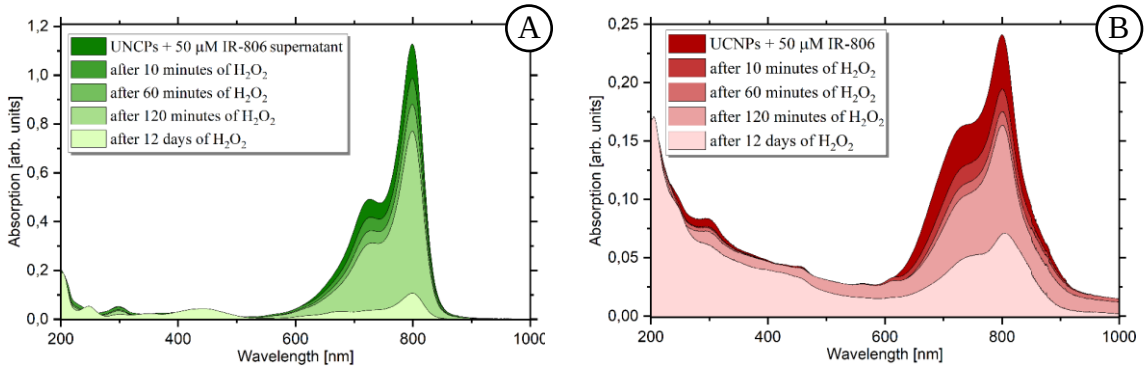

Figure 40. Long-term chemical degradation of IR-806 exposed to extracellular levels of H_2O_2 | Extension of experiment presented in figure 33. Absorption spectra of A) 50 µM dye solution and B) UCNPs@$mSiO_2$ silica-embedded dye incubated with 50 µM of dye solution. Experiments carried for additional 11 days. Experiments performed in 1 mM of H_2O_2 akin to the threshold of extracellular concentration of hydrogen peroxide for induction of apoptosis.

For the silica-embedded dye, about 32,25% of the IR-806 was left. In comparison around 9,81% of the dye in the solution was left. Considering the results of time-dependent degradation, the presence of hydrogen peroxide caused significant degradation of silica-embedded dye. From 64,1% remaining after 12 days of storage, to 32,25% in parallel 13 days old sample with H_2O_2. A similar effect was observed for the free dye molecules in the solution. The remaining dye dropped from 33% of the original quantity to 9,81%.

These results suggest that mesoporous coating of nanoparticles is not an efficient approach to protect, sensitizing agents, diagnostic compounds, therapeutic drugs, or other carried molecules, from a highly reactive environment.

■□□□ Cytotoxicity

THP-1, a monocyte-like cell line isolated from an acute monocytic leukemia patient, MDA-MB-231 epithelial-like line isolated from an adenocarcinoma patient, and an epithelial-like A375 line from a patient with malignant melanoma, were obtained from the collection of Institute of Immunology and Experimental Therapy and were selected for the cytotoxic experiments. These cell lines correspond to original American Type Culture Collection (ATCC) lines. Different silica-coated, as well as uncoated core- and core@shell-type of $NaYF_4$ nanoparticles, were used for cytotoxic assessment. The concentration of nanoparticles ranged from 20 to 200 μg/mL across all experiments. Cells were stimulated for 24 hours.

□□□ MTT assay assessment of cytotoxic effect of core, core@shell, and silica-coated UCNPS on the THP-1 and MDA-MB-231 lines.

For the macrophage-like THP-1 cell line, smaller core-type nanoparticles increased proliferation on average by 9% and up to 17% in the highest tested concentration in the experiments. The impact of the bigger core@shell-type UCNPs was higher, reaching on average 17% of increment over the control sample and up to 28% in the highest tested concentration (figure 41A). Before the stimulation, all monocyte-like THP-1 were treated for 72 hours with PMA to stimulate macrophage-like differentiation of the cells.

For the epithelial-like MDA-MB-231 cell line, stimulatory properties for both core- and core@shell-type nanoparticles were not observed (figure 41B).

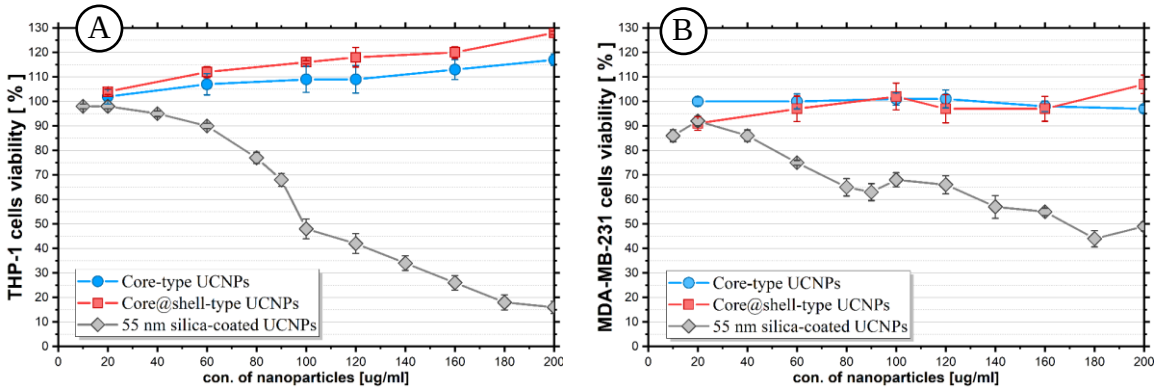

Figure 41. THP-1 and MDA-MB-231 viability after stimulation | Cytotoxic effect of core, core-shell, and silica-coated nanoparticles on the A) THP-1 and B) MD-MB-231 cell cultures after 24 hours of stimulation with various concentrations of nanoparticles.

Stimulation with 55 nm silica-coated upconversion nanoparticles showed significant cell toxicity of these nanoparticles (figure 41). Compared to the untreated control group, the viability of the THP1 cell culture decreases to 16% for the highest chosen concentration (200 µg/mL), while MDA-MB-231 drops to 49% of the control group.

□□□ MTT assay assessment of cytotoxic effect of 55 nm and 96 nm silica-coated nanoparticles and IR-806 dye on a THP-1 and A375 cell line.

The macrophage-like THP-1 cell line was selected for the cytotoxicity experiments involving various sizes of silica shell. Nanoparticles 55 nm and 96 nm core@shell-type $NaYF_4$ of the same composition, with two different sizes of silica shell, were chosen (figure 42).

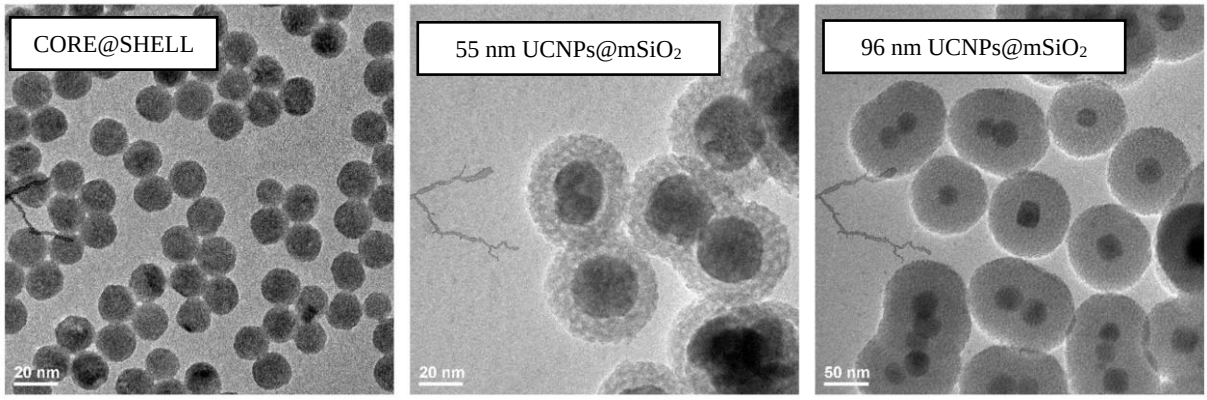

Figure 42. Nanoparticles used in cytotoxicity experiments | TEM images of uncoated and silica-coated nanoparticles used.

The THP-1 cell cultures were stimulated for 24 hours with 55 and 96 nm silica-coated $NaYF_4$ nanoparticles (figure 43). As seen with the results in the preceding section, the 55 nm nanoparticles exhibit highly toxic nature. Cell viability dropped sharply above concentration of around 40 μg/mL. In contrast, the 96 nm nanoparticles do not induce clear cell death during 24 hours stimulation of cell culture with the concentration up to 200 μg/mL.

The human melanoma A375 cell line was selected for additional cytotoxicity experiments involving various sizes of silica shell as well as assessment of cytotoxicity of IR-806 dye used is studies as a potential luminescent enhancing antenna from UCNPs (figure 44). Cells were stimulated for 24 hours. Various volumes of stock suspension of 200 μg/mL silica-coated NPs with 1.33 μM of embedded IR-806 dye were used for all experiments. In all samples, IR-806 is embedded into the mesoporous structure of the silica. The concentration of

embedded dye was chosen based on the loading capacity of mesoporous silica, to avoid the presence of any free molecules in the solution. layer.

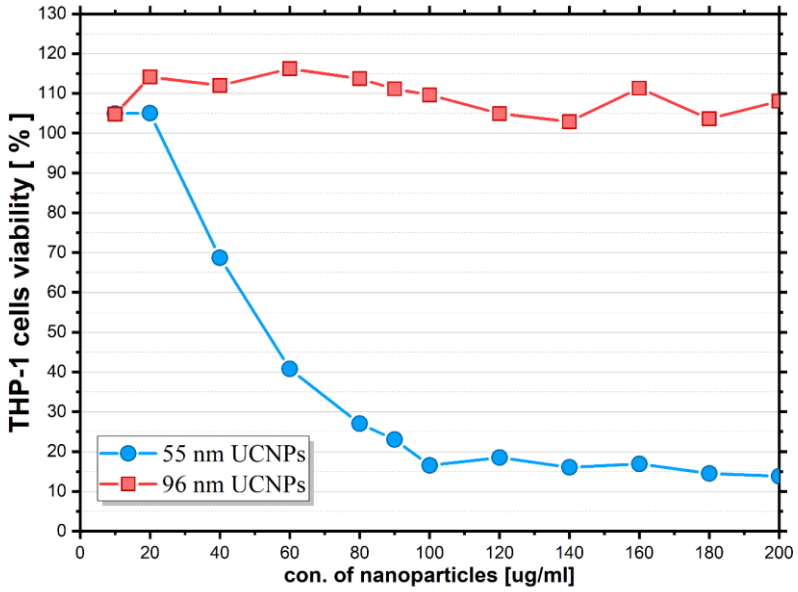

Figure 43. THP-1 cells viability after stimulation with different-sized UCNPs | Cytotoxic effect of 55 nm (blue line) and 96 nm (red line) silica-coated lanthanide-doped $NaYF_4$ nanoparticles.

Similarly, to the results of THP-1 and MDA-MB-231 experiments, the 55 nm silica-coated upconverting nanoparticles reduced the viability of the A375 cells. There was no observed additional cytotoxic effect from the dye embedded in the silica layer (figure 44A and B). For the thicker coating on 96 nm UCNPs@$mSiO_2$, there was no major cytotoxic effect observed in both, the dye-free nanoparticles and silica-embedded dye in nanoparticles.

Media-dissolved dye did not impact the viability of cell culture (figure 44C). No significant cytotoxicity of IR-806 dye was observed in all samples up to the concentration of 50 μM.

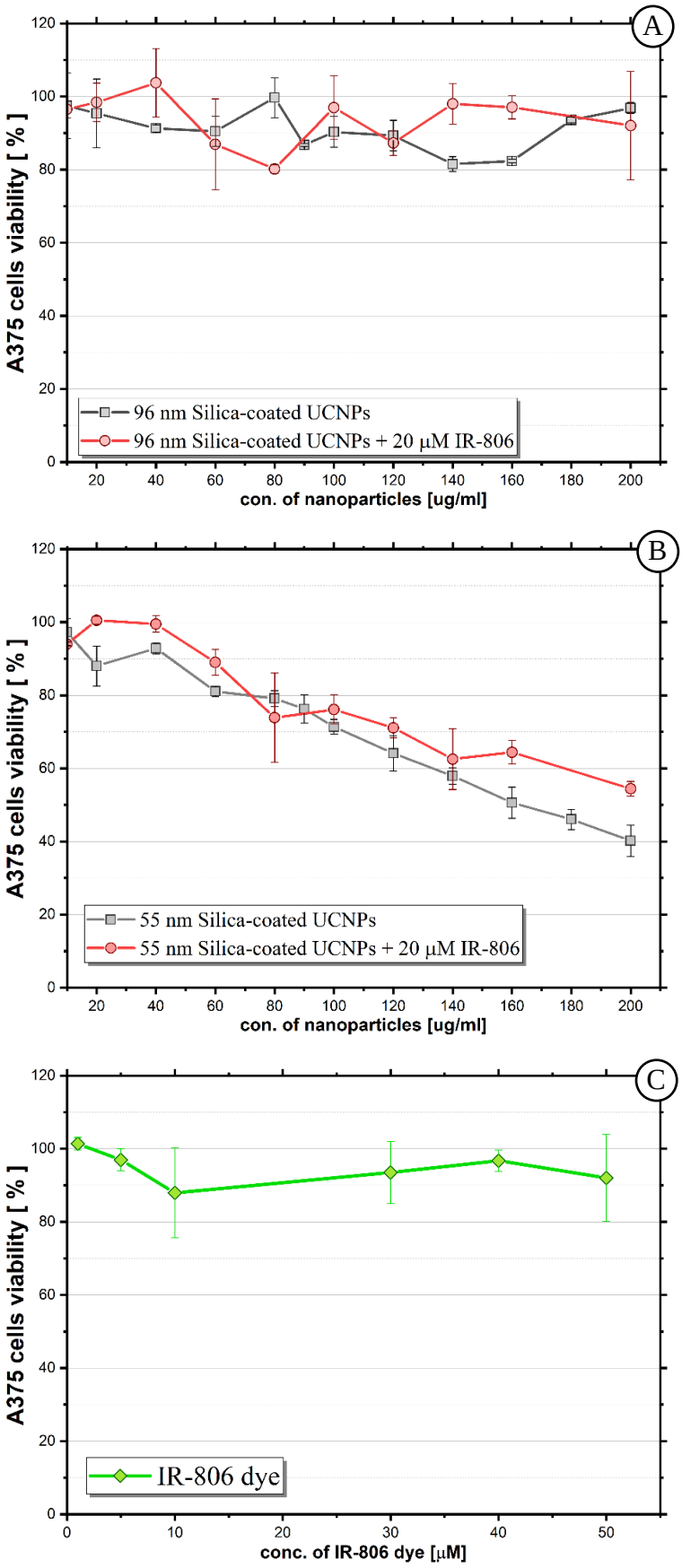

Figure 44. A375 cells viability after stimulation with UCNPs and IR-806 | Cytotoxic effect of A) 55 nm and B) 96 nm silica-coated nanoparticles as well as C) IR-806 dye solution. Experiments with UCNPs were carried for both UCNPs alone and UCNPs with silica-embedded IR-806 dye.

□□□ Flow cytometry

MTT assay gives a general overview of the viability of the cells, stimulated with a potentially toxic factor, without distinguishing between types of the cellular death. It cannot be used to assess if $NaYF_4$@$mSiO_2$ nanoparticles induce necrotic or apoptotic processes. Because of it, a flow cytometry method was used. Experiments were performed on macrophage-like THP-1 cell line. Cells were incubated with 55 nm and 96 nm silica-coated NaYF4 nanoparticles at the concentration of 90 µg/mL based on the toxicity of THP-1 assay (figure 41, page 74). Cells, with silica-coated UCNPs, were incubated for 24 and 48 hours before the analysis. Table 2 (page 80) presents statistical average from four separate experiments.

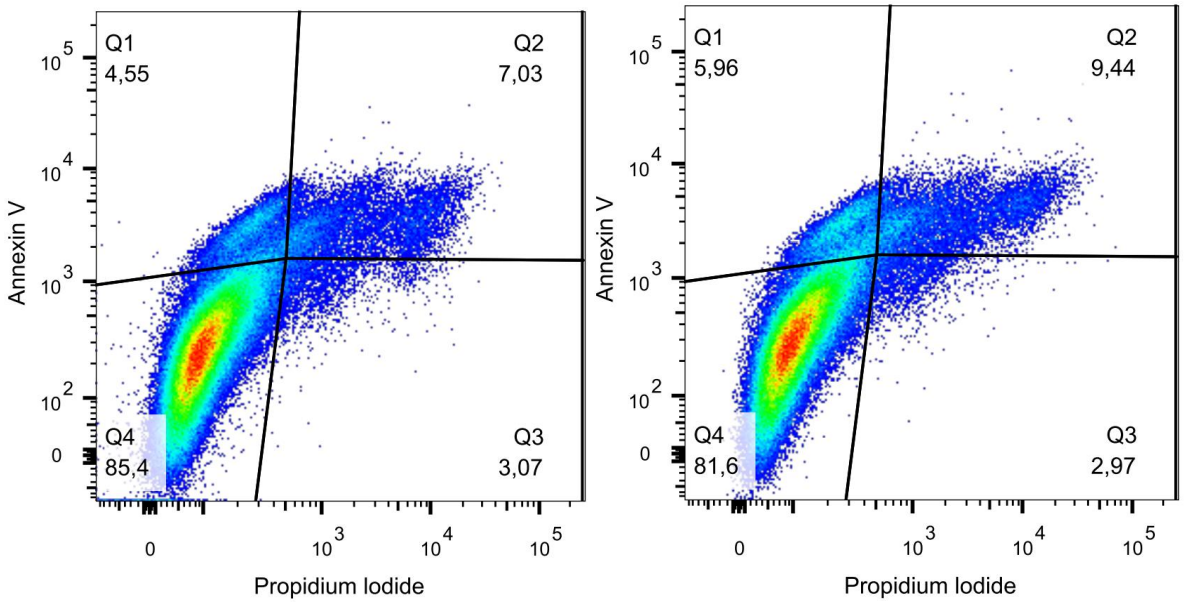

Figure 45. Control group | Dot plots of THP-1 control samples after 24 (left) and 48 (right) hours.

The control sample (figure 45) showed a healthy population of cells after 24 hours and 48 hours of culturing in flow cytometry tubes in the volume of 500 µL. The number of cells in the early and late apoptotic state as well as necrotic cells was low. After two days, around 87% of cells were not stained by Annexin V or propidium iodide, indicating that the control culture was in good condition.

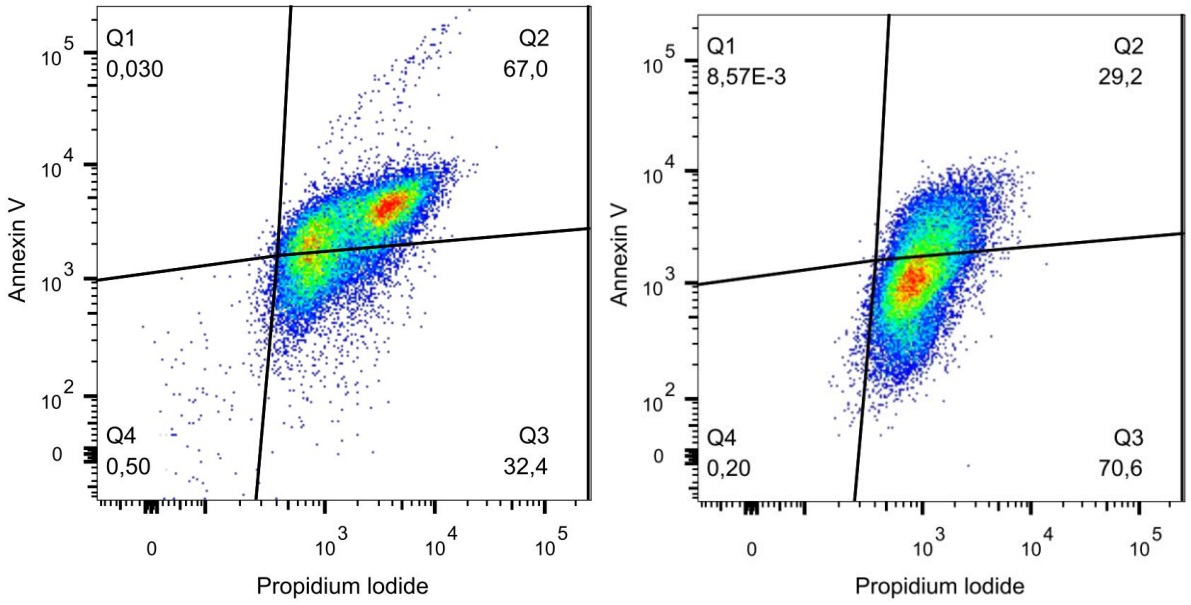

Figure 46. Stimulation with 55 nm UCNPs@mSiO₂ | Dot plots of samples of the THP-1 cells treated with 55 nm silica-coated nanoparticles. Samples analysed after 24 (left) and 48 (right) hours.

The 55 nm, in diameter, silica coated $NaYF_4$ upconversion nanoparticles showed significant toxicity by inducing apoptosis after 24 hours of incubation (figure 46). On average 34% of cells stained positively for both Annexin V and PI indicating necrosis. Around 57% of cell population was in late apoptotic stage. Less than 10 percent of cells were both Annexin- and PI-negative. After 48 hours almost 60% of population was in the necrotic state while 39% exhibited late apoptotic features.

The 96 nm, β-$NaYF_4$: 2% Er^{3+}, 20% Yb^{3+} @ β-$NaYF_4$: 30% Nd^{3+}, 20% Yb^{3+} @ $mSiO_2$ UCNPs exhibited toxicity as well, however, the toxicity exhibited was less than 55 nm counterparts in the first 24 hours of exposition. After 24 hours of incubation (figure 47), apoptosis was detected in around 57% of population, for both early and late stage apoptosis. About 37% of cells did not bind Annexin V or stained with PI, indicating integrity of the cells and an overall good condition. Only less than 6% of population showed signs of necrosis. On the other hand 48 hours of incubation presented a quite significant jump in toxicity. Less than

two percent of the cells showed non-necrotic or –apoptotic features. Around 88% of the cell population was in the late apoptosis stage while 10% exhibited necrotic markers.

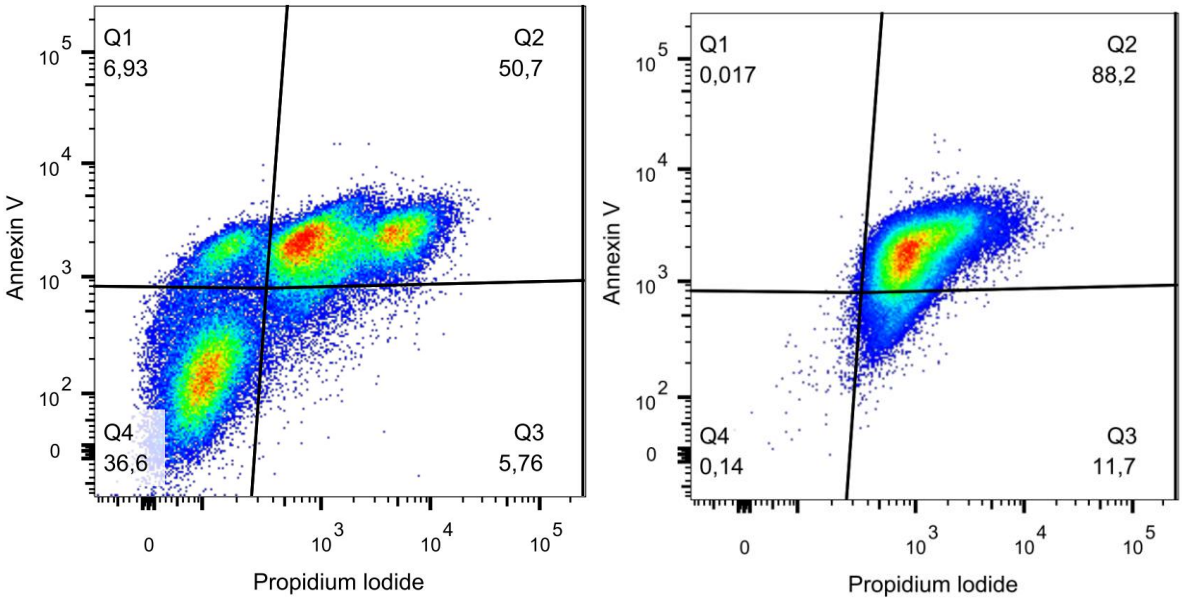

Figure 47. Stimulation with 96 nm UCNPs@mSiO₂ | Dot plots of samples of the THP-1 cells treated with 96 nm silica-coated nanoparticles. Samples analysed after 24 (left) and 48 (right) hours.

Name of the group and time	**Stage**			
Control groups	**Early apoptotic**	**Late apoptotic**	**Necrosis**	**Live cells**
24 hours	6,7%	13,3%	2,1%	77,8%
48 hours	4,2%	6,2%	1,9%	87,6%
Stimulation with 96 nm UCNPs@mSiO₂	**Early apoptotic**	**Late apoptotic**	**Necrosis**	**Live cells**
24 hours	8,8%	48,2%	5,9%	37,1%
48 hours	0,4%	87,5%	10,3%	1,7%
Stimulation with 55 nm UCNPs@mSiO₂	**Early apoptotic**	**Late apoptotic**	**Necrosis**	**Live cells**
24 hours	0,1%	57,2%	34,2%	8,5%
48 hours	0,0%	39,5%	58,7%	1,7%

Table 2. Average percent of population at different stages of apoptosis | Table presents the average percentage values of cells in different stages of UCNPs-induced apoptotic process.

□□□ Light microscopy imaging of UCNPs-treated THP-1 cells

The morphology of THP-1 cells treated with 55 nm and 96 nm upconversion $NaYF_4$ nanoparticles was assessed with an inverted light microscope Nikon Eclipse Ti2. Images were captured with NIS-Elements software.

Cells were cultured at the density of 2×10^5 cells per 500 µL of media. Cells were stimulated with 55 and 96 nm UCNPs at the concentration of 90 µg/mL to mirror the cytotoxicity assessment done with the flow cytometry described in a previous section.

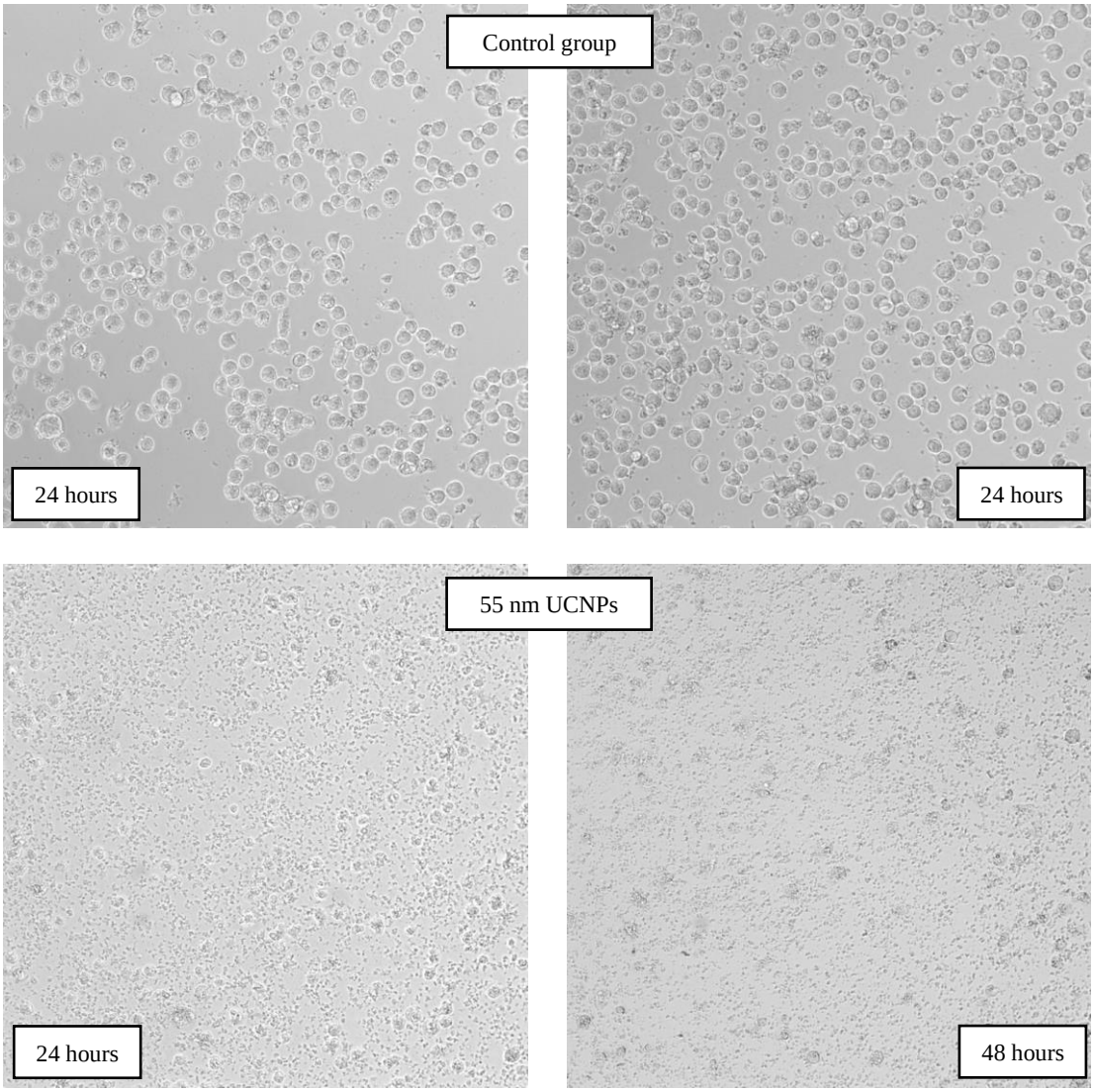

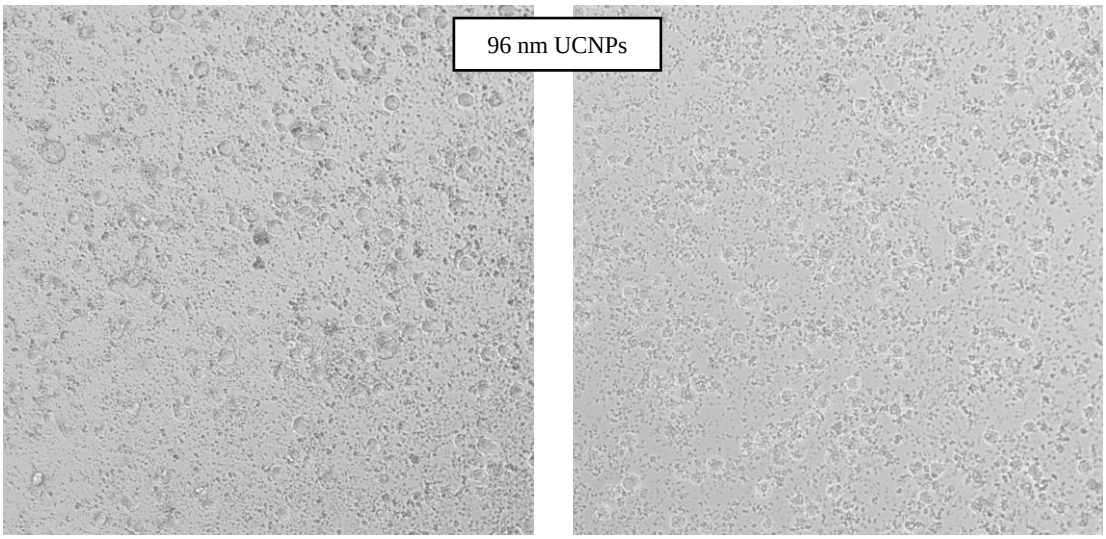

Figure 48. Microscopy images of THP-1 cells treated with $NaYF_4$ nanoparticles | Microscope images of THP-1 cells. Samples were analysed after 24 (left) and 48 (right) hours. Control group (upper images), 55 nm (middle images) and 96 (lower images) nm silica-coated nanoparticles.

Microscope imaging, presented in the figure 48, shows significant cellular membrane integrity disruption in all performed experiments in comparison to the control group untread with silica-coated nanoparticles. These results align with the results obtained with flow cytometry. After 24 hours of stimulation with both 55 and 96 nm nanoparticles, a clear cytotoxic effect can be observed. Both cell cultures contain significant amount of small bodies, presumably apoptotic bodies previously detected in flow cytometry measurements. The visual inspection with the microscope after 48 hours, showed that most of the cells treated with 55 nm UCNPs@$mSiO_2$ fragmented into smaller bodies. For the simulation with 96 nm nanoparticles, a few structurally undisrupted cells could be still observed while most of the sample contained smaller vesicles.

DISCUSSION

A new tool, based on $NaYF_4$ upconverting nanoparticles, for therapy and diagnostics (often combined in an emerging field of theranostics), bioimaging,[30,101,102] biosensing, [103–106] and other applications[4] mentioned in section *Application of Upconversion Nanoparticles* (page 27) could provide significant benefits over presently used fluorescent dyes, proteins, and other kinds of detection molecules.[25]

The lack of a photobleaching effect present in many organic dye and fluorescent proteins makes the $NaYF_4$ promising option for long-term imaging and observation of a studied subject. The cytotoxicity of the $NaYF_4$ nanoparticles, given an adequate surface modification strategy applied, is less than of the other small fluorescent objects that gained traction on recent years, quantum dots.[24,253] The upconversion phenomena displayed by the $NaYF_4$ nanoparticles removes some of the background noise.[131] The volume of noise generating visible light is limited to the light emitted by nanoparticles. The reduction stems from the usage of near-infrared light which is absorbed less by the various cellular structures of a tissue.[132] As previously mentioned, surface modifications, which were described in more details in the *Surface Modification of $NaYF_4$ Nanoparticles* section (page 18), offer a wide scope of approaches in rendering the nanoparticles more biocompatible. Silica-coating is especially an interesting approach as the shell is resistant to chemical and physical factors and it can be designed with a porous structure that is capable of adsorbing various molecules.[93,94] These molecules could include drugs, labelling agents and *etc*.[163–166]

For all of the reasons listed above as well as other more specific properties of $NaYF_4$ upconverting nanoparticles and silica coating mentioned throughout introductory sections, this

work aimed to focus on preliminary assessment of silica-coated $NaYF_4$ upconversion nanoparticles as a stable and reliable platform for delivering specific molecules.

The 23 nm core- and core@shell-type of $NaYF_4$ nanoparticles, doped with Er^{3+}, Nd^{3+}, and Yb^{3+} ions were synthesized following a previously established protocols by the group at the Włodzimierz Trzebiatowski's Institute of Low Temperature and Structure Research in Wrocław. In this dissertation, the obtained nanocrystals were coated with a layer of porous silica *via* the modified Strober method of tetraethyl orthosilicate (TEOS) hydrolysis. The low success rate, of about 10%, of silica syntheses of the nanoparticles may suggest that TEOS is not a suitable precursor compound for this kind of surface modification, or the method of synthesis requires major evaluation and the investigation of alternative techniques that will ensure a more uniform coating in conditions of synthesis that can be easier manipulated.

The pores of the silica structure were used to host infrared IR-806 cyanine dye. Potential protective characteristics of various factors were studied. In comparison to an aqueous solution, adsorption to the silica lowered the rate of the spontaneous degradation of IR-806 stored in dark and cold conditions. Active attempts of degradation by the utilization of UV light were performed. Investigation with UV source of light producing 254 and 366 nm UV wavelengths was chosen. As with the spontaneous degradation, silica-coating lowered the destruction of IR-806 molecules embedded in the mesoporous structure. Opaque characteristics of suspension suggest that the silica coating may scatter the light and thus protect the load by reducing the number of photons reaching it.

Chemical-based degradation is the second major concern studied in the context of the protective properties of silica coating. Obtained experimental data shows that silica does not protect IR-806 molecules from reactive oxygen species. H_2O_2 was chosen as an example of ROS. The degradation rate remained similar to the degradation of water-dissolved dye, suggesting that silica-coating does not protect against these chemical factors. These results suggest that the silica shell should not be employed for payloads susceptible to chemical environment.

The silica-based delivery system can be used for the protection of molecules susceptible to physical factors such as light-induced degradation, but it will not be as effective in a scenario where there are reactive molecules in the environment.

Silica-coated $NaYF_4$ nanoparticles of around 55 nm, could be suitable for biological application. The MTT assay results show a high cytotoxic effect of all tested cell lines. Within a 24-hour stimulation period, THP-1, MD-MB-231, and A375 cell cultures showed a major decrease in the number of living cells. The flow cytometry analysis showed that 55 nm UCNPs@$mSiO_2$ induces apoptosis of macrophage-like THP-1 cell line in the first 24 hours of stimulation and by the 48 hour most of the population enters the necrotic stage. The cytotoxic effect could be a result of the internalization *via* the caveolin-mediated endocytosis pathway which subsequently induced some signals for apoptosis. However, this would require further investigation into the subject by employing antibody cytometry or Western-blot-based methods of to detect various apoptotic factors. Currently, the silica-coated UCNPs with diameter of 55 nm induced apoptosis. An additional step, such as coating in a thin layer of polymer or specific protein corona, must be used to ensure a high biocompatibility necessary for the utilization of the nanoparticles in medicine.

The lack of cytotoxic effect from the sub-20 nm nanoparticles, without silica coating, could come from the non-specific internalization of such small nanoparticles. Internalization without specific membrane and cytoplasmic proteins would not induce apoptotic signaling. Uncoated $NaYF_4$ nanoparticles with their ligands removed, showed to induce cellular division of the THP-1, MD-MB-231 cancer-derived cell cultures. This would have to be further researched due to two puzzling aspects, the first being the induction of more frequent cellular division in comparison to the control group, and the second relates to the fact that as the nanoparticles could degrade there would be a release of lanthanide and fluoride ions that could negatively affect viability of the cultures.

Substantially bigger nanoparticles of around 96 nm in diameter, showed neither a negative nor positive impact on the viability of the THP-1 and A375 cell cultures during the 24 hour of stimulation with the MTT assay method. However, this could be a result of the reduced toxic effect of the 96 nm UCNPs@ $mSiO_2$ in comparison to their 55 nm counterparts. The flow cytometry study showed that after 24 hours, the population of THP-1 cells were still in a viable condition and were not expressing markers of late stage apoptosis or necrosis. Metabolically active cells in the early stages of apoptosis were shown to metabolize MTT.[254] Flow cytometry results after 48 hours showed a clear induction of apoptotic pathway as the most population shows signs of late-stage apoptotic or necrotic state. Particles of around 100 nm in size are reported to penetrate the cellular membrane *via* the Clathrin-mediated endocytosis, with an ease that can be observed with their smaller counterparts.[255] Further research into internalization would require a specialized microscope with a source of IR light for the detection of nanoparticles and assessing their presence or lack in the cytoplasm, as well as an inquiry into

changes in expression levels of the protein component of the clathrin-mediated endocytic system.

These results align with other reports that showed a cytotoxic effect from smaller sub-40 nm nanoparticles, where the viability of bone marrow-derived mesenchymal stem cells (BMSCs) and myoblast cells cultures, dropped below 70%, 66.8% for the BMSCs and 68.2% for skeletal myoblasts.[225] Regarding the 10-100 nm size range of typical $NaYF_4$ nanoparticles (figure 20), multiple reports have shown that ~80 nm UCNPs either do not cause cell death of L929 fibroblast cell line[165] or that the cell cultures of L929 maintain 80% of cell viability after the period of 24 hours of incubation.[256]

The results presented in this work, as well as reports cited throughout it, could indicate the existence of a cytotoxic peak for silica-coated $NaYF_4$ upconversion nanoparticles, or nanoparticles in general, related to unspecified size-dependent cellular mechanism of endocytosis. That peak would exist somewhere around the diameter of 50 nm.

Further inquiry into this subject is necessary for developing a viable diagnostic or therapeutic tool based of $NaYF_4$ upconversion nanoparticles.

CONCLUSIONS

1. Synthesis of the silica shell *via* TEOS condensation method in a basic environment is a suitable approach for an efficient coating of the kind of UCNPs used in this work, although the catalysis conditions need further improvements.

2. Exposure to damaging UV radiation showed that silica-coating on nanoparticles protects photolabile IR-806 dye against light.

3. Long-term storage in a cold environment without access to light showed that the mesoporous structure of silica-coating slowed down the spontaneous degradation of carried IR-806 dye.

4. Silica-coating was not a suitable approach for the protection of carried molecules that are susceptible to reactive elements present in the environment.

5. Cytotoxicity experiments showed that 55 nm nanoparticles coated in a silica shell caused the induction of apoptosis within the 24 hours-long stimulation period and by 48 hours cell population is mostly necrotic. In contrary to the 55 nm UCNPs@$mSiO_2$, smaller uncoated nanoparticles did not show cytotoxic effects within 24 hours of stimulation. The 96 nm nanoparticles with a thicker silica coating exhibited a strong cytotoxic effect after 48 hours of stimulation. These results may suggest a range, centred around the diameter of 55 nm, in which the silica-coated $NaYF_4$ nanoparticles are the most toxic to the cells and should be avoided while designing therapeutic tools.

INDEX OF FIGURES AND TABLES

Figure or Table **page**

REFERENCES

1. Auzel, F. History of upconversion discovery and its evolution. *J Lumin* **223**, 116900 (2020).
2. Auzel, F. Compteur quantique par transfert denergie de Yb3+ a Tm3+ dans un tungstate mixte et dans un verre germanate. *Comptes Rendus Hebdomadaires Des Seances De L Academie Des Sciences Serie B 263.14* (1966).
3. Auzel, F. Upconversion and Anti-Stokes Processes with f and d Ions in Solids. *Chem Rev* **104**, 139–173 (2004).
4. Gnach, A. & Bednarkiewicz, A. Lanthanide-doped up-converting nanoparticles: Merits and challenges. *Nano Today* **7**, 532–563 (2012).
5. Bednarkiewicz, A., Nyk, M., Samoc, M. & Strek, W. Up-conversion FRET from Er 3+ /Yb 3+ :NaYF 4 Nanophosphor to CdSe Quantum Dots. *The Journal of Physical Chemistry C* **114**, 17535–17541 (2010).
6. Prorok, K., Pawlyta, M., Strek, W. & Bednarkiewicz, A. Energy Migration Up-conversion of Tb3+ in Yb3+ and Nd3+ Codoped Active-Core/Active-Shell Colloidal Nanoparticles. *Chemistry of Materials* **28**, 2295–2300 (2016).
7. Heer, S., Lehmann, O., Haase, M. & Güdel, H. U. Blue, green, and red upconversion emission from lanthanide-doped LuPo4 and YbPO4 nanocrystals in a transparent colloidal solution. *Angewandte Chemie - International Edition* **42**, 3179–3182 (2003).
8. Krämer, K. W. *et al.* Hexagonal Sodium Yttrium Fluoride Based Green and Blue Emitting Upconversion Phosphors. *Chemistry of Materials* **16**, 1244–1251 (2004).
9. Abel, K. A., Boyer, J. C. & van Veggel, F. C. J. M. Hard proof of the NaYF4/NaGdF4 nanocrystal core/shell structure. *J Am Chem Soc* **131**, 14644–14645 (2009).
10. Suyver, J. F. *et al.* Novel materials doped with trivalent lanthanides and transition metal ions showing near-infrared to visible photon upconversion. *Opt Mater (Amst)* **27**, 1111–1130 (2005).
11. Prorok, K. *et al.* Near-infrared excited luminescence and in vitro imaging of HeLa cells by using Mn 2+ enhanced Tb 3+ and Yb 3+ cooperative upconversion in NaYF 4 nanocrystals. *Nanoscale Adv* (2019) doi:10.1039/C9NA00336C.
12. Mai, H. X. *et al.* High-quality sodium rare-earth fluoride nanocrystals: Controlled synthesis and optical properties. *J Am Chem Soc* **128**, 6426–6436 (2006).
13. Boyer, J. C., Vetrone, F., Cuccia, L. A. & Capobianco, J. A. Synthesis of colloidal upconverting NaYF4 nanocrystals doped with Er3+, Yb3+ and Tm3+, Yb3+ via thermal decomposition of lanthanide trifluoroacetate precursors. *J Am Chem Soc* **128**, 7444–7445 (2006).
14. Kömpe, K. *et al.* Green-Emitting CePO4:Tb/LaPO4 Core-Shell Nanoparticles with 70 % Photoluminescence Quantum Yield. *Angewandte Chemie - International Edition* **42**, 5513–5516 (2003).
15. Wang, Z. L. *et al.* A facile synthesis and photoluminescent properties of redispersible CeF 3, CeF 3:Tb 3+, and CeF 3:Tb 3+/LaF 3 (core/shell) nanoparticles. *Chemistry of Materials* **18**, 2030–2037 (2006).
16. Yi, G. & Chow, G. Core / Shell / Shell Nanoparticles with Significant Enhancement of Upconversion Fluorescence. **298**, 341–343 (2007).
17. Vetrone, F., Naccache, R., Mahalingam, V., Morgan, C. G. & Capobianco, J. A. The active-core/active-shell approach: A strategy to enhance the upconversion luminescence in lanthanide-doped nanoparticles. *Adv Funct Mater* **19**, 2924–2929 (2009).
18. Qian, H. S. & Zhang, Y. Synthesis of hexagonal-phase core-shell NaYF4 nanocrystals with tunable upconversion fluorescence. *Langmuir* **24**, 12123–12125 (2008).

19. Johnson, N. J. J., Korinek, A., Dong, C. & van Veggel, F. C. J. M. Self-focusing by Ostwald ripening: A strategy for layer-by-layer epitaxial growth on upconverting nanocrystals. *J Am Chem Soc* **134**, 11068–11071 (2012).
20. Chen, Z. *et al.* Versatile synthesis strategy for carboxylic acid-functionalized upconverting nanophosphors as biological labels. *J Am Chem Soc* **130**, 3023–3029 (2008).
21. Li, Z. & Zhang, Y. An efficient and user-friendly method for the synthesis of hexagonal-phase NaYF 4 :Yb, Er/Tm nanocrystals with controllable shape and upconversion fluorescence. *Nanotechnology* **19**, 345606 (2008).
22. Guller, A. E. *et al.* Cytotoxicity and non-specific cellular uptake of bare and surface-modified upconversion nanoparticles in human skin cells. *Nano Res* **8**, 1546–1562 (2015).
23. Zhou, J., Liu, Z. & Li, F. Upconversion nanophosphors for small-animal imaging. *Chem Soc Rev* **41**, 1323–1349 (2012).
24. Wang, M., Abbineni, G., Clevenger, A., Mao, C. & Xu, S. Upconversion nanoparticles: Synthesis, surface modification and biological applications. *Nanomedicine* **7**, 710–729 (2011).
25. Sun, L., Wei, R., Feng, J. & Zhang, H. Tailored lanthanide-doped upconversion nanoparticles and their promising bioapplication prospects. *Coord Chem Rev* **364**, 10–32 (2018).
26. Prorok, K. *et al.* Near-infrared excited luminescence and in vitro imaging of HeLa cells by using Mn 2+ enhanced Tb 3+ and Yb 3+ cooperative upconversion in NaYF 4 nanocrystals. *Nanoscale Adv* (2019) doi:10.1039/C9NA00336C.
27. Esipova, T. v. *et al.* Dendritic upconverting nanoparticles enable in vivo multiphoton microscopy with low-power continuous wave sources. *Proceedings of the National Academy of Sciences* **109**, 20826–20831 (2012).
28. Jiang, G., Pichaandi, J., Johnson, N. J. J., Burke, R. D. & van Veggel, F. C. J. M. An effective polymer cross-linking strategy to obtain stable dispersions of upconverting NaYF 4 nanoparticles in buffers and biological growth media for biolabeling applications. *Langmuir* **28**, 3239–3247 (2012).
29. Sun, C., Simke, J. R. J. & Gradzielski, M. An efficient synthetic strategy for ligand-free upconversion nanoparticles. *Mater Adv* **1**, 1602–1607 (2020).
30. Generalova, A. N. *et al.* PEG-modified upconversion nanoparticles for in vivo optical imaging of tumors. *RSC Adv* **6**, 30089–30097 (2016).
31. Li, Z. & Zhang, Y. Monodisperse Silica-Coated Polyvinylpyrrolidone/NaYF4 Nanocrystals with Multicolor Upconversion Fluorescence Emission. *Angewandte Chemie* **118**, 7896–7899 (2006).
32. Kostiv, U. *et al.* Versatile Bioconjugation Strategies of PEG-Modified Upconversion Nanoparticles for Bioanalytical Applications. *Biomacromolecules* **21**, 4502–4513 (2020).
33. Li, C. & Lin, J. Rare earth fluoride nano-/microcrystals: Synthesis, surface modification and application. *J Mater Chem* **20**, 6831–6847 (2010).
34. Li, Z., Guo, H., Qian, H. & Hu, Y. Facile microemulsion route to coat carbonized glucose on upconversion nanocrystals as high luminescence and biocompatible cell-imaging probes. *Nanotechnology* **21**, (2010).
35. Wang, D., Rogach, A. L. & Caruso, F. Semiconductor Quantum Dot-Labeled Microsphere Bioconjugates Prepared by Stepwise Self-Assembly. *Nano Lett* **2**, 857–861 (2002).
36. Wang, L. *et al.* Fluorescence resonant energy transfer biosensor based on upconversion-luminescent nanoparticles. *Angewandte Chemie - International Edition* **44**, 6054–6057 (2005).
37. Poon, Z., Chang, D., Zhao, X. & Hammond, P. T. Layer-by-layer nanoparticles with a pH-sheddable layer for in vivo targeting of tumor hypoxia. *ACS Nano* **5**, 4284–4292 (2011).
38. Liu, Q. *et al.* Multifunctional rare-earth self-assembled nanosystem for tri-modal upconversion luminescence /fluorescence /positron emission tomography imaging. *Biomaterials* **32**, 8243–8253 (2011).
39. Ohmori, M. & Matijević, E. Preparation and properties of uniform coated colloidal particles. VII. Silica on hematite. *J Colloid Interface Sci* **150**, 594–598 (1992).

40. Liz-marza, L. M., Giersig, M. & Mulvaney, P. Synthesis of Nanosized Gold - Silica Core - Shell Particles. **7463**, 4329–4335 (1996).
41. Hu, H. *et al.* Multimodal-luminescence core-shell nanocomposites for targeted imaging of tumor cells. *Chemistry - A European Journal* **15**, 3577–3584 (2009).
42. Xu, J. *et al.* Yolk-Structured Upconversion Nanoparticles with Biodegradable Silica Shell for FRET Sensing of Drug Release and Imaging-Guided Chemotherapy. *Chemistry of Materials* **29**, 7615–7628 (2017).
43. Karami, A. *et al.* Facile Multistep Synthesis of ZnO-Coated β-NaYF 4 :Yb/Tm Upconversion Nanoparticles as an Antimicrobial Photodynamic Therapy for Persistent Staphylococcus aureus Small Colony Variants. *ACS Appl Bio Mater* **4**, 6125–6136 (2021).
44. Johnson, N. J. J., Oakden, W., Stanisz, G. J., Scott Prosser, R. & van Veggel, F. C. J. M. Size-Tunable, Ultrasmall NaGdF $_4$ Nanoparticles: Insights into Their T $_1$ MRI Contrast Enhancement. *Chemistry of Materials* **23**, 3714–3722 (2011).
45. Bogdan, N., Vetrone, F., Roy, R. & Capobianco, J. A. Carbohydrate-coated lanthanide-doped upconverting nanoparticles for lectin recognition. *J Mater Chem* **20**, 7543 (2010).
46. Cheng, L. *et al.* Facile Preparation of Multifunctional Upconversion Nanoprobes for Multimodal Imaging and Dual-Targeted Photothermal Therapy. *Angewandte Chemie International Edition* **50**, 7385–7390 (2011).
47. Naccache, R., Vetrone, F., Mahalingam, V., Cuccia, L. A. & Capobianco, J. A. Controlled Synthesis and Water Dispersibility of Hexagonal Phase NaGdF $_4$:Ho $^{3+}$ /Yb $^{3+}$ Nanoparticles. *Chemistry of Materials* **21**, 717–723 (2009).
48. Dai, Y. *et al.* In Vivo Multimodality Imaging and Cancer Therapy by Near-Infrared Light-Triggered *trans* -Platinum Pro-Drug-Conjugated Upconverison Nanoparticles. *J Am Chem Soc* **135**, 18920–18929 (2013).
49. Dong, A. *et al.* A Generalized Ligand-Exchange Strategy Enabling Sequential Surface Functionalization of Colloidal Nanocrystals. *J Am Chem Soc* **133**, 998–1006 (2011).
50. Shen, J. *et al.* Engineering the Upconversion Nanoparticle Excitation Wavelength: Cascade Sensitization of Tri-doped Upconversion Colloidal Nanoparticles at 800 nm. *Adv Opt Mater* **1**, 644–650 (2013).
51. Kang, D., Song, X. & Xing, J. Synthesis and characterization of upconversion nanoparticles with shell structure and ligand-free hydrophilic modification. *RSC Adv* **5**, 83149–83154 (2015).
52. Himmelstoß, S. F. & Hirsch, T. Long-Term Colloidal and Chemical Stability in Aqueous Media of NaYF 4 -Type Upconversion Nanoparticles Modified by Ligand-Exchange. *Particle & Particle Systems Characterization* **36**, 1900235 (2019).
53. Kong, W. *et al.* A general strategy for ligand exchange on upconversion nanoparticles. *Inorg Chem* **56**, 872–877 (2017).
54. Chen, Y. *et al.* Dispersion stability and biocompatibility of four ligand-exchanged NaYF4: Yb, Er upconversion nanoparticles. *Acta Biomater* **102**, 384–393 (2020).
55. Das, G. K., Stark, D. T. & Kennedy, I. M. Potential Toxicity of Up-Converting Nanoparticles Encapsulated with a Bilayer Formed by Ligand Attraction. *Langmuir* **30**, 8167–8176 (2014).
56. Cheng, L. *et al.* Highly-sensitive multiplexed in vivo imaging using pegylated upconversion nanoparticles. *Nano Res* **3**, 722–732 (2010).
57. Wu, Z. *et al.* A pluronic F127 coating strategy to produce stable up-conversion NaYF4:Yb,Er(Tm) nanoparticles in culture media for bioimaging. *J Mater Chem* **22**, 18596 (2012).
58. Yi, G.-S. & Chow, G.-M. Water-Soluble NaYF 4 :Yb,Er(Tm)/NaYF 4 /Polymer Core/Shell/Shell Nanoparticles with Significant Enhancement of Upconversion Fluorescence. *Chemistry of Materials* **19**, 341–343 (2007).
59. Li, L.-L. *et al.* Biomimetic Surface Engineering of Lanthanide-Doped Upconversion Nanoparticles as Versatile Bioprobes. *Angewandte Chemie International Edition* **51**, 6121–6125 (2012).

60. Yao, C. *et al.* Highly Biocompatible Zwitterionic Phospholipids Coated Upconversion Nanoparticles for Efficient Bioimaging. *Anal Chem* **86**, 9749–9757 (2014).
61. Zhou, H.-P., Xu, C.-H., Sun, W. & Yan, C.-H. Clean and Flexible Modification Strategy for Carboxyl/Aldehyde-Functionalized Upconversion Nanoparticles and Their Optical Applications. *Adv Funct Mater* **19**, 3892–3900 (2009).
62. Hu, H. *et al.* Facile Epoxidation Strategy for Producing Amphiphilic Up-Converting Rare-Earth Nanophosphors as Biological Labels. *Chemistry of Materials* **20**, 7003–7009 (2008).
63. Bogdan, N., Vetrone, F., Ozin, G. A. & Capobianco, J. A. Synthesis of Ligand-Free Colloidally Stable Water Dispersible Brightly Luminescent Lanthanide-Doped Upconverting Nanoparticles. *Nano Lett* **11**, 835–840 (2011).
64. Niu, W. *et al.* NaYF 4 :Yb,Er–MoS 2 : from synthesis and surface ligand stripping to negative infrared photoresponse. *Chemical Communications* **51**, 9030–9033 (2015).
65. Zhang, L., Jin, D. & Stenzel, M. H. Polymer-Functionalized Upconversion Nanoparticles for Light/Imaging-Guided Drug Delivery. *Biomacromolecules* **22**, 3168–3201 (2021).
66. Jin, J. *et al.* Polymer-Coated NaYF 4 :Yb 3+ , Er 3+ Upconversion Nanoparticles for Charge-Dependent Cellular Imaging. *ACS Nano* **5**, 7838–7847 (2011).
67. Cheng, L., Yang, K., Shao, M., Lu, X. & Liu, Z. In vivo pharmacokinetics, long-term biodistribution and toxicology study of functionalized upconversion nanoparticles in mice. *Nanomedicine* **6**, 1327–1340 (2011).
68. Johnson, N. J. J., Sangeetha, N. M., Boyer, J.-C. & van Veggel, F. C. J. M. Facile ligand-exchange with polyvinylpyrrolidone and subsequent silica coating of hydrophobic upconverting β-NaYF4:Yb3+/Er3+ nanoparticles. *Nanoscale* **2**, 771 (2010).
69. Liras, M. *et al.* Thin Amphiphilic Polymer-Capped Upconversion Nanoparticles: Enhanced Emission and Thermoresponsive Properties. *Chemistry of Materials* **26**, 4014–4022 (2014).
70. Gwon, K. *et al.* Improved near infrared-mediated hydrogel formation using diacrylated Pluronic F127-coated upconversion nanoparticles. *Materials Science and Engineering: C* **90**, 77–84 (2018).
71. Generalova, A. N. *et al.* Submicron polyacrolein particles in situ embedded with upconversion nanoparticles for bioassay. *Nanoscale* **7**, 1709–1717 (2015).
72. Li, Z. & Zhang, Y. Monodisperse Silica-Coated Polyvinylpyrrolidone/NaYF4 Nanocrystals with Multicolor Upconversion Fluorescence Emission. *Angewandte Chemie International Edition* **45**, 7732–7735 (2006).
73. Tang, J., Lei, L., Feng, H., Zhang, H. & Han, Y. Preparation of K+-Doped Core-Shell NaYF4:Yb, Er Upconversion Nanoparticles and its Application for Fluorescence Immunochromatographic Assay of Human Procalcitonin. *J Fluoresc* **26**, 2237–2246 (2016).
74. Lv, R. *et al.* Plasmonic modulated upconversion fluorescence by adjustable distributed gold nanoparticles. *J Lumin* **220**, 116974 (2020).
75. Harada, A., Takashima, Y. & Nakahata, M. Supramolecular Polymeric Materials via Cyclodextrin–Guest Interactions. *Acc Chem Res* **47**, 2128–2140 (2014).
76. Wang, A. *et al.* Drug delivery function of carboxymethyl-β-cyclodextrin modified upconversion nanoparticles for adamantine phthalocyanine and their NIR-triggered cancer treatment. *Dalton Transactions* **45**, 3853–3862 (2016).
77. Ding, Y., Zhu, H., Zhang, X., Zhu, J.-J. & Burda, C. Rhodamine B derivative-functionalized upconversion nanoparticles for FRET-based Fe3+-sensing. *Chemical Communications* **49**, 7797 (2013).
78. Ou, J. *et al.* pH-sensitive nanocarriers for Ganoderma applanatum polysaccharide release via host–guest interactions. *J Mater Sci* **53**, 7963–7975 (2018).
79. Wang, X. *et al.* Facile surface functionalization of upconversion nanoparticles with phosphoryl pillar[5]arenes for controlled cargo release and cell imaging. *Chemical Communications* **54**, 12990–12993 (2018).

80. Li, H. *et al.* Smart Self-Assembled Nanosystem Based on Water-Soluble Pillararene and Rare-Earth-Doped Upconversion Nanoparticles for pH-Responsive Drug Delivery. *ACS Appl Mater Interfaces* **10**, 4910–4920 (2018).
81. Stöber, W., Fink, A. & Bohn, E. Controlled growth of monodisperse silica spheres in the micron size range. *J Colloid Interface Sci* **26**, 62–69 (1968).
82. Qian, L. P., Zhou, L. H., Too, H.-P. & Chow, G.-M. Gold decorated NaYF4:Yb,Er/NaYF4/silica (core/shell/shell) upconversion nanoparticles for photothermal destruction of BE(2)-C neuroblastoma cells. *Journal of Nanoparticle Research* **13**, 499–510 (2011).
83. Brinker, J. C. & Scherer, G. W. *Sol-Gel Science: The Physics and Chemistry of Sol–Gel Processing*. (Elsevier, 1990). doi:10.1016/C2009-0-22386-5.
84. Liu, J.-N., Bu, W.-B. & Shi, J.-L. Silica Coated Upconversion Nanoparticles: A Versatile Platform for the Development of Efficient Theranostics. *Acc Chem Res* **48**, 1797–1805 (2015).
85. Han, R., Shi, J., Liu, Z., Wang, H. & Wang, Y. Fabrication of Mesoporous-Silica-Coated Upconverting Nanoparticles with Ultrafast Photosensitizer Loading and 808 nm NIR-Light-Triggering Capability for Photodynamic Therapy. *Chemistry - An Asian Journal* vol. 12 2197–2201 Preprint at https://doi.org/10.1002/asia.201700836 (2017).
86. Nooney, R. I., Thirunavukkarasu, D., Chen, Y., Josephs, R. & Ostafin, A. E. Synthesis of Nanoscale Mesoporous Silica Spheres with Controlled Particle Size. *Chemistry of Materials* **14**, 4721–4728 (2002).
87. Gorelikov, I. & Matsuura, N. Single-Step Coating of Mesoporous Silica on Cetyltrimethyl Ammonium Bromide-Capped Nanoparticles. *Nano Lett* **8**, 369–373 (2008).
88. Qian, H. S., Guo, H. C., Ho, P. C.-L., Mahendran, R. & Zhang, Y. Mesoporous-Silica-Coated Up-Conversion Fluorescent Nanoparticles for Photodynamic Therapy. *Small* **5**, 2285–2290 (2009).
89. Wang, M. *et al.* Immunolabeling and NIR-Excited Fluorescent Imaging of HeLa Cells by Using NaYF 4 :Yb,Er Upconversion Nanoparticles. *ACS Nano* **3**, 1580–1586 (2009).
90. Liu, X. *et al.* A simple and efficient synthetic route for preparation of NaYF 4 upconversion nanoparticles by thermo-decomposition of rare-earth oleates. *CrystEngComm* **16**, 5650–5661 (2014).
91. Liu, J. *et al.* Controlled synthesis of uniform and monodisperse upconversion core/mesoporous silica shell nanocomposites for bimodal imaging. *Chemistry - A European Journal* **18**, 2335–2341 (2012).
92. Wiercigroch-Walkosz, K., Cichos, J. & Karbowiak, M. Growth of silica shell on hydrophobic upconverting nanocrystals – Mechanism and control of porosity. *Colloids Surf A Physicochem Eng Asp* **572**, 1–9 (2019).
93. Joo, S. H. *et al.* Thermally stable Pt/mesoporous silica core-shell nanocatalysts for high-temperature reactions. *Nat Mater* **8**, 126–131 (2009).
94. Allen, L. H. & Matijević, E. Stability of colloidal silica. *J Colloid Interface Sci* **31**, 287–296 (1969).
95. *Luminescent Materials and Applications*. (John Wiley & Sons, Ltd, 2008). doi:10.1002/9780470985687.
96. Tu, D. *et al.* Time-Resolved FRET Biosensor Based on Amine-Functionalized Lanthanide-Doped NaYF4 Nanocrystals. *Angewandte Chemie International Edition* **50**, 6306–6310 (2011).
97. Argyo, C., Weiss, V., Bräuchle, C. & Bein, T. Multifunctional Mesoporous Silica Nanoparticles as a Universal Platform for Drug Delivery. *Chemistry of Materials* **26**, 435–451 (2014).
98. Mi, C. *et al.* Novel Microwave-Assisted Solvothermal Synthesis of $NaYF_4$:Yb,Er Upconversion Nanoparticles and Their Application in Cancer Cell Imaging. *Langmuir* **27**, 14632–14637 (2011).
99. Liu, F., Zhao, Q., You, H. & Wang, Z. Synthesis of stable carboxy-terminated NaYF4: Yb3+, Er3+@SiO2 nanoparticles with ultrathin shell for biolabeling applications. *Nanoscale* **5**, 1047–1053 (2013).

100. Jesu Raj, J. G. *et al.* Sensitive Detection of ssDNA Using an LRET-Based Upconverting Nanohybrid Material. *ACS Appl Mater Interfaces* **7**, 18257–18265 (2015).
101. Chen, J. *et al.* Controllable synthesis of NaYF4:Yb,Er upconversion nanophosphors and their application to in vivo imaging of Caenorhabditis elegans. *J Mater Chem* **21**, 2632–2638 (2011).
102. Nyk, M., Kumar, R., Ohulchanskyy, T. Y., Bergey, E. J. & Prasad, P. N. High Contrast in Vitro and in Vivo Photoluminescence Bioimaging Using Near Infrared to Near Infrared Up-Conversion in Tm^{3+} and Yb^{3+} Doped Fluoride Nanophosphors. *Nano Lett* **8**, 3834–3838 (2008).
103. Rabie, H. *et al.* NIR Biosensing of Neurotransmitters in Stem Cell-Derived Neural Interface Using Advanced Core–Shell Upconversion Nanoparticles. *Advanced Materials* **31**, 1806991 (2019).
104. Wu, S. *et al.* Aptamer-based fluorescence biosensor for chloramphenicol determination using upconversion nanoparticles. *Food Control* **50**, 597–604 (2015).
105. Xu, S. *et al.* A novel upconversion, fluorescence resonance energy transfer biosensor (FRET) for sensitive detection of lead ions in human serum. *Nanoscale* **6**, 12573–12579 (2014).
106. Yi, G. *et al.* Synthesis, Characterization, and Biological Application of Size-Controlled Nanocrystalline $NaYF_4$:Yb,Er Infrared-to-Visible Up-Conversion Phosphors. *Nano Lett* **4**, 2191–2196 (2004).
107. Liu, J., Bu, W., Pan, L. & Shi, J. NIR-Triggered Anticancer Drug Delivery by Upconverting Nanoparticles with Integrated Azobenzene-Modified Mesoporous Silica. *Angewandte Chemie* **125**, 4471–4475 (2013).
108. Wang, H. *et al.* Design and Synthesis of Core-Shell-Shell Upconversion Nanoparticles for NIR-Induced Drug Release, Photodynamic Therapy, and Cell Imaging. *ACS Appl Mater Interfaces* **8**, 4416–4423 (2016).
109. Wang, C., Cheng, L. & Liu, Z. Upconversion nanoparticles for photodynamic therapy and other cancer therapeutics. *Theranostics* **3**, 317–330 (2013).
110. Deisseroth, K. Optogenetics. *Nat Methods* **8**, 26–29 (2011).
111. You, M. *et al.* Inkjet printing of upconversion nanoparticles for anti-counterfeit applications. *Nanoscale* **7**, 4423–4431 (2015).
112. He, M. *et al.* Monodisperse Dual-Functional Upconversion Nanoparticles Enabled Near-Infrared Organolead Halide Perovskite Solar Cells. *Angewandte Chemie* **128**, 4352–4356 (2016).
113. Zhang, Y. & Liu, X. Nanocrystals: Shining a light on upconversion. *Nat Nanotechnol* **8**, 702–703 (2013).
114. Gao, L. *et al.* Video-rate upconversion display from optimized lanthanide ion doped upconversion nanoparticles. *Nanoscale* **12**, 18595–18599 (2020).
115. Wu, X. *et al.* Dye-Sensitized Core/Active Shell Upconversion Nanoparticles for Optogenetics and Bioimaging Applications. *ACS Nano* **10**, 1060–1066 (2016).
116. Chien, Y.-H. *et al.* Near-Infrared Light Photocontrolled Targeting, Bioimaging, and Chemotherapy with Caged Upconversion Nanoparticles *in Vitro* and *in Vivo*. *ACS Nano* **7**, 8516–8528 (2013).
117. Rostami, I., Rezvani, H., Hu, Z. & Shahmoradian, S. H. Breakthroughs in medicine and bioimaging with up-conversion nanoparticles. *Int J Nanomedicine* **Volume 14**, 7759–7780 (2019).
118. González-Béjar, M., Francés-Soriano, L. & Pérez-Prieto, J. Upconversion nanoparticles for bioimaging and regenerative medicine. *Front Bioeng Biotechnol* **4**, 1–9 (2016).
119. Rafique, R., Kailasa, S. K. & Park, T. J. Recent advances of upconversion nanoparticles in theranostics and bioimaging applications. *TrAC Trends in Analytical Chemistry* **120**, 115646 (2019).
120. Han, X., Lui, H., McLean, D. I. & Zeng, H. Near-infrared autofluorescence imaging of cutaneous melanins and human skin in vivo. *J Biomed Opt* **14**, 024017 (2009).

121. Xu, S. *et al.* Mesoporous silica coating NaYF4:Yb,Er@NaYF4 upconversion nanoparticles loaded with ruthenium(II) complex nanoparticles: Fluorometric sensing and cellular imaging of temperature by upconversion and of oxygen by downconversion. *Microchimica Acta* **185**, (2018).
122. Wang, F. *et al.* Microscopic inspection and tracking of single upconversion nanoparticles in living cells. *Light Sci Appl* **7**, 18007–18007 (2018).
123. Hischemöller, A., Nordmann, J., Ptacek, P., Mummenhoff, K. & Haase, M. In-Vivo Imaging of the Uptake of Upconversion Nanoparticles by Plant Roots. *J Biomed Nanotechnol* **5**, 278–284 (2009).
124. Jin, B. *et al.* Upconversion nanoparticles based FRET aptasensor for rapid and ultrasenstive bacteria detection. *Biosens Bioelectron* **90**, 525–533 (2017).
125. Yin, M., Jing, C., Li, H., Deng, Q. & Wang, S. Surface chemistry modified upconversion nanoparticles as fluorescent sensor array for discrimination of foodborne pathogenic bacteria. *J Nanobiotechnology* **18**, 41 (2020).
126. Kim, J. *et al.* Rapid and background-free detection of avian influenza virus in opaque sample using NIR-to-NIR upconversion nanoparticle-based lateral flow immunoassay platform. *Biosens Bioelectron* **112**, 209–215 (2018).
127. Han, S. *et al.* Upconversion nanoparticles coated organic photovoltaics for near infrared light controlled drug delivery systems. *Nano Energy* **81**, 105650 (2021).
128. Denk, W., Strickler, J. H. & Webb, W. W. Two-photon laser scanning fluorescence microscopy. *Science (1979)* **248**, 73–76 (1990).
129. Zhou, J., Liu, Q., Feng, W., Sun, Y. & Li, F. Upconversion luminescent materials: Advances and applications. *Chem Rev* **115**, 395–465 (2015).
130. Farka, Z. *et al.* Surface design of photon-upconversion nanoparticles for high-contrast immunocytochemistry. *Nanoscale* **12**, 8303–8313 (2020).
131. del Rosal, B., Villa, I., Jaque, D. & Sanz-Rodríguez, F. In vivo autofluorescence in the biological windows: the role of pigmentation. *J Biophotonics* **9**, 1059–1067 (2016).
132. Shi, L., Sordillo, L. A., Rodríguez-Contreras, A. & Alfano, R. Transmission in near-infrared optical windows for deep brain imaging. *J Biophotonics* **9**, 38–43 (2016).
133. Liu, Q. *et al.* Sub-10 nm hexagonal lanthanide-doped NaLuF 4 upconversion nanocrystals for sensitive bioimaging in vivo. *J Am Chem Soc* **133**, 17122–17125 (2011).
134. Chen, G. *et al.* (alpha-NaYbF4:Tm3+)/CaF2 Core/ShellNanoparticles with Efficient Upconversion for High-Contrast Deep Tissue Bioimaging. *ACS Nano* **6**, 8280–8287 (2012).
135. Weissleder, R. A clearer vision for in vivo imaging. *Nat Biotechnol* **19**, 316–317 (2001).
136. Zhang, P., Steelant, W., Kumar, M. & Scholfield, M. Versatile Photosensitizers for Photodynamic Therapy at Infrared Excitation. *J Am Chem Soc* **129**, 4526–4527 (2007).
137. Nadort, A. *et al.* Quantitative Imaging of Single Upconversion Nanoparticles in Biological Tissue. *PLoS One* **8**, e63292 (2013).
138. Zhao, M. *et al.* Supramolecularly Engineered NIR-II and Upconversion Nanoparticles In Vivo Assembly and Disassembly to Improve Bioimaging. *Advanced Materials* **30**, 1804982 (2018).
139. Jia, T. *et al.* Mesoporous cerium oxide-coated upconversion nanoparticles for tumor-responsive chemo-photodynamic therapy and bioimaging. *Chem Sci* **10**, 8618–8633 (2019).
140. Tian, G. *et al.* Mn2+ Dopant-Controlled Synthesis of NaYF4:Yb/Er Upconversion Nanoparticles for in vivo Imaging and Drug Delivery. *Advanced Materials* **24**, 1226–1231 (2012).
141. Himmelstoß, S. F. & Hirsch, T. A critical comparison of lanthanide based upconversion nanoparticles to fluorescent proteins, semiconductor quantum dots, and carbon dots for use in optical sensing and imaging. *Methods Appl Fluoresc* **7**, 022002 (2019).
142. Li, X., Yi, Z., Xue, Z., Zeng, S. & Liu, H. Multifunctional BaYbF 5 : Gd/Er upconversion nanoparticles for in vivo tri-modal upconversion optical, X-ray computed tomography and magnetic resonance imaging. *Materials Science and Engineering: C* **75**, 510–516 (2017).

143. Kostiv, U. *et al.* A simple neridronate-based surface coating strategy for upconversion nanoparticles: highly colloidally stable ^{125} I-radiolabeled $NaYF_4$:Yb^{3+} /Er^{3+} @PEG nanoparticles for multimodal *in vivo* tissue imaging. *Nanoscale* **9**, 16680–16688 (2017).
144. Shen, J.-W. *et al.* Incorporation of Computed Tomography and Magnetic Resonance Imaging Function into $NaYF_4$:Yb/Tm Upconversion Nanoparticles for in Vivo Trimodal Bioimaging. *Anal Chem* **85**, 12166–12172 (2013).
145. Du, K. *et al.* In situ decorating of ultrasmall Ag2Se on upconversion nanoparticles as novel nanotheranostic agent for multimodal imaging-guided cancer photothermal therapy. *Appl Mater Today* **18**, 100497 (2020).
146. Tang, S.-H. *et al.* Ultrasonic assisted preparation of lanthanide-oleate complexes for the synthesis of multifunctional monodisperse upconversion nanoparticles for multimodal imaging. *Nanoscale* **6**, 8037 (2014).
147. Zhou, L. *et al.* Mesoporous NaYbF4@NaGdF4 core-shell up-conversion nanoparticles for targeted drug delivery and multimodal imaging. *Biomaterials* **35**, 7666–7678 (2014).
148. Liu, L., Zhang, H., Wang, Z. & Song, D. Peptide-functionalized upconversion nanoparticles-based FRET sensing platform for Caspase-9 activity detection in vitro and in vivo. *Biosens Bioelectron* **141**, 111403 (2019).
149. Liu, M., Ye, Y., Yao, C., Zhao, W. & Huang, X. Mn 2+ -doped NaYF 4 :Yb/Er upconversion nanoparticles with amplified electrogenerated chemiluminescence for tumor biomarker detection. *J. Mater. Chem. B* **2**, 6626–6633 (2014).
150. Gong, L. *et al.* A versatile luminescent resonance energy transfer (LRET)-based ratiometric upconversion nanoprobe for intracellular miRNA biosensing. *J Mater Chem B* **8**, 5952–5961 (2020).
151. Wilhelm, S. *et al.* Multicolor Upconversion Nanoparticles for Protein Conjugation. *Theranostics* **3**, 239–248 (2013).
152. Lai, J., Shah, B. P., Zhang, Y., Yang, L. & Lee, K.-B. Real-Time Monitoring of ATP-Responsive Drug Release Using Mesoporous-Silica-Coated Multicolor Upconversion Nanoparticles. *ACS Nano* **9**, 5234–5245 (2015).
153. Chen, S. *et al.* Size-dependent cytotoxicity of europium doped NaYF4 nanoparticles in endothelial cells. *Materials Science and Engineering C* **43**, 330–342 (2014).
154. Nagarajan, S., Li, Z., Marchi-Artzner, V., Grasset, F. & Zhang, Y. Imaging gap junctions with silica-coated upconversion nanoparticles. *Med Biol Eng Comput* **48**, 1033–1041 (2010).
155. Li, C., Liu, J., Alonso, S., Li, F. & Zhang, Y. Upconversion nanoparticles for sensitive and in-depth detection of Cu2+ ions. *Nanoscale* **4**, 6065 (2012).
156. Peltomaa, R., Benito-Peña, E., Gorris, H. H. & Moreno-Bondi, M. C. Biosensing based on upconversion nanoparticles for food quality and safety applications. *Analyst* **146**, 13–32 (2021).
157. Wu, S. *et al.* Magnetic nanobead-based immunoassay for the simultaneous detection of aflatoxin B1 and ochratoxin A using upconversion nanoparticles as multicolor labels. *Biosens Bioelectron* **30**, 35–42 (2011).
158. Idris, N. M. *et al.* Tracking transplanted cells in live animal using upconversion fluorescent nanoparticles. *Biomaterials* **30**, 5104–5113 (2009).
159. Ma, Y. *et al.* Labeling and long-term tracking of bone marrow mesenchymal stem cells in vitro using NaYF 4 :Yb 3+ ,Er 3+ upconversion nanoparticles. *Acta Biomater* **42**, 199–208 (2016).
160. Xiang, J. *et al.* Antigen-Loaded Upconversion Nanoparticles for Dendritic Cell Stimulation, Tracking, and Vaccination in Dendritic Cell-Based Immunotherapy. *ACS Nano* **9**, 6401–6411 (2015).
161. Dong, Y. *et al.* Non-invasive tracking of hydrogel degradation using upconversion nanoparticles. *Acta Biomater* **55**, 410–419 (2017).
162. Verma, A. & Stellacci, F. Effect of surface properties on nanoparticle-cell interactions. *Small* **6**, 12–21 (2010).

163. Li, K. *et al.* Ratiometric Monitoring of Intracellular Drug Release by an Upconversion Drug Delivery Nanosystem. *ACS Appl Mater Interfaces* **7**, 12278–12286 (2015).
164. Reddy, K. L. *et al.* Amine-functionalized, porous silica-coated NaYF4:Yb/Er upconversion nanophosphors for efficient delivery of doxorubicin and curcumin. *Materials Science and Engineering: C* **96**, 86–95 (2019).
165. Liu, B. *et al.* Upconversion-Luminescent Core/Mesoporous-Silica-Shell-Structured β-NaYF 4 :Yb 3+ ,Er 3+ @SiO 2 @mSiO 2 Composite Nanospheres: Fabrication and Drug-Storage/Release Properties. *Eur J Inorg Chem* **2014**, 1906–1913 (2014).
166. Jiang, S., Zhang, Y., Lim, K. M., Sim, E. K. W. & Ye, L. NIR-to-visible upconversion nanoparticles for fluorescent labeling and targeted delivery of siRNA. *Nanotechnology* **20**, 155101 (2009).
167. Li, C. *et al.* Multifunctional Upconversion Mesoporous Silica Nanostructures for Dual Modal Imaging and In Vivo Drug Delivery. *Small* **9**, 4150–4159 (2013).
168. Liu, S. *et al.* pH-sensitive polymer-gated multifunctional upconversion NaYF 4 :Yb/Er@mSiO 2 nanocomposite for oral drug delivery. *Microporous and Mesoporous Materials* **264**, 151–158 (2018).
169. Wang, C., Cheng, L. & Liu, Z. Drug delivery with upconversion nanoparticles for multi-functional targeted cancer cell imaging and therapy. *Biomaterials* **32**, 1110–1120 (2011).
170. Jia, X. *et al.* Polyacrylic Acid Modified Upconversion Nanoparticles for Simultaneous pH-Triggered Drug Delivery and Release Imaging. *J Biomed Nanotechnol* **9**, 2063–2072 (2013).
171. Lin, M. *et al.* Facial Layer-by-Layer Engineering of Upconversion Nanoparticles for Gene Delivery: Near-Infrared-Initiated Fluorescence Resonance Energy Transfer Tracking and Overcoming Drug Resistance in Ovarian Cancer. *ACS Appl Mater Interfaces* **9**, 7941–7949 (2017).
172. Yan, B., Boyer, J.-C., Branda, N. R. & Zhao, Y. Near-Infrared Light-Triggered Dissociation of Block Copolymer Micelles Using Upconverting Nanoparticles. *J Am Chem Soc* **133**, 19714–19717 (2011).
173. Jayakumar, M. K. G., Idris, N. M. & Zhang, Y. Remote activation of biomolecules in deep tissues using near-infrared-to-UV upconversion nanotransducers. *Proceedings of the National Academy of Sciences* **109**, 8483–8488 (2012).
174. Dai, Y. *et al.* Doxorubicin conjugated NaYF4:Yb3+/Tm3+ nanoparticles for therapy and sensing of drug delivery by luminescence resonance energy transfer. *Biomaterials* **33**, 8704–8713 (2012).
175. Qiu, H., Tan, M., Ohulchanskyy, T. Y., Lovell, J. F. & Chen, G. Recent progress in upconversion photodynamic therapy. *Nanomaterials* **8**, 1–18 (2018).
176. Liu, Y., Meng, X. & Bu, W. Upconversion-based photodynamic cancer therapy. *Coord Chem Rev* **379**, 82–98 (2019).
177. Hong, S. ho & Choi, Y. Mesoporous silica-based nanoplatforms for the delivery of photodynamic therapy agents. *J Pharm Investig* **48**, 3–17 (2018).
178. Wezgowiec, J. *et al.* Cyanines in photodynamic reaction assisted by reversible electroporation—in vitro study on human breast carcinoma cells. *Photodiagnosis Photodyn Ther* **10**, 490–502 (2013).
179. Ding, B. *et al.* Large-Pore Mesoporous-Silica-Coated Upconversion Nanoparticles as Multifunctional Immunoadjuvants with Ultrahigh Photosensitizer and Antigen Loading Efficiency for Improved Cancer Photodynamic Immunotherapy. *Advanced Materials* **30**, 1802479 (2018).
180. Loh, X. J., Dou, Q. Q., Ye, E. & Teng, C. P. Effective near-infrared photodynamic therapy assisted by upconversion nanoparticles conjugated with photosensitizers. *Int J Nanomedicine* 419 (2015) doi:10.2147/IJN.S74891.
181. Idris, N. M. *et al.* In vivo photodynamic therapy using upconversion nanoparticles as remote-controlled nanotransducers. *Nat Med* **18**, 1580–1585 (2012).

182. Xu, F. *et al.* Mesoporous-silica-coated upconversion nanoparticles loaded with vitamin B12 for near-infrared-light mediated photodynamic therapy. *Mater Lett* **167**, 205–208 (2016).
183. Lu, F., Yang, L., Ding, Y. & Zhu, J.-J. Highly Emissive Nd 3+ -Sensitized Multilayered Upconversion Nanoparticles for Efficient 795 nm Operated Photodynamic Therapy. *Adv Funct Mater* **26**, 4778–4785 (2016).
184. Wang, H. *et al.* Near-infrared light activated photodynamic therapy of THP-1 macrophages based on core-shell structured upconversion nanoparticles. *Microporous and Mesoporous Materials* **239**, 78–85 (2017).
185. Yang, C. *et al.* Dual-modal imaging and photodynamic therapy using upconversion nanoparticles for tumor cells. *Analyst* **139**, 6414–6420 (2014).
186. Fan, W. *et al.* A smart upconversion-based mesoporous silica nanotheranostic system for synergetic chemo-/radio-/photodynamic therapy and simultaneous MR/UCL imaging. *Biomaterials* **35**, 8992–9002 (2014).
187. Grüner, M. C., Arai, M. S., Carreira, M., Inada, N. & de Camargo, A. S. S. Functionalizing the Mesoporous Silica Shell of Upconversion Nanoparticles To Enhance Bacterial Targeting and Killing via Photosensitizer-Induced Antimicrobial Photodynamic Therapy. *ACS Appl Bio Mater* **1**, 1028–1036 (2018).
188. Kuk, S., Lee, B. il, Lee, J. S. & Park, C. B. Rattle-Structured Upconversion Nanoparticles for Near-IR-Induced Suppression of Alzheimer's β-Amyloid Aggregation. *Small* **13**, 1603139 (2017).
189. Yadav, K. *et al.* Targeted and efficient activation of channelrhodopsins expressed in living cells via specifically-bound upconversion nanoparticles. *Nanoscale* **9**, 9457–9466 (2017).
190. Yu, N. *et al.* Near-Infrared-Light Activatable Nanoparticles for Deep-Tissue-Penetrating Wireless Optogenetics. *Adv Healthc Mater* **8**, 1801132 (2019).
191. Pliss, A. *et al.* Subcellular Optogenetics Enacted by Targeted Nanotransformers of Near-Infrared Light. *ACS Photonics* **4**, 806–814 (2017).
192. Lin, X. *et al.* Multiplexed Optogenetic Stimulation of Neurons with Spectrum-Selective Upconversion Nanoparticles. *Adv Healthc Mater* **6**, 1700446 (2017).
193. Bansal, A., Liu, H., Jayakumar, M. K. G., Andersson-Engels, S. & Zhang, Y. Quasi-Continuous Wave Near-Infrared Excitation of Upconversion Nanoparticles for Optogenetic Manipulation of C. elegans. *Small* **12**, 1732–1743 (2016).
194. Huang, X. Broadband dye-sensitized upconversion: A promising new platform for future solar upconverter design. *J Alloys Compd* **690**, 356–359 (2017).
195. Dibaba, S. T., Xiaoqian Ge, Ren, W. & Sun, L. Recent progress of energy transfer and luminescence intensity boosting mechanism in Nd3+-sensitized upconversion nanoparticles. *Journal of Rare Earths* **37**, 791–805 (2019).
196. Zhang, X. *et al.* Boosting Luminance Energy Transfer Efficiency in Upconversion Nanoparticles with an Energy-Concentrating Zone. *Angewandte Chemie - International Edition* **58**, 12117–12122 (2019).
197. Liang, T. *et al.* Removing the Obstacle of Dye-Sensitized Upconversion Luminescence in Aqueous Phase to Achieve High-Contrast Deep Imaging In Vivo. *Adv Funct Mater* **30**, 1–8 (2020).
198. Shao, Q. *et al.* Enhancing the upconversion luminescence and photothermal conversion properties of ~800 nm excitable core/shell nanoparticles by dye molecule sensitization. *J Colloid Interface Sci* **486**, 121–127 (2017).
199. Chen, G. *et al.* Energy-Cascaded Upconversion in an Organic Dye-Sensitized Core/Shell Fluoride Nanocrystal. *Nano Lett* **15**, 7400–7407 (2015).
200. Wei, Y. *et al.* Molecular antenna-sensitized upconversion nanoparticle for temperature monitored precision photothermal therapy. *Int J Nanomedicine* **15**, 1409–1420 (2020).

201. Song, D. *et al.* Upconversion System with Quantum Dots as Sensitizer: Improved Photoluminescence and PDT Efficiency. *ACS Appl Mater Interfaces* **11**, 41100–41108 (2019).
202. Ansari, A. A., Nazeeruddin, M. K. & Tavakoli, M. M. Organic-inorganic upconversion nanoparticles hybrid in dye-sensitized solar cells. *Coord Chem Rev* **436**, 213805 (2021).
203. Zhang, J., Shade, C. M., Chengelis, D. A. & Petoud, S. A Strategy to Protect and Sensitize Near-Infrared Luminescent Nd^{3+} and Yb^{3+} : Organic Tropolonate Ligands for the Sensitization of Ln^{3+} -Doped $NaYF_4$ Nanocrystals. *J Am Chem Soc* **129**, 14834–14835 (2007).
204. Zou, W., Visser, C., Maduro, J. A., Pshenichnikov, M. S. & Hummelen, J. C. Broadband dye-sensitized upconversion of near-infrared light. *Nat Photonics* **6**, 560–564 (2012).
205. Alyatkin, S. *et al.* In-Depth Analysis of Excitation Dynamics in Dye-Sensitized Upconversion Core and Core/Active Shell Nanoparticles. *Journal of Physical Chemistry C* **122**, 18177–18184 (2018).
206. Xu, J. *et al.* Highly Emissive Dye-Sensitized Upconversion Nanostructure for Dual-Photosensitizer Photodynamic Therapy and Bioimaging. *ACS Nano* **11**, 4133–4144 (2017).
207. Zou, X. *et al.* A water-dispersible dye-sensitized upconversion nanocomposite modified with phosphatidylcholine for lymphatic imaging. *Chemical Communications* **52**, 13389–13392 (2016).
208. Wei, W. *et al.* Alleviating Luminescence Concentration Quenching in Upconversion Nanoparticles through Organic Dye Sensitization. *J Am Chem Soc* **138**, 15130–15133 (2016).
209. Wang, D. *et al.* ICG-Sensitized $NaYF_4$:Er Nanostructure for Theranostics. *Adv Opt Mater* **6**, 1701142 (2018).
210. Zhao, X. *et al.* Optimizing the performance of dye-sensitized upconversion nanoparticles. *Dyes and Pigments* **192**, 109428 (2021).
211. Xue, B. *et al.* Ultrastrong Absorption Meets Ultraweak Absorption: Unraveling the Energy-Dissipative Routes for Dye-Sensitized Upconversion Luminescence. *J Phys Chem Lett* **9**, 4625–4631 (2018).
212. Saleh, M. I. *et al.* Sensitization of upconverting nanoparticles with a NIR-emissive cyanine dye using a micellar encapsulation approach. *Methods Appl Fluoresc* **7**, 014003 (2019).
213. Wang, J. & Deng, R. Energy Transfer in Dye-Coupled Lanthanide-Doped Nanoparticles: From Design to Application. *Chemistry - An Asian Journal* vol. 13 614–625 Preprint at https://doi.org/10.1002/asia.201701817 (2018).
214. Lv, R. *et al.* Stable ICG-loaded upconversion nanoparticles: silica core/shell theranostic nanoplatform for dual-modal upconversion and photoacoustic imaging together with photothermal therapy. *Sci Rep* **7**, 15753 (2017).
215. Doughan, S., Uddayasankar, U., Peri, A. & Krull, U. J. A paper-based multiplexed resonance energy transfer nucleic acid hybridization assay using a single form of upconversion nanoparticle as donor and three quantum dots as acceptors. *Anal Chim Acta* **962**, 88–96 (2017).
216. Li, Z., Zhang, Y. & Jiang, S. Multicolor Core/Shell-Structured Upconversion Fluorescent Nanoparticles. *Advanced Materials* **20**, 4765–4769 (2008).
217. Jeong, S. *et al.* Multiplexed near-infrared in vivo imaging complementarily using quantum dots and upconverting NaYF4:Yb3+,Tm3+ nanoparticles. *Chemical Communications* **47**, 8022 (2011).
218. Gu, Y.-P., Cui, R., Zhang, Z.-L., Xie, Z.-X. & Pang, D.-W. Ultrasmall Near-Infrared Ag_2Se Quantum Dots with Tunable Fluorescence for *in Vivo* Imaging. *J Am Chem Soc* **134**, 79–82 (2012).
219. Schmid, S. L. & Conner, S. D. Regulated portals of entry into the cell. *Nature* **422**, 37–44 (2003).
220. Plohl, O. *et al.* Optically Detected Degradation of NaYF 4 :Yb,Tm-Based Upconversion Nanoparticles in Phosphate Buffered Saline Solution. *Langmuir* **33**, 553–560 (2017).
221. Sarkander, H. I. & Brade, W. P. On the mechanism of lanthanide-induced liver toxicity. *Arch Toxicol* **36**, 1–17 (1976).

222. Thunus, L. & Lejeune, R. Overview of transition metal and lanthanide complexes as diagnostic tools. *Coord Chem Rev* **184**, 125–155 (1999).
223. Tai, P., Zhao, Q., Su, D., Li, P. & Stagnitti, F. Biological toxicity of lanthanide elements on algae. *Chemosphere* **80**, 1031–1035 (2010).
224. Wang, Z.-L., Hao, J., Chan, H. L. W., Wong, W.-T. & Wong, K.-L. A Strategy for Simultaneously Realizing the Cubic-to-Hexagonal Phase Transition and Controlling the Small Size of NaYF4:Yb3+,Er3+ Nanocrystals for In Vitro Cell Imaging. *Small* **8**, 1863–1868 (2012).
225. Abdul Jalil, R. & Zhang, Y. Biocompatibility of silica coated NaYF4 upconversion fluorescent nanocrystals. *Biomaterials* **29**, 4122–4128 (2008).
226. Zhao, L. *et al.* The endocytic pathway of Pt nanoclusters and their induced apoptosis of A549 and A549/Cis cells through c-Myc/p53 and Bcl-2/caspase-3 signaling pathways. *Biomedicine & Pharmacotherapy* **144**, 112360 (2021).
227. Reis, C. R., Chen, P.-H., Bendris, N. & Schmid, S. L. TRAIL-death receptor endocytosis and apoptosis are selectively regulated by dynamin-1 activation. *Proceedings of the National Academy of Sciences* **114**, 504–509 (2017).
228. Xiong, L. Q. *et al.* Synthesis, characterization, and in vivo targeted imaging of amine-functionalized rare-earth up-converting nanophosphors. *Biomaterials* **30**, 5592–5600 (2009).
229. Li, X. *et al.* Peptide-enhanced tumor accumulation of upconversion nanoparticles for sensitive upconversion luminescence/magnetic resonance dual-mode bioimaging of colorectal tumors. *Acta Biomater* **104**, 167–175 (2020).
230. Krüger, M. & Richter, P. To Die or Not to Die: Cell Death in Biology and Disease. *Int J Mol Sci* **23**, 6734 (2022).
231. Green, D. R. The End and After: How Dying Cells Impact the Living Organism. *Immunity* **35**, 441–444 (2011).
232. Kiraz, Y., Adan, A., Kartal Yandim, M. & Baran, Y. Major apoptotic mechanisms and genes involved in apoptosis. *Tumor Biology* **37**, 8471–8486 (2016).
233. Wong, R. S. Apoptosis in cancer: from pathogenesis to treatment. *Journal of Experimental & Clinical Cancer Research* **30**, 87 (2011).
234. Portt, L., Norman, G., Clapp, C., Greenwood, M. & Greenwood, M. T. Anti-apoptosis and cell survival: A review. *Biochimica et Biophysica Acta (BBA) - Molecular Cell Research* **1813**, 238–259 (2011).
235. Favaloro, B., Allocati, N., Graziano, V., Di Ilio, C. & De Laurenzi, V. Role of Apoptosis in disease. *Aging* **4**, 330–349 (2012).
236. Novus Biologicals. Apoptosis, Necroptosis & Autophagy Poster. (2023).
237. Galluzzi, L., Kepp, O., Krautwald, S., Kroemer, G. & Linkermann, A. Molecular mechanisms of regulated necrosis. *Semin Cell Dev Biol* **35**, 24–32 (2014).
238. D'Arcy, M. S. Cell death: a review of the major forms of apoptosis, necrosis and autophagy. *Cell Biol Int* **43**, 582–592 (2019).
239. Kung, G., Konstantinidis, K. & Kitsis, R. N. Programmed Necrosis, Not Apoptosis, in the Heart. *Circ Res* **108**, 1017–1036 (2011).
240. Lotfi, R., Kaltenmeier, C., Lotze, M. T. & Bergmann, C. Until Death Do Us Part: Necrosis and Oxidation Promote the Tumor Microenvironment. *Transfusion Medicine and Hemotherapy* **43**, 120–132 (2016).
241. Strzyz, P. Pulling the apoptotic trigger for necrosis. *Nat Rev Mol Cell Biol* **18**, 72–72 (2017).
242. Kumar, P., Nagarajan, A. & Uchil, P. D. Analysis of Cell Viability by the MTT Assay. *Cold Spring Harb Protoc* **2018**, pdb.prot095505 (2018).
243. Supino, R. MTT Assays. in *In Vitro Toxicity Testing Protocols* 137–149 (Humana Press, 1995). doi:10.1385/0-89603-282-5:137.

244. Crowley, L. C., Marfell, B. J., Scott, A. P. & Waterhouse, N. J. Quantitation of Apoptosis and Necrosis by Annexin V Binding, Propidium Iodide Uptake, and Flow Cytometry. *Cold Spring Harb Protoc* **2016**, pdb.prot087288 (2016).
245. Han, Y., Gu, Y., Zhang, A. C. & Lo, Y.-H. Review: imaging technologies for flow cytometry. *Lab Chip* **16**, 4639–4647 (2016).
246. Adan, A., Alizada, G., Kiraz, Y., Baran, Y. & Nalbant, A. Flow cytometry: basic principles and applications. *Crit Rev Biotechnol* **37**, 163–176 (2017).
247. McKinnon, K. M. Flow Cytometry: An Overview. *Curr Protoc Immunol* **120**, (2018).
248. Robinson, J. P. Flow cytometry: past and future. *Biotechniques* **72**, 159–169 (2022).
249. Chiu, Y.-H., Chang, T.-F., Chen, C.-Y., Sone, M. & Hsu, Y.-J. Mechanistic Insights into Photodegradation of Organic Dyes Using Heterostructure Photocatalysts. *Catalysts* **9**, 430 (2019).
250. Winterbourn, C. C. Reconciling the chemistry and biology of reactive oxygen species. *Nat Chem Biol* **4**, 278–286 (2008).
251. Samadi, M. *et al.* Design and tailoring of one-dimensional ZnO nanomaterials for photocatalytic degradation of organic dyes: a review. *Research on Chemical Intermediates* **45**, 2197–2254 (2019).
252. Gardner, A. M. *et al.* Apoptotic vs. Nonapoptotic Cytotoxicity Induced by Hydrogen Peroxide. *Free Radic Biol Med* **22**, 73–83 (1997).
253. Muhr, V., Wilhelm, S., Hirsch, T. & Wolfbeis, O. S. Upconversion nanoparticles: From hydrophobic to hydrophilic surfaces. *Acc Chem Res* **47**, 3481–3493 (2014).
254. Lobner, D. Comparison of the LDH and MTT assays for quantifying cell death: validity for neuronal apoptosis? *J Neurosci Methods* **96**, 147–152 (2000).
255. Kaksonen, M. & Roux, A. Mechanisms of clathrin-mediated endocytosis. *Nat Rev Mol Cell Biol* **19**, 313–326 (2018).
256. Li, C. *et al.* A facile fabrication of upconversion luminescent and mesoporous core–shell structured β-$NaYF_4$:Yb^{3+}, Er^{3+}@$mSiO_2$ nanocomposite spheres for anti-cancer drug delivery and cell imaging. *Biomater. Sci.* **1**, 213–223 (2013).